Supplementary Material

Theoretical spectroscopy for unraveling the intensity mechanism of the optical and photoluminescent spectra of chiral Re(I) transition metal complexes.

Rami Shafei,[1,2] Ai Hamano,[3,4] Christophe Gourlaouen,[3] Dimitrios Maganas,[1]

Keiko Takano,[4] Chantal Daniel,[*3] and Frank Neese[*1]

[1]*Max-Planck-Institut für Kohlenforschung, Kaiser-Wilhelm-Platz 1, 45470 Mülheim an der Ruhr,* Germany

[2]*Department of Chemistry, Faculty of Science, Beni-Suef University, Salah Salem Str., 62511 Beni-Suef, Egypt*

[3]*Laboratoire de Chimie Quantique Institut de Chimie UMR 7177 CNRS-Université de Strasbourg, 4, Rue Blaise Pascal CS 90032, F-67081 Strasbourg Cedex, France.*

[4]*Department of Chemistry and Biochemistry, Graduate School of Humanities and Sciences Ochanomizu University 2-1-1 Otsuka, Bunkyo-ku, Tokyo 112-8610, Japan*

Table of Contents

List of Schemes

List of Figures

List of Tables

I. Abbreviations

NHC	N-Heterocyclic Carbene Ligand
ABS	Absorption
PL	Photoluminescence
CP	Circular Polarized
CD	Circular Dichroism
ECD	Electronic Circular Dichroism
MCD	Magnetic Circular Dichroism
CPL	Circular Polarized Luminescence
CPP	Circular Polarized Phosphorescence
PLQY	Photoluminescence Quantum Yield
C-	Right-handed Center
A-	Left-handed Center
P-	Right-handed Helix
M-	Left-handed Helix
MLCT	Metal to ligand charge transfer
XLCT	Halogen to ligand charge transfer
LCCT	Ligand centered charge transition
ILCT	Intraligand charge transfer
ZFS	Zero Field Splitting
SH	Spin Hamiltonian

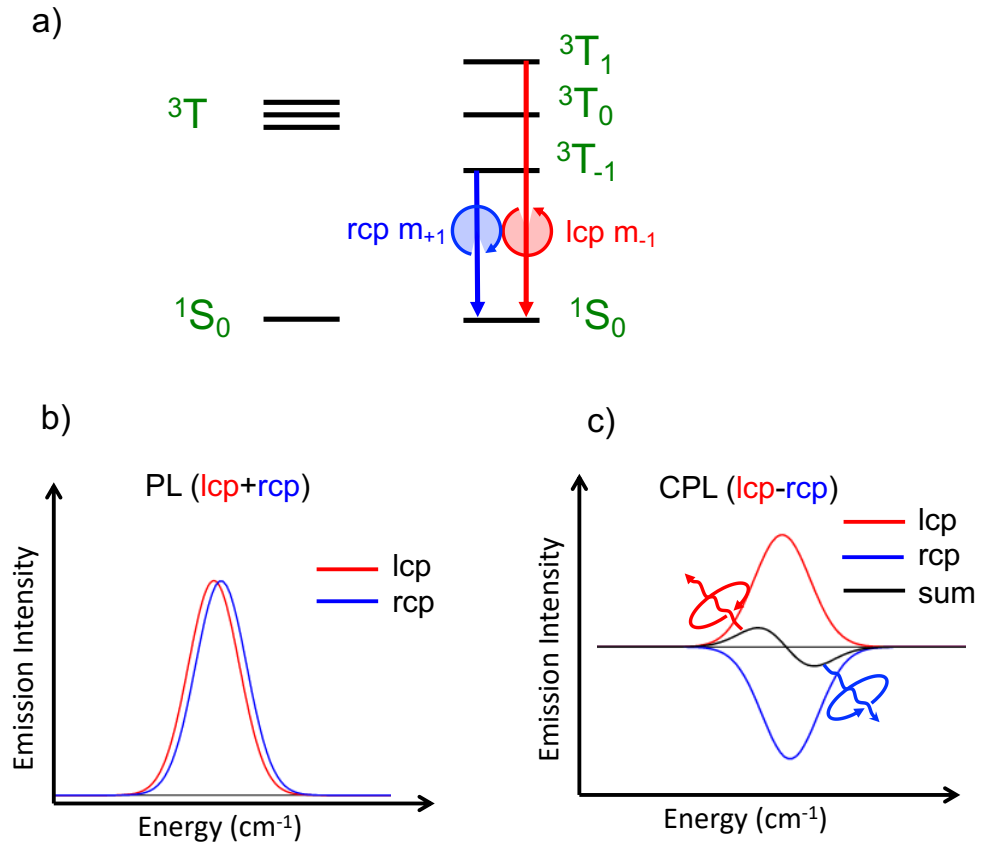

Scheme S 1

a) CPL selection rules for a ground singlet S and an excited triplet T states interacting through SOC. b) The resulted lcp and rcp components of the photoluminescent (PL) spectrum. c) The resulted lcp-rpl circularly polarized photoluminescence (CPL) spectrum together with the lcp and rcp CPL components.

II. Theory

1. Absorption and photoluminescence spectroscopies (ABS, PL)

The absorption or the spontaneous photoluminescence cross section between a set of stationary initial $|I\rangle$ and final $|F\rangle$ state(s) is given, at first-order perturbation theory and within the weak field approximation, by the general expression of the Fermi's golden rule:

$$\sigma_{ABS/PL}(\omega) = \frac{4\pi^2}{c(\omega_{ABS/PL}-\omega_{FI})} |T_{IF}|^2 \delta\left(E_{FI} \pm \omega_{ABS/PL}\right) \quad (1)$$

where $\omega_{ABS/PL}$ are the excitation and emission photon energies, respectively while ω_{FI} is the energy difference between the initial and final states reached in the absorption or the photoluminescence processes. $T_{IF} = \langle I | e^{i\mathrm{kr}_j} (\varepsilon \cdot \hat{p}_j) | F \rangle$ denotes the transition probability employing the full field-matter interaction operator (FFMIO), r_j and $\hat{p}_j$ are the position and the momentum operators of the *j*-th particle, k and ε denote the wave and polarization vectors of the incident radiation field. E_{FI} is the transition energy, δ refers to the line-broadening arising from the lifetimes of the relevant final states, and c being the speed of light. The most straightforward way of computing oscillator strengths relies on a series expansion of the spatial part of the radiation field of the interaction Hamiltonian contained in T_{IF}, i.e. $e^{i\boldsymbol{k}\cdot\boldsymbol{r}} = 1 + i\boldsymbol{k} \cdot \boldsymbol{r} - 1/2\,(\boldsymbol{k} \cdot \boldsymbol{r})^2 + \cdots$, that eventually results in the *multipole expansion* of T_{IF} as $T_{IF}^{mult} = T_{IF}^{(0)} + T_{IF}^{(1)} + T_{IF}^{(2)} + \ldots$, which in principle is infinite.

Within the electric dipole approximation (ED) the respective radiative rates for the absorption and the spontaneous photoluminescence, are given by equations (2) and (3), respectively.

$$k_{ABS}(\omega) = \frac{4\pi^2 \omega_{ABS}}{3} \sum_F |\langle \Psi_I | \hat{\mu} | \Psi_F \rangle|^2 \delta(E_{FI} \pm \omega_{ABS}) \quad (2)$$

$$k_{PL}(\omega) = \frac{4{\omega_{PL}}^3 n^2}{3\hbar c^3} \sum_F |\langle \Psi_I | \hat{\mu} | \Psi_F \rangle|^2 \delta(E_{FI} \pm \omega_{PL}) \quad (3)$$

where $\hat{\mu}$ defines the electric dipole operator as $\hat{\mu} = \sum_A Z_A \hat{R}_A - \sum_i \hat{r}_i$, here A sums over nuclei with charges Z_A at positions $\hat{R}_A, i$ over the electrons, n is the refractive index, and $\hbar$ is the Planck constant divided by 2π.

2. Circularly polarized absorption and photoluminescence spectroscopies (ECD, CPL)

As it has been shown within the context of magnetic circular dichroism (MCD), [1-3] by defining a laboratory frame in which the $\hat{z}$-axis defines the direction of the light trajectory, circular polarized light interactions can be generated with the use of the complex vectors $\mathcal{E}_{\pm} = \frac{1}{\sqrt{2}}(\hat{x} \pm i\hat{y})$. In this framework the FFMIO operator transforms as:

$$T_{IF}^{\pm} = \frac{1}{\sqrt{2}}\sum_{j=1}^{N}\langle I|e^{-i\mathrm{k}r_j}(\varepsilon \cdot \hat{p}_x)|F\rangle \pm \langle I|e^{-i\mathrm{k}r_j}(\varepsilon \cdot \hat{p}_y)|F\rangle \quad (4)$$

In both ECD and/or CPL spectroscopies, the measured intensities reflect the difference of absorption and/or photoluminescence between the left and right polarized transition moments given by:

$$\Delta_{IF}^{L\pm R}(\mathrm{k}, \mathcal{E}) = |T_{IF}^{-}|^2 \pm |T_{IF}^{+}|^2 \quad (5)$$

which leads to the following expressions for the sum and the difference of the square moduli $|T_{IF}^{\pm}|^2$:

$$\Delta_{IF}^{L+R}(\mathrm{k}, \mathcal{E}) = \frac{1}{2}\langle I|\sum_{j=1}^{N} e^{-i\mathrm{k}r_j}(\varepsilon \cdot \hat{p}_x)|F\rangle\langle I|\sum_{j=1}^{N} e^{-i\mathrm{k}r_j}(\varepsilon \cdot \hat{p}_y)|F\rangle \quad (6)$$

$$\Delta_{IF}^{L-R}(\mathrm{k}, \mathcal{E}) = -\mathbf{Im}\left(\langle I|\sum_{j=1}^{N} e^{-i\mathrm{k}r_j}(\varepsilon \cdot \hat{p}_x)|F\rangle\langle I|\sum_{j=1}^{N} e^{-i\mathrm{k}r_j}(\varepsilon \cdot \hat{p}_y)|F\rangle\right) \quad (7)$$

Performing orientational averaging on expression (7) in presence of a magnetic field and taking into account Zeeman interactions leads to the formulation of MCD expressions in the framework of FFMIO operator.[1]

Alternatively, within the ED approximation and upon orientational averaging, equation (6) can be used to generate ABS and PL cross sections presented in equations (2) and (3). Likewise, equation (7) including ED and magnetic dipole (MD) interactions upon orientational averaging will generate the respective ECD and CPL radiative transition rates:

$$k_{ECD}(\omega) = \frac{16\pi^2\omega_{ECD}}{3}\sum_F \mathbf{Im}(|\langle\Psi_I|\hat{\mu}|\Psi_F\rangle\langle\Psi_F|\hat{m}|\Psi_I\rangle|)\delta(E_{FI} \pm \omega_{ECD}) \quad (8)$$

$$k_{CPL}(\omega) = \frac{16{\omega_{CPL}}^3 n^2}{3\hbar c^3}\sum_F \mathbf{Im}(|\langle\Psi_I|\hat{\mu}|\Psi_F\rangle\langle\Psi_F|\hat{m}|\Psi_I\rangle|)\delta(E_{FI} \pm \omega_{CPL}) \quad (9)$$

leading to a unified formulation of ABS, PL, ECD and CPL spectroscopies.

In the above expressions, $\hat{\mu}$ defines electric dipole operator while $\hat{m}$ is the respective magnetic dipole operator $\hat{m} = \frac{1}{2m_e c}\sum_i r_i \times \hat{p}_i$, m_e is the electron mass and $\mathbf{Im}(|\langle\Psi_I|\hat{\mu}|\Psi_F\rangle\langle\Psi_F|\hat{m}|\Psi_I\rangle|)$ represents the rotatory strength (R_{IF}).

Quite commonly the ECD and CPL (or CPP) spectral intensities are represented against normalized absorption and photoluminescent intensities defining, similar expressions for, the respective dissymmetry factors g_{abs} and g_{lum}:

$$g_{abs}\,(ECD)\ or\ g_{lum}(CPL) = 2\frac{I_{LCP} - I_{RCP}}{I_{LCP} + I_{RCP}} \sim \frac{4R}{D}, -2 < g_{abs}\ or\ g_{lum} < 2 \qquad (10)$$

where $I_{LCP/RCP}$ is the left and right polarized components of the involved absorption or emission process. D and R are the square of the transition electric dipole and the rotatory strength, respectively.

3. Spin-orbit coupling (SOC) effects

Spin-orbit coupling (SOC) along with the Zeeman interaction can be introduced in the framework of quasi-degenerate perturbation theory (QDPT). [4] In the QDPT scheme, SOC and Zeeman interactions act as perturbation to the non-relativistic Hamiltonian which takes the form [5]:

$$\langle\Psi_I^{SM}|H_{BO} + H_{SOC} + H_Z|\Psi_F^{S'M'}\rangle = \delta_{IF}\delta_{SS'}\delta_{MM'}E_I^S + \langle\Psi_I^{SM}|H_{SOC} + H_Z|\Psi_F^{S'M'}\rangle \qquad (11)$$

In this approach, the SOC operator is approximated by the spin-orbit mean field (SOMF) operator,[5] which is an effective one-electron operator that contains one- and two-electron SOC integrals and also incorporates the spin-other orbit interaction. Hence in equation (11) H_{SOC} is given by

$$H_{SOC} = \sum_i \mathbf{h}^{SOC}(x_i)s(i) \qquad (12)$$

where $\mathbf{h}^{SOC}(x_i)$ is the effective mean-field one-electron spin-orbit operator, x_i and $s(i)$ refer to the coordinates and spin-operators of electron *i,* respectively. Finally the Zeeman Hamiltonian may be included in the form of:

$$H_Z = \mu_B(\hat{\mathbf{L}} + g_e\hat{\mathbf{S}}) \cdot \mathbf{B} \qquad (13)$$

with

$$\hat{\mathbf{L}} = \sum_i l(i)$$

4. Photoluminescence and CPL transition rates with excited state dynamics

Assuming an emissive triplet state within the Frank-Condon approximation and neglecting SOC between ground and excited states as well as vibronic coupling, the observed radiative photoluminescence (PL) or CPL rates $k_{PL/CPL}^{obs}$ can be evaluated from relations (3) and (9) considering the Boltzmann population for the each state[6] at temperature (T) according to equation (14):

$$k_{PL/CPL}^{obs} = \sum_M k_M \, e^{-(\Delta E_{M,1}/k_B T)} \, / \, Z \tag{14}$$

where k_M is the rate constant of each magnetic sublevel $M = 1 - 3$, $\Delta E_{M,1}$ is the energy difference between the magnetic sublevel M and the low-lying sublevel ($M = 1$) and Z is the partition function defined as $\sum_M e^{-(\Delta E_{M,1}/k_B T)}$.

It has been shown that a more direct way to compute unpolarized as well as, circularly polarized transition rates proceeds through the path integral approach[7-15] in which it is possible to calculate $k_{PL/CPL}^{obs}$ from the Fourier Transform (FT) of the respective correlation function $\chi_{(t)}$ that is computed from the path integral of the multidimensional harmonic oscillator according to:

$$k_{ABS/PL/ECD/CPL}^{obs}(\omega) = 2\alpha \mathcal{R}e \int_0^\infty \chi_{(t)} \, e^{\pm i\omega t} dt \tag{15}$$

with α being a collection of constants while, in the exponential time-dependent treatment, one selects the positive sign and the negative sign for the ABS/ ECD, and PL/CPL processes, respectively. Hence in the case of one-photon transition rates (ABS, PL) within the ED approximation the correlation function takes the form[7, 8, 16]:

$$\chi_{(t)} = e^{\pm i\omega t} \left[|\mu_e|^2 \rho^{FC}(t) + \sum_k \frac{\partial \mu_e^*}{\partial \bar{Q}_k} \mu_e \rho_k^{HT/FC}(t) \; + \sum_k \mu_e^* \frac{\partial \mu_e}{\partial \bar{Q}_k} \rho_k^{HT/FC}(t) \; + \right.$$
$$\left. \sum_{kl} \frac{\partial \mu_e^*}{\partial \bar{Q}_k} \frac{\partial \mu_e}{\partial \bar{Q}_l} \rho_k^{HT}(t) \right] \tag{16}$$

where FC and HT denote Frank-Condon and Herzberg–Teller interactions. Similarly the circularly polarized one-photon transition rates (ECD, CPL), considering electric dipole and magnetic dipole interactions in the expression of the rotatory strengths, it takes the form[16]:

$$\chi_{(t)} = e^{\pm i\omega t} \left[\mathbf{Im}[\mu_e m_e^*] \rho^{FC}(t) + \sum_k \mathbf{Im} \left[\mu_e \frac{\partial m_e^*}{\partial \bar{Q}_k} \right] \rho_k^{HT/FC}(t) \; + \right.$$
$$\left. \sum_k \mathbf{Im} \left[\frac{\partial \mu_e}{\partial \bar{Q}_k} m_e^* \right] \rho_k^{HT/FC}(t) \; + \; \sum_{kl} \mathbf{Im} \left[\frac{\partial \mu_e}{\partial \bar{Q}_k} \frac{\partial m_e^*}{\partial \bar{Q}_l} \right] \rho_k^{HT}(t) \right] \tag{17}$$

where μ_e and m_e represent the respective transition dipole $\langle \Psi_I | \hat{\mu} | \Psi_F \rangle$ and magnetic dipole $\langle \Psi_F | \hat{m} | \Psi_I \rangle$ moment integrals between initial and final states I, F while:

$$\rho^{FC} = Tr(e^{-i\hat{H}\tau}e^{-i\hat{H}\tau}) \quad (18)$$

$$\rho_k^{HT/FC} = Tr(\bar{Q}_k e^{-i\hat{H}\tau}e^{-i\hat{H}\tau}) \quad (19)$$

$$\rho_{kl}^{HT} = Tr(\bar{Q}_k e^{-i\hat{H}\tau}\bar{Q}_l e^{-i\hat{H}\tau}) \quad (20)$$

It has been shown recently[7, 8] that the above equations can be very efficiently implemented for absorption and emission transition rates.

5. Non-Radiative transition rates and quantum yields

The luminescence photophysics may be perturbed by non-radiative processes such as internal conversion (IC) and intersystem crossing (ISC). Both unpolarized and circularly polarized radiative rates should take into account excited states that undergo temperature dependent non-radiative relaxation. Within the harmonic approximation and weak coupling limit between the emissive and ground states, non-radiative rates follow the so called weak-coupling limit of "energy gap law" as derived by Englman and Jortner.[17] In the 'classical' description the respective potential energy surfaces PESs show only small displacement, with small Huang Rhys factor ($S \lesssim 1$), from each other and the excited state relaxation process proceeds through the zeroth order vibronic states. Quantum mechanically non-radiative ISC rates between initial $|I\rangle$ and final $|F\rangle$ state(s), can be estimated by,[18, 19]

$$k_{ISC} = \frac{2\pi}{\hbar} \sum_F |\langle \Psi_F | H_{SOC} | \Psi_I \rangle|^2 \delta(E_{FI}) \quad (21)$$

Hence, similar to radiative rates $k_{ABS/PL}$, k_{ISC} can be calculated in the framework of ESD through the path integral approach and within the FC/HT approximations. Hence, similarly to radiative phosphorescence, the non-radiative rate of $(T_1 \rightsquigarrow S_0\ ISC)$ can be calculated employing equation (21) considering the Boltzmann populations over sublevels with spin projections $Ms = 0, \pm 1$, as shown in equation (14).

Knowledge of the radiative (k_r) and non-radiative (k_{nr}) rates provides access to the respective relaxation times (τ_r and τ_{nr}) as well as to the PLQY quantity $\Phi_{PL} = {k_r}/{k_r + k_{nr}}$.

6. Spin-vibronic coupling effects

Inclusion of spin-vibronic coupling effects in photoluminescent processes requires treatment of the magnetic properties induced within the emissive multiplet. Let us define an excited state

Spin-Hamiltonian (SH) which at zero field and by excluding nuclei interactions reduces to the zero-field splitting (ZFS) term

$$\widehat{H}_{S,ZFS} = \hat{S}^T D \hat{S} = \sum_{i,j} D_{ij} \hat{S}_i \hat{S}_j \quad (22)$$

Typically, ZFS matrix in the SH is set to be traceless and symmetric (e.g. the ZFS matrix is diagonal in its eigenframe) so that

$$\widehat{H}_{S,ZFS} = D\left(\hat{S}_z^2 - \frac{S(S+1)}{3}\right) + E(\hat{S}_x^2 - \hat{S}_y^2) \quad (23)$$

and within an S=1 excited multiplet it takes the matrix form

$$D_{ZFS} = \begin{pmatrix} -1/3D + E & 0 & 0 \\ 0 & -1/3D - E & 0 \\ 0 & 0 & 2/3D \end{pmatrix} \quad (24)$$

with $D = 2/3D_z, E = (D_x - D_y)/3$

Under vibronic coupling conditions the effective Hamiltonian takes the form:

$$\widehat{H}_{eff} = \widehat{H}_S + \widehat{H}_{vib} + \widehat{H}_{S-vib} \quad (25)$$

where $\widehat{H}_S$ corresponds to the static SH, including only the zero-field terms in absence of external field as defined in equation (23) while $\widehat{H}_{vib}$ corresponds to the Vibrational-Hamiltonian (VH) which in the harmonic oscillator approximation is expressed as:

$$\widehat{H}_{vib} = \hbar\omega\left(n + \frac{1}{2}\right), \quad n = 0,1,\ldots \quad (26)$$

Restricting the SH expansion to linear terms in a series of normal modes Q_i and taking into account equation (23), the Spin-vibronic Hamiltonian $\widehat{H}_{S-vib}$ takes the form:

$$\widehat{H}_{S-vib} = \frac{\partial D}{\partial Q_0} Q_i \left(\hat{S}_z^2 - \frac{1}{4}\right) + \frac{\partial E}{\partial Q_0} Q_i (\hat{S}_x^2 - \hat{S}_y^2) \quad (27)$$

The basis of the Spin-vibronic Hamiltonian consists of a set of functions expressed by products of magnetic sublevels $|S = 1, M_S\rangle$, $M_S = 0, \pm 1$ and harmonic oscillator wavefunctions $|n\rangle$, with n-vibrational number and energies given by equation (26). Assuming weak vibronic coupling limit:

$$\hbar\omega \gg \left\langle M_S \middle| \hat{S}_z^2 - \frac{1}{4} \middle| M_S' \right\rangle \langle 0|Q_i|1'\rangle \quad (28)$$

$$\hbar\omega \gg \langle M_S|\hat{S}_x^2 - \hat{S}_y^2|M_S' \pm 2\rangle \langle 0|Q_i|1'\rangle \quad (29)$$

the basis functions consist of the ground and first excited state M_S, M_S' manifolds where one vibrational quantum state has been excited $\langle 0|Q_i|1'\rangle$.

In the presence of n coupled vibrational quantum states the effective Hamiltonian $\widehat{H}_{eff}$ takes the general form:

$$\widehat{H}_{eff} = \begin{pmatrix} \widehat{H}_S & \widehat{H}_{S-vib1} & \widehat{H}_{S-vib2} & \widehat{H}_{S-vib3} & \cdots \\ \widehat{H}^*_{S-vib1} & \widehat{H}_S + \hbar\omega_1 I & 0 & 0 & 0 \\ \widehat{H}^*_{S-vib2} & 0 & \widehat{H}_S + \hbar\omega_2 I & 0 & 0 \\ \widehat{H}^*_{S-vib3} & 0 & 0 & \widehat{H}_S + \hbar\omega_3 I & 0 \\ \vdots & \vdots & \vdots & \vdots & \ddots \end{pmatrix} \tag{30}$$

This implies that in the concept of spin-vibronic coupling along a photoluminescent process it is possible to determine the static $\hat{H}_S$ ZFS parameters of the emissive excited multiplet by employing the effective Hamiltonian approach at the equilibrium geometry. In a second step formulation of the ground and excited state potential energy surface (PES) scans, along the different contributing normal modes, calculated within the relativistic framework, provides access to the various spin-vibronic coupling constants per contributing normal mode.

III. Absorption and Emission processes. A qualitative electronic structure analysis

We enter our analysis by first discussing the most important factors that influence the absorption and emission processes of chiral Re(I) enantiomeric pair structures **1** and **2**. In both complexes the Re(I) center is imposed in a pseudo-octahedral (O_h) coordination environment, surrounded by one halogen, three carbonyl groups and one chelating bidentate: C^N NHC N-heterocyclic carbene ligands. Under approximately C_{3v} symmetry around the Re(I) complexes **1** and **2** obtain a low-spin d^6 singlet ground state $S_0(^1A_1)$. It follows that valence single electron excitations or electron decays will give rise to CT type of transitions (MLCT, XLCT, LLCT and ILCT) of $2S+1=1$ and $2S+1=3$ multiplets of A_2 and E symmetries along the absorption and emission processes respectively.

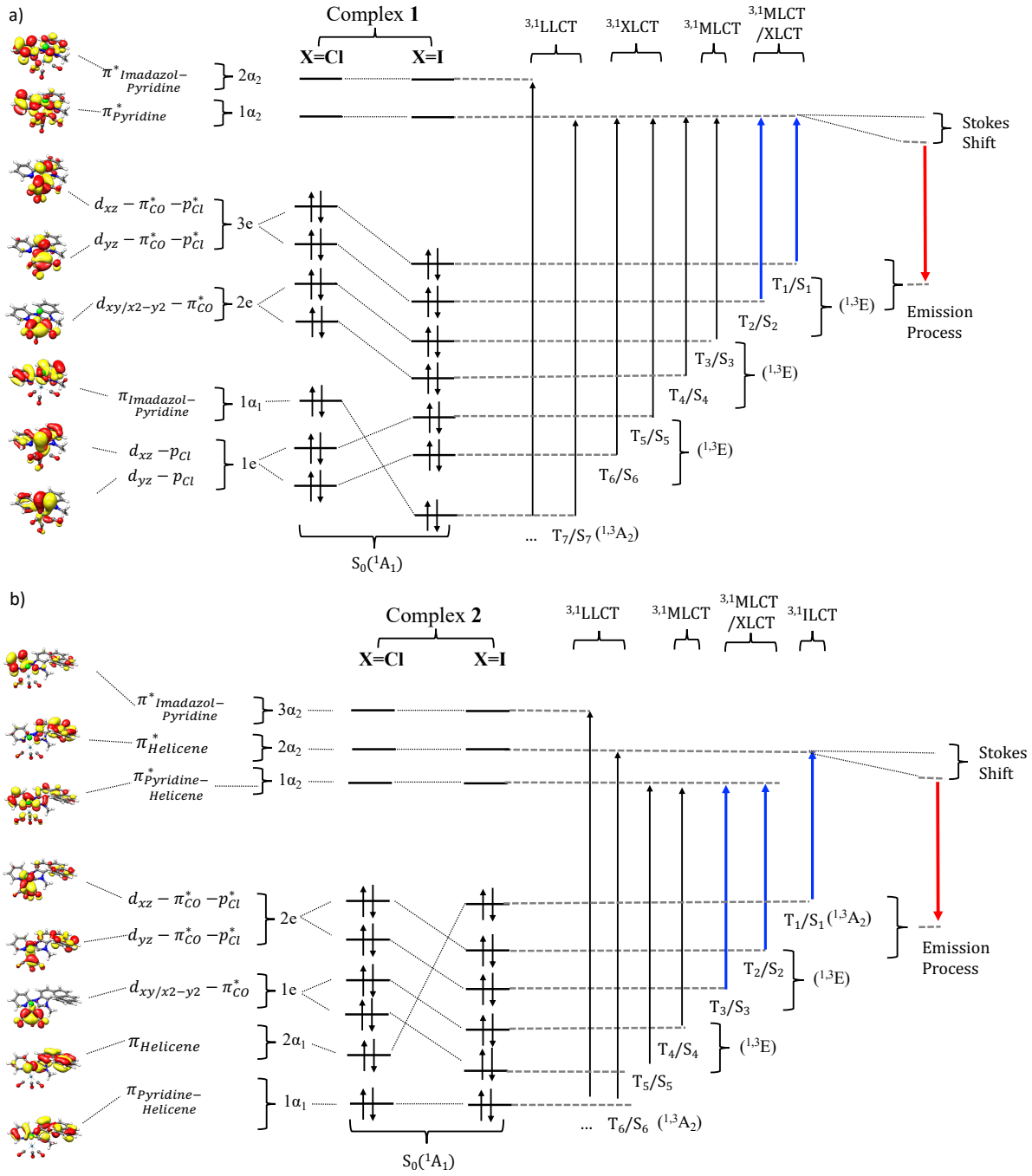

Figure S 1

PBE0/def2-TZVP MO diagram of the Cl and I derivatives of complexes **1** and **2** adapted in an 'ideal' C_{3v} symmetry around the Re centers. In both complexes the different type of single electron excitations depicted within the 1-electron picture are giving rise to E-symmetric MLCT and/or XLCT, as well as, A_2 symmetric LLCT types of transitions. In the case of complexes type **2**, $(\pi_{Helicene})^2 \rightarrow (\pi^*_{Helicene})^0$ excitations withing the Helicenic ligand give in addition rise to A_2 symmetric ILCT types of transitions.

In particular the enantiomeric pairs **1** C-/A-Cl and **1** C-/A-I have valence electron configuration:

$$(d_{xy} - \pi^*_{CO})^{\,2}(d_{yz} - \pi^*_{CO} - p^*_{Cl/I})^2(d_{xz} - \pi^*_{CO} - p^*_{Cl/I})^{\,2}(\pi^*_{Pyridine})^{\,0}(\pi^*{}_{\substack{Imadazol-\\Pyridine}})^{\,0}$$

As is seen in Figure S1a excitations $(d_{yz/xz} - \pi^*_{CO} - p^*_{Cl/I})^2 \rightarrow (\pi^*_{Pyridine})^{\,0}$ give rise to a pair of E-symmetric ^{1,3}MLCT/^{1,3}XLCT transitions which dominate the emission process. Similarly, $(d_{xy} - \pi^*_{CO})^2 \rightarrow (\pi^*_{Pyridine})^{\,0}$, $(\pi_{\substack{Imadazol-\\Pyridine}})^2 \rightarrow (\pi^*_{Pyridine})^{\,0}$ and $(d_{xz/yz} - p_{Cl})^2 \rightarrow (\pi^*_{Pyridine})^{\,0}$ excitations give rise to E-symmetric ^{1,3}MLCT, ^{1,3}XLCT and A_2-symmetric ^{1,3}LLCT type of transitions which will consist the high energy region of the absorption spectrum.

The Helicenic containing enantiomeric pair **2** M,A-/P,C-Cl has valence electron configuration (Figure S1b):

$$(d_{xy} - \pi^*_{CO})^2(\pi_{Helicene})^{\,2}(d_{yz} - \pi^*_{CO} - p^*_{Cl})^2(d_{xz} - \pi^*_{CO} - p^*_{Cl})^{\,2}(\pi^*_{\substack{Pyridine-\\Helicene}})^{\,0}(\pi^*_{Helicene})^{\,0}(\pi^*{}_{\substack{Imadazol-\\Pyridine}})^{\,0}$$

Likewise to the **1** C-/A-Cl/I diastereomers $(d_{yz/xz} - \pi^*_{CO} - p^*_{Cl/I})^2 \rightarrow (\pi^*_{Helicene})^{\,0}$ excitations give rise to a pair of E-symmetric ^{1,3}MLCT/^{1,3}XLCT transitions while $(\pi_{Helicene})^2 \rightarrow (\pi^*_{Helicene})^{\,0}$ give rise to an A_2-symmetric ^{1,3}ILCT type of transitions. This set of transitions dominate the emission process.

In the iodide derivative the increase of the Re-I covalency stabilizes the Re-based $d_{yz/xz} - \pi^*_{CO} - p^*_I$ below the $\pi_{Helicene}$ orbital, hence the enantiomeric pair **2** M,A-/P,C-I has valence electron configuration:

$$(d_{xy} - \pi^*_{CO})^{\,2}d_{yz} - \pi^*_{CO} - p^*_{Cl/I})^2(d_{xz} - \pi^*_{CO} - p^*_{Cl/I})^{\,2}(\pi_{Helicene})^{\,2}(\pi^*_{\substack{Pyridine-\\Helicene}})^{\,0}(\pi^*_{Helicene})^{\,0}(\pi^*{}_{\substack{Imadazol-\\Pyridine}})^{\,0}$$

As in the case of the **2** M,A-/P,C-Cl enantiomeric pair, the $(d_{yz/xz} - \pi^*_{CO} - p^*_I)^2 \rightarrow (\pi^*_{Helicene})^{\,0}$ and $(\pi_{Helicene})^2 \rightarrow (\pi^*_{Helicene})^{\,0}$ transitions give rise to a set of E-symmetric ^{1,3}MLCT/^{1,3}XLCT and A_2-symmetric ^{1,3}ILCT transitions which dominate the emission process. In both **2** M,A-/P,C-Cl/I enantiomeric pairs the high energy part of the absorption spectrum consist once again by a set of ^{,3}MLCT and ^{1,3}LLCT transitions owning to $(d_{xy} - \pi^*_{CO})^2 \rightarrow (\pi^*_{Pyridine})^{\,0}$, $(\pi_{\substack{Imadazol-\\Pyridine}})^2 \rightarrow (\pi^*_{Pyridine})^{\,0}$ and $(\pi_{\substack{Imadazol-\\Pyridine}})^2 \rightarrow (\pi^*_{Helicene})^{\,0}$ single

electron excitations. It should be noted that while MLCT and XLCT transitions can be both z- or xy- polarized transitions, LLCT and ILCT transitions are in principle $\pi \rightarrow \pi^*$ z-polarized transitions. As in practice under C_{3v} symmetry the A_2-symmetric $\pi \rightarrow \pi^*$ transitions involve orbital symmetries a_1 and a_2 ($a_1 \rightarrow a_2$) they are electric dipole forbidden but magnetic dipole allowed. In a first approximation this is expected to influence both the ECD, CPP intensities as well as the g_{abs} and g_{lum} values.

Based on the above qualitative analysis one may conclude that in the non-Helicenic diastereomers **1** C-/A-Cl/I MLCT/XLCT transitions will dominate the emission process while in the Helicenic diastereomers **2** M,A-/P,C-Cl/I the emission process will be dominated by a mixture of MLCT/XLCT and ILCT (within the Helicenic ligand) transitions.

In practice MLCT transitions involving transitions from $Re_{3d_{yz/xz}} - CO_{\pi^*}$ occupied MO will weaken the $\pi -$ backdonation $\mathrm{CO} \rightarrow \mathrm{Re(I)}$. This is expected to show up in the IR spectra leading to a blue shift in the CO stretching modes in the excited states that consist of MLCT transitions. This is in fact the case in the computed IR spectra of complexes **1** and **2** presented in Figure S2a and S2b for the non-relativistic ground state S_0 and the 1st excited 2S+1=1(S_1) and 2S+1=3 (T_1) states respectively. We focus in the spectral region around 2000 cm^{-1} in which the CO symmetric and asymmetric stretching vibration shows up. Comparing to the 'ideal' [O_h-Re(I)$(CO)_6$]$^+$ model complex[20] with complexes **1** and **2** the CO vibrations appear at lower energies indicating weakening for the CO bond strength due to the coordination of the halogen and the N-heterocyclic carbene ligands. In the 1st singlet and triplet excited states the asymmetric CO stretching vibration of complexes of type **1** is shifted at higher energies with respect to complexes of type **2** indicating a weaker Re-CO bond (Figure S2). This is consistent with the fact that in complexes of type **2** the absorption and emission processes contain in addition to MLCT/XLCT contributions from ILCT type of excitations within the Helicene unit. This also indicates that vibronic coupling should play a significant role in the emission processes of these complexes and has to be taken into account at least to some extent.

One may conclude that the above described excitation problem is more complicated as the coordination of the Halogen and the N-heterocyclic carbene ligands reduces further the local symmetry around Re(I) to C_s, hence all the remaining orbital degeneracy is lifted and all the non-relativistic 2S+1=1 and 2S+1=3 multiplets will be of $A'$and A'' symmetries. In principle the transitions consisting the absorption and emission processes will be a linear combination of the parent MLCT, XLCT, LLCT and ILCT transitions represented as

$$^{3,1}CT = \alpha\ ^{3,1}MLCT_{n=1,2\ldots} + \beta\ ^{3,1}XLCT + \gamma\ ^{3,1}LLCT + \delta\ ^{3,1}ILCT$$

where, $\alpha, \beta, \gamma, \delta$ define the mixing coefficients.

Further mixing of the different singlet and triplet ^{1,3}CT transitions is provided through SOC leading to state manifolds consisting magnetic sublevels with $M_S = 0, \pm 1$. In a further step vibrations that have the correct symmetry to interact with the non-relativistic states may add a dynamic band shape character to the absorption and emission processes while they might influence the excited state magnetic properties and hence the nature of the intensity mechanism and the relaxation times of the observed phosphorescence and the circularly polarized phosphorescence spectra of diastereomers **1** and **2.** In following we will develop a computational protocol that is able to tackle all the above aspects.

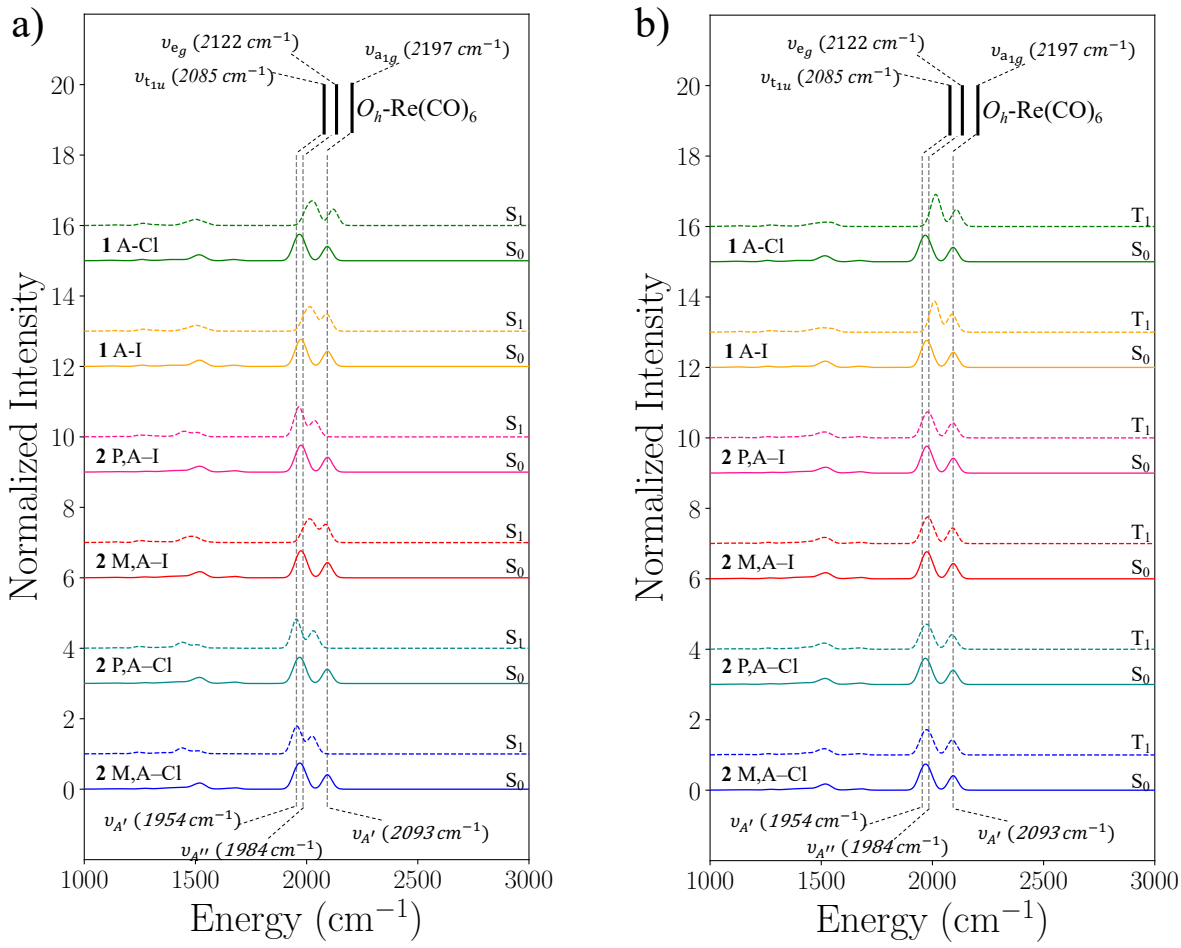

Figure S 2

IR spectra of a) ground and first singlet geometries, b) ground and first triplet geometries, all compared with experiments of $[O_h$-Re(CO)$_6]^+$.

IV. Choice of TD-DFT Functionals

Prior entering the spectra computation section and analysis we evaluate the performance of various TD-DFT functionals in computing the Absorption and ECD spectra of the diastereomers **1** and **2.** In a preliminary step B3LYP/TD-DFT was evaluated to perform similarly in both ORCA and ADF computational frameworks, knowing that both basis sets (Gaussian vs. Slater atomic orbitals) and relativistic effects (level of approximation) are not described by the same formalism in the two quantum chemistry softwares. These results are provided in Figures S8-10 and Table S2. As discussed in the computational section all productive calculations were performed with the ORCA computational package where the newly developed protocol, presented in the previous sections, has been implemented.

As a matter of fact, choice of "best" DFT functional with the desired level of accuracy is not trivial and depends on the specific system and the targeted property. In a first step, the ABS and ECD spectra of complex **1** A-Cl are computed employing the STEOM-DLPNO-CCSD[21-24] and full TD-DFT[25] levels of theory employing a collection of DFT functionals belonging to the GGA: BP86,[26, 27] PBE,[28] hybrid: PBE0,[29-31] BHLYP,[32] B3LYP,[26, 33-35] hybrid meta-GGA: M06,[36] range separated hybrid: CAM-B3LYP[37], wB97,[38] and double hybrid: B2PLYP[39] families. The computed non-relativistic and relativistic ABS and ECD spectra of complex **1** A-Cl compared with the respective experimental spectra are collectively provided in Figures S3 and S4.

As is seen the MAE errors with respect to experiment drop below 10% when employing STEOM-DLPNO-CCSD + SOC to compute the ABS and ECD spectra of **1** A-Cl, respectively. This is not surprising as in fact STEOM-DLPNO-CCSD level of theory has been successfully used to evaluate the performance of TD-DFT protocols in computing band gap energies of organic and inorganic semiconductors[40] and inorganic phosphor materials.[41] At the TD-DFT + SOC level functionals containing no Hartree Fock (HF) exchange e.g. the GGA BP86 and PBE and those with small HF exchange (e.g. in range separated hybrid wB97, 10%HF) or large HF exchange (e.g. in hybrid BHLYP , 50%HF) show avg MAEs $\geq$ 25 %. Such behavior can be attributed to the fact that none of the above functionals is able to provide a balance description of the diverse nature of the involved CT transitions (MLCT, XLCT, ILCT).

In contrast, the situation improves when hybrid functionals with moderate HF exchange, such as M06, PBE0, and B3LYP (with 27%, 25% and 20%HF, respectively) are employed. They in fact perform satisfactorily showing MAE values of (18, 14, and 22)%,

respectively. Interestingly the range separated hybrid performs worst in comparison to its hybrid variant (MAE=26%).

In a next step we select the bottom and upper limits of the above "best" performing functionals namely the PBE0 and B3LYP and we compare their performance across all complexes in the study set in the framework of ABS and ECD TD-DFT (+ SOC) computations. These results are collectively presented in Figures S6-8 and Table S2. Once again PBE0/TD-DFT + SOC shows the smallest errors in comparison to the experimental Absorption and ECD spectra. These errors amount to about 12% and 19% respectively. The respective errors employing the B3LYP/TD-DFT methods are ranked a bit higher, amounting in average to ~19% and ~33% for the Absorption and ECD spectra respectively.

Based on the above results while all the TD-DFT computed absorption and ECD spectra across the study set exhibit satisfactory agreement with experiment, PBE0/TD-DFT + SOC method shows the smallest MAE errors across the study set, hence it is chosen for all the production Absorption, ECD, PL and CPL calculations.

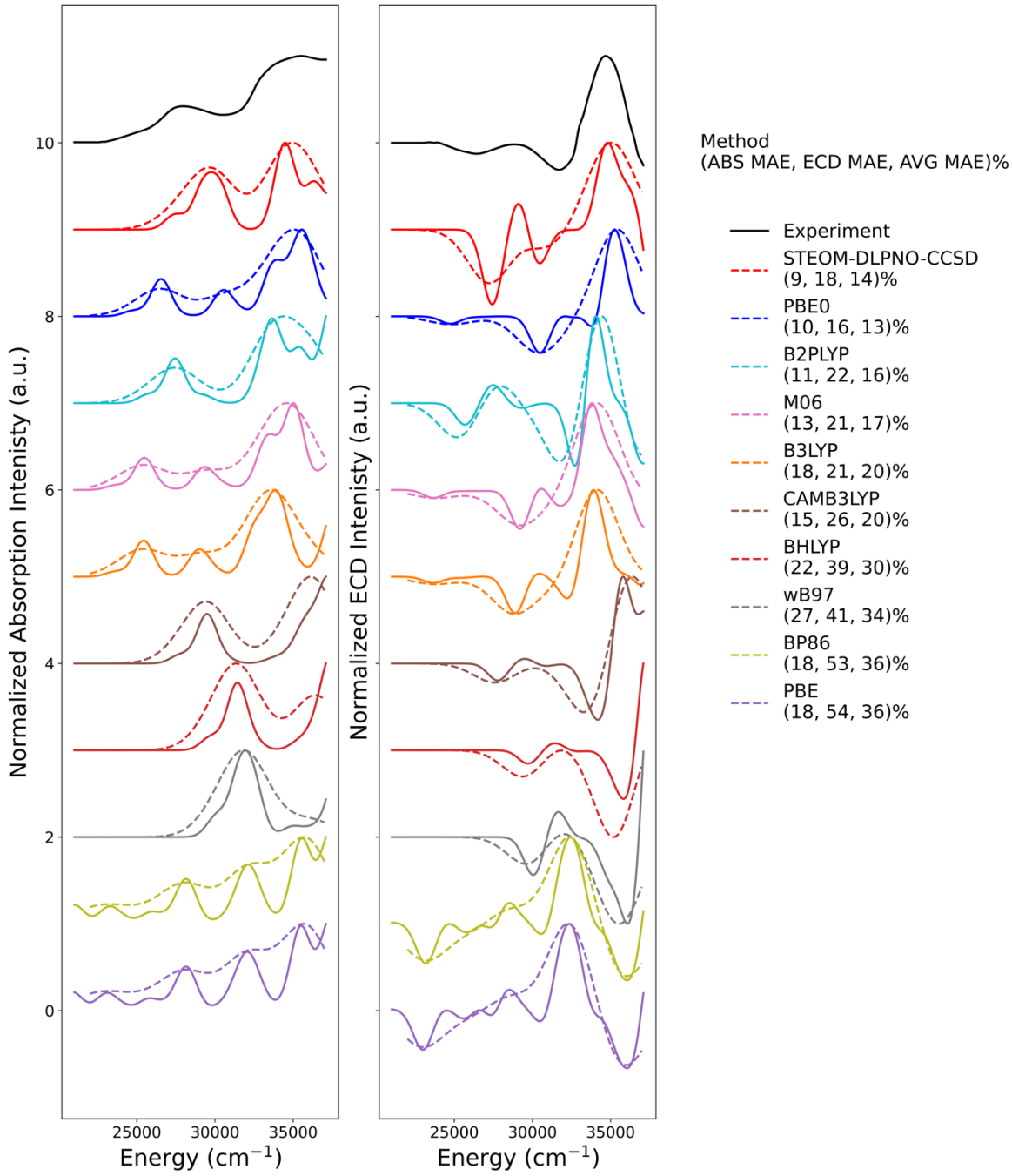

Figure S 3

Experimental (black) vs. calculated non-relativistic STEOM-DLPNO-CCSD (red), non-relativistic TD-DFT/BP86 (olive), PBE (purple), BHLYP (pale red), PBE0 (blue), B3LYP (orange), M06 (pink), CAMB3LYP (brown), wB97 (gray), B2PLYP(cyan) ABS (left side) and ECD (right side) spectra of complex **1** A-Cl. Solid lines indicate constant Gaussian broadening of 1500 cm^{-1} while dotted lines indicate constant Gaussian broadening of 3000 cm^{-1}. Given in parenthesis are the %MAE errors with respect to experiment, for (ABS, ECD and their average).

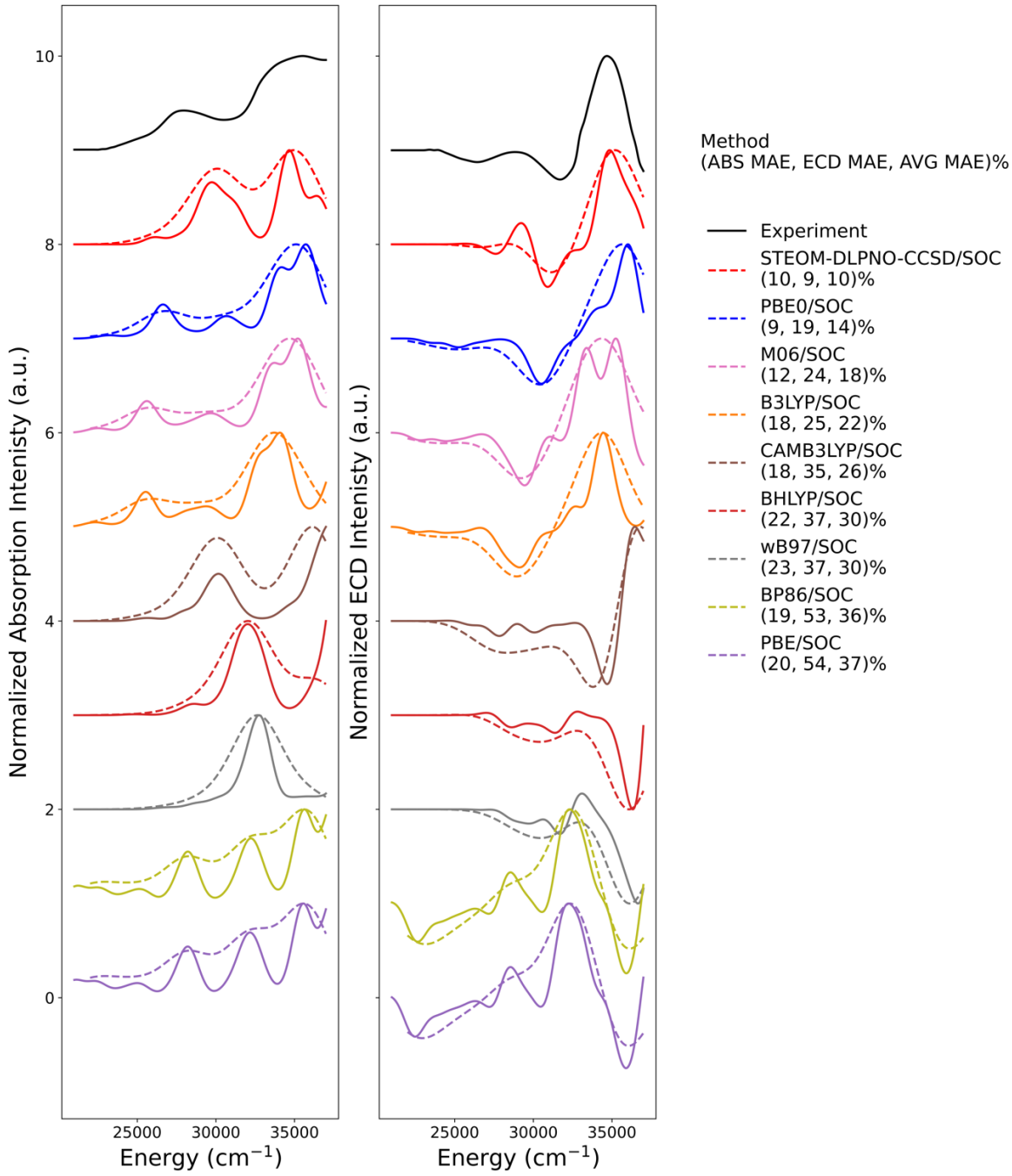

Figure S 4

Experimental (black) vs. calculated relativistically corrected STEOM-DLPNO-CCSD (red), non-relativistic TD-DFT/BP86 (olive), PBE (purple), BHLYP (pale red), PBE0 (blue), B3LYP (orange), M06 (pink), CAMB3LYP (brown), wB97 (gray) ABS (left side) and ECD (right side) spectra of complex **1** A-Cl. Solid lines indicate constant Gaussian broadening of 1500 cm^{-1} while dotted lines indicate constant Gaussian broadening of 3000 cm^{-1}. Given in parenthesis are the %MAE errors with respect to experiment, for (ABS, ECD and their average).

V. Absorption and ECD Spectra

1. Non-Relativistic Absorption and ECD spectra

1.1. Parent Non-Helicenic Complexes

(1 A-Cl / 1 C-Cl and 1 A-I / 1 C-I)

The experimental versus PBE0/TD-DFT calculated Absorption and ECD spectra of **1** A-Cl and **1** A-I are provided in Figure S5a and S5b. Note that for clarity only the spectra of the left-handed (A-) enantiomers are discussed. The complementary spectra of the right-handed (C-) models are in Figure S11. In principle the absorption spectra can be divided into three main regions. The first region extends between 24000-26000 cm^{-1} and includes the weak intensity bands 1-3. NTO analysis shows that bands 1, 2 have mixed MLCT/XLCT characters consisting of $Re - d_{yz/xz} - Cl/I - p^*_{x/y} \rightarrow \pi^*_{Pyridine}$ single electron excitations. As expected, the XLCT character of the excitation increases from Cl to I. On the contrary band 3 has basically a pure MLCT transition consisting of $Re - d_{xy} \rightarrow \pi^*_{Pyridine}$ single electron excitation. The second region extends between 32000-40000 cm^{-1} and includes bands 4-6. According to the NTO analysis these bands have mainly XLCT character ($Cl/I - p^*_{x/y} \rightarrow \pi^*_{Pyridine}$) containing small contributions from MLCT ($Re - d_{yz/xz} - Cl/I - p^*_{x/y} \rightarrow \pi^*_{Pyridine}$) and LLCT ($\pi_{Pyridine} \rightarrow \pi^*_{Pyridine}$ and $\pi_{Imidazole} \rightarrow \pi^*_{Pyridine}$) characters respectively. Finally, the high energy region > 40000 cm^{-1} consisting of bands 7-8 that have mainly XLCT character ($Cl/I - p^*_{x/y} \rightarrow \pi^*_{Pyridine/Imidazole}$). It should be noted that these results are also consistent with the TheoDore analysis presented in Figures S16 and S17 and Tables S3 and S4. Looking into the respective ECD spectra, bands 1-3 show weak ECD intensities due to fact that they consist of mainly MLCT characters with pronounced experimental g_{abs} ~0.003 (Figure S15a). Moving at higher energies (bands 4-6) where the respective ECD intensities increase as also the XLCT and LLCT characters in these transitions increase. This is also reflected to the experimental g_{abs} values that are now smaller (g_{abs} ~0.002, Figure S15a). At higher energy regions, bands 7 and 8 in the case of **1** A-Cl the ECD intensity drops while in the case of **1** A-I maintains its high intensity in comparison to bands 4-6. This indicates a more complex ECD intensity mechanism in this bands as they consist of a multitude of XLCT, LLCT types of excitations. At these energies the experimental g_{abs} values drop below 0.001, Figure S15a.

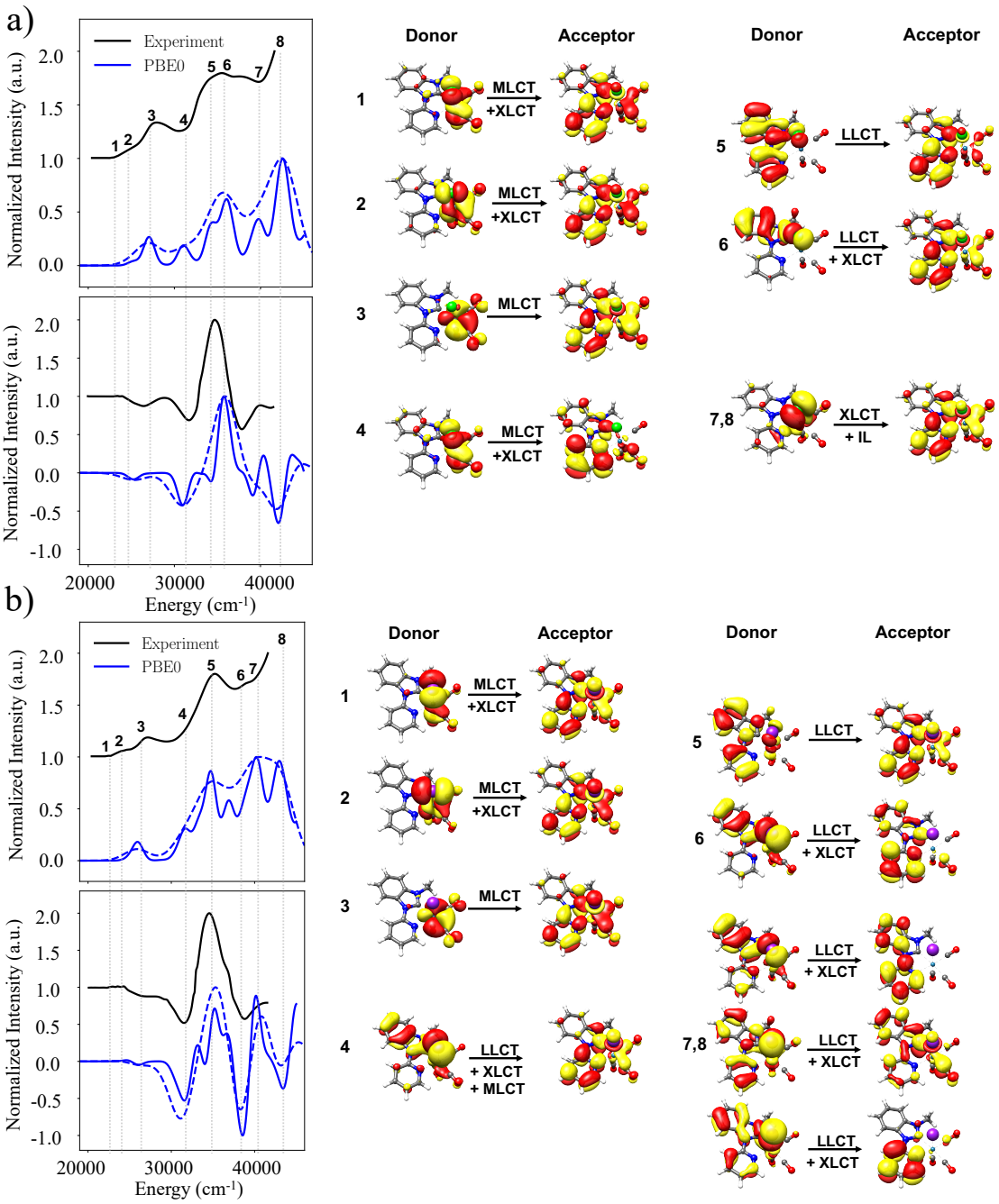

Figure S 5

Experimental (black) PBE0/TD-DFT (blue) of Absorption and ECD spectra of non-helicenic enantiomer a) **1** A-Cl and b) **1** A-I. The nature of the most important bands 1-8 is discussed in the framework of NTO analysis. Solid lines indicate constant Gaussian broadening of 1500 cm^{-1} while dotted lines indicate constant Gaussian broadening of 3000 cm^{-1}.

1.2. Helicenic complexes

X-Helicenic parallel (2 M,A-Cl / P,C-Cl and 2 M,A-I / P,C-I) and anti-parallel (2 M,C-Cl / P,A-Cl and 2 M,C-I / P,A-I) aligned

The experimental versus PBE0/TD-DFT calculated Absorption and ECD spectra of **2** M,A-Cl and **2** P,A-Cl are provided in Figures 6a and 6b while for the respective **2** M,A-I and **2** P,A-I are provided in Figures S12a and S12b. Once again, the complementary spectra of the right-handed (C-) models are in Figures S13 and S14. In all these cases there are 3 weak intensity bands around 25000 and 27000 cm^{-1}. According to the NTO analysis these bands are assigned as MLCT/XLCT transitions consisting of $Re - d_{yz/xz} - Cl/I - p^*_{x/y} \rightarrow \pi^*_{Pyridine}$ single electron excitations while band 3 has an ILCT character consisting of $\pi_{Helicene} \rightarrow \pi^*_{Helicene}$ single electron excitation. This is in contrast to the diastereomer complexes **1** in which the first bands are all MLCT/XLCT in nature. At energies between 30000 and 40000 cm^{-1} bands 4-6 consist from a mixture of MLCT/XLCT and ILCT transitions while > 40000 cm^{-1} band 7 and 8 consist from a mixture of XLCT and ILCT transitions. Once again, these results are consistent with the TheoDore analysis presented in Figures S18 and S19 and Tables S5 and S6.

As in the case of diastereomers **1** the ECD intensities increase at higher energies bands (4-7). In all bands there is in principle a pronounce mixing between MLCT/XLCT and ILCT transitions. This together with a more pronounced symmetry reduction around the Re(I) center to C_s, renders all the transitions both electric dipole and magnetic dipole allowed. This is reflected in the experimental and calculated g_{abs} values (Figure S15b) that vary only between g_{abs} ~0.002 and 0.001 across the experimentally observed and computed bands.

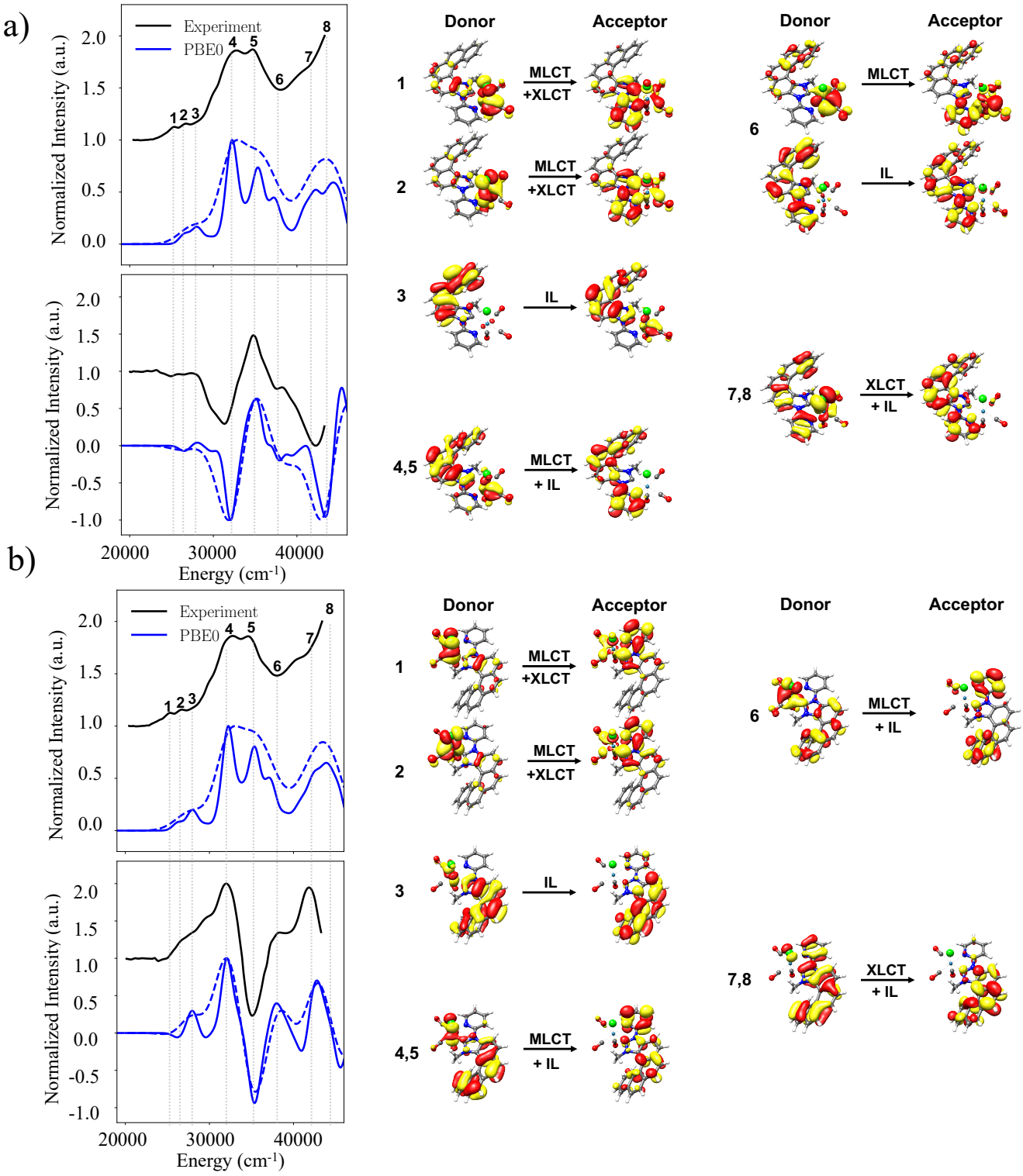

Figure S 6

Experimental (black) PBE0/TD-DFT (blue) of Absorption and ECD spectra of helicenic enantiomer a) **2** M,A-Cl and b) **2** P,A-Cl. The nature of the most important bands 1-8 is discussed in the framework of NTO analysis. Solid lines indicate constant Gaussian broadening of 1500 cm^{-1} while dotted lines indicate constant Gaussian broadening of 3000 cm^{-1}.

2. Relativistically corrected Absorption and ECD spectra.

In a next step we turn on SOC interactions. The relevant relativistically corrected Absorption and ECD spectra are presented in Figure S7 for the non-Helicenic enantiomers **1** A-Cl and **1** A-I and the respective Helicenic enantiomers, **2** M,A-Cl and **2** M,A-I. The complementary spectra of the C-, M,C-, and P,A/C enantiomers are presented in Figures S20-S22.

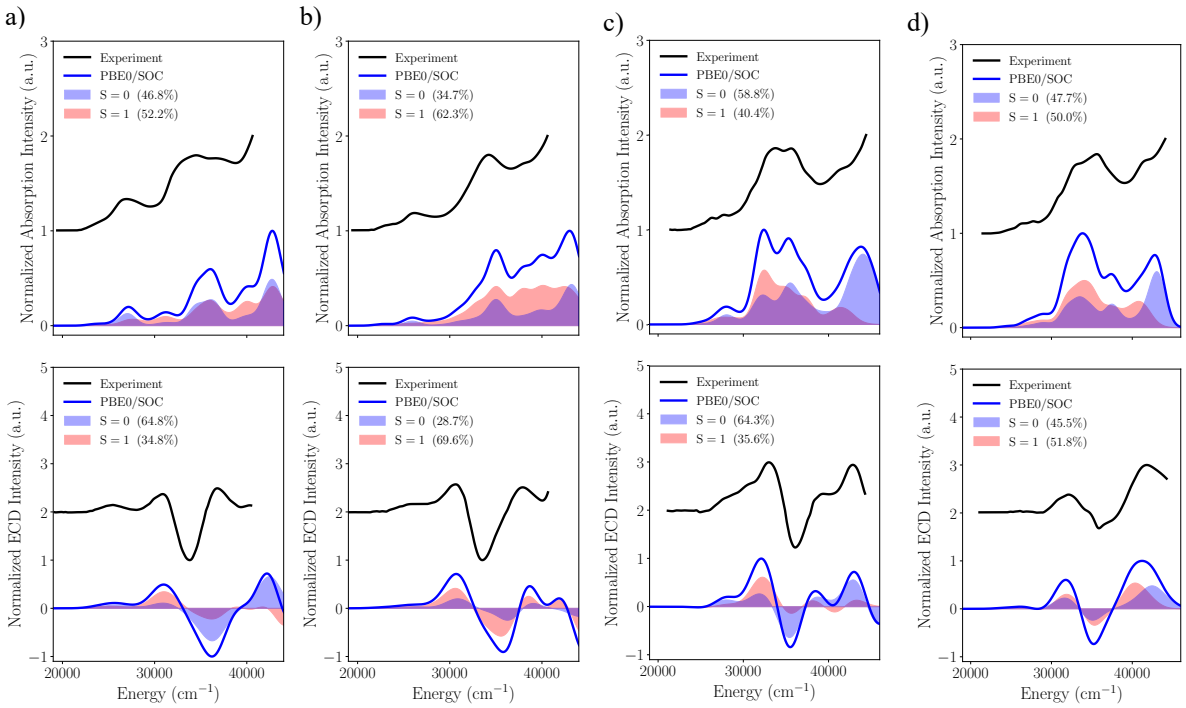

Figure S 7

Experimental (black) PBE0/TD-DFT + SOC (blue) Absorption and ECD spectra of non-helicenic enantiomers a) **1** A-Cl and b) **1** A-I and of helicenic enantiomers, c) **2** M,A-Cl and d) **2** M,A-I. The spectra are analyzed in terms of contributing parent non-relativistic singlet (light red) and triplet (light blue). Solid lines indicate constant Gaussian broadening of 1500 cm^{-1}.

As seen in Figure S7 analysis of the spectral features in terms of parent non-relativistic singlet (light blue) and triplet (light red) states reveals that all spectral features consist of a significant amount of parent not-relativistic triplet states which ranges between ~40-60%. Analysis of the individual contributions presented in Tables S7-S10 reveals that the low-lying

excitation problem in both **1** and **2** diastereomers involves 6-states which at the non-relativistic limit consists of the ground the excited states singlets S_0, S_1 and S_2 as well as the respective excited state Triplets T_1, T_2 and T_3. Interestingly while in both **1** and **2** diastereomers states S_1-S_2 and T_2-T_3 are all MLCT/XLCT with contributions from LLCT in the case of **1** or ILCT in the case of **2** the character of the T_1 state differs significantly. It is again an MLCT/XLCT character in the case of **1** diastereomers but it is a pure ILCT in the case of **2** diastereomers. In a similar fashion at the relativistic limit the SOC states $|\Psi_{0-9}\rangle$ consist of magnetic sublevels $M_S = 0, \pm 1$ with contributions from the various non-relativistic states Tables S7-S10.

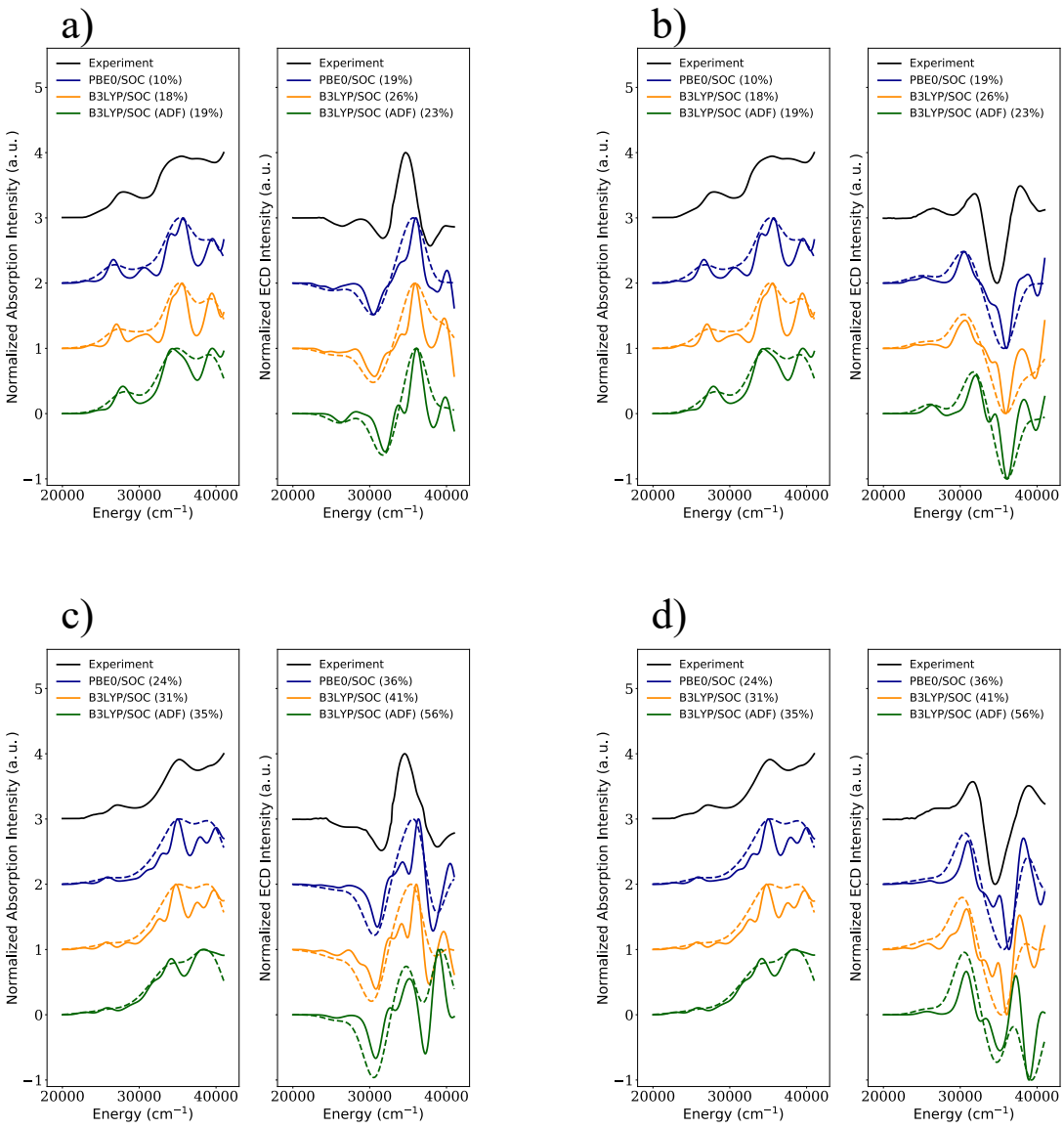

Figure S 8

Experimental (black) versus calculated relativistically corrected Absorption and ECD spectra PBE0/TD-DFT (blue), B3LYP/TD-DFT (orange) B3LYP/TD-DFT (green) of non-helicene Complex **1** a) A-Cl b) C-Cl c) A-I and d) C-I. %MAE errors in comparison to experiment are provided in parenthesis. Solid lines indicate constant Gaussian broadening of 1500 cm^{-1} while dotted lines indicate constant Gaussian broadening of 3000 cm^{-1}.

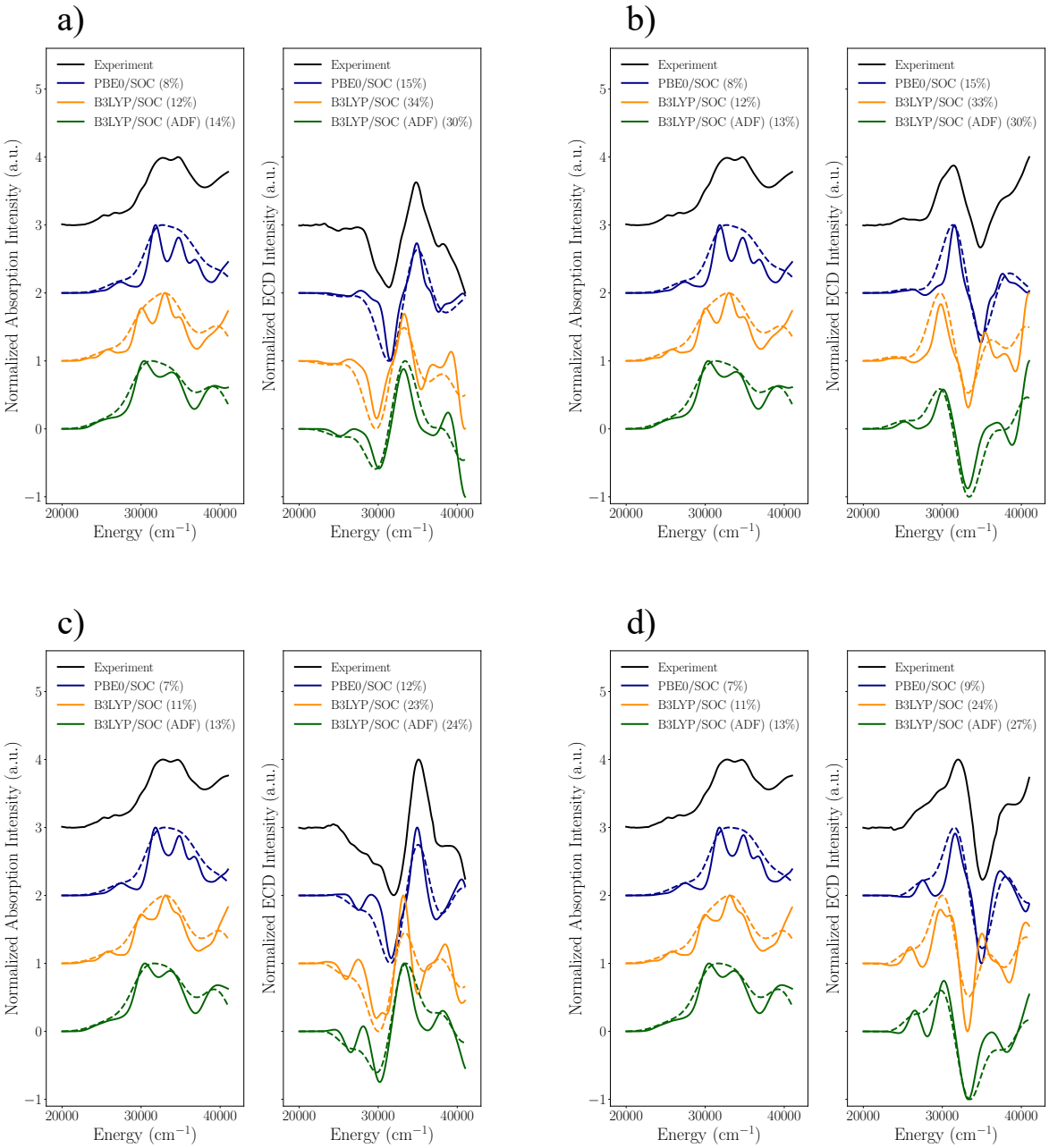

Figure S 9

Experimental (black) versus calculated relativistically corrected Absorption and ECD spectra PBE0/TD-DFT (blue), B3LYP/TD-DFT (orange) B3LYP/TD-DFT (green) of helicene Complex **2** a) M,A-Cl b) P,C-Cl c) M,C-Cl d) P,A-Cl. %MAE errors in comparison to experiment are provided in parenthesis. Solid lines indicate constant Gaussian broadening of 1500 cm^{-1} while dotted lines indicate constant Gaussian broadening of 3000 cm^{-1}.

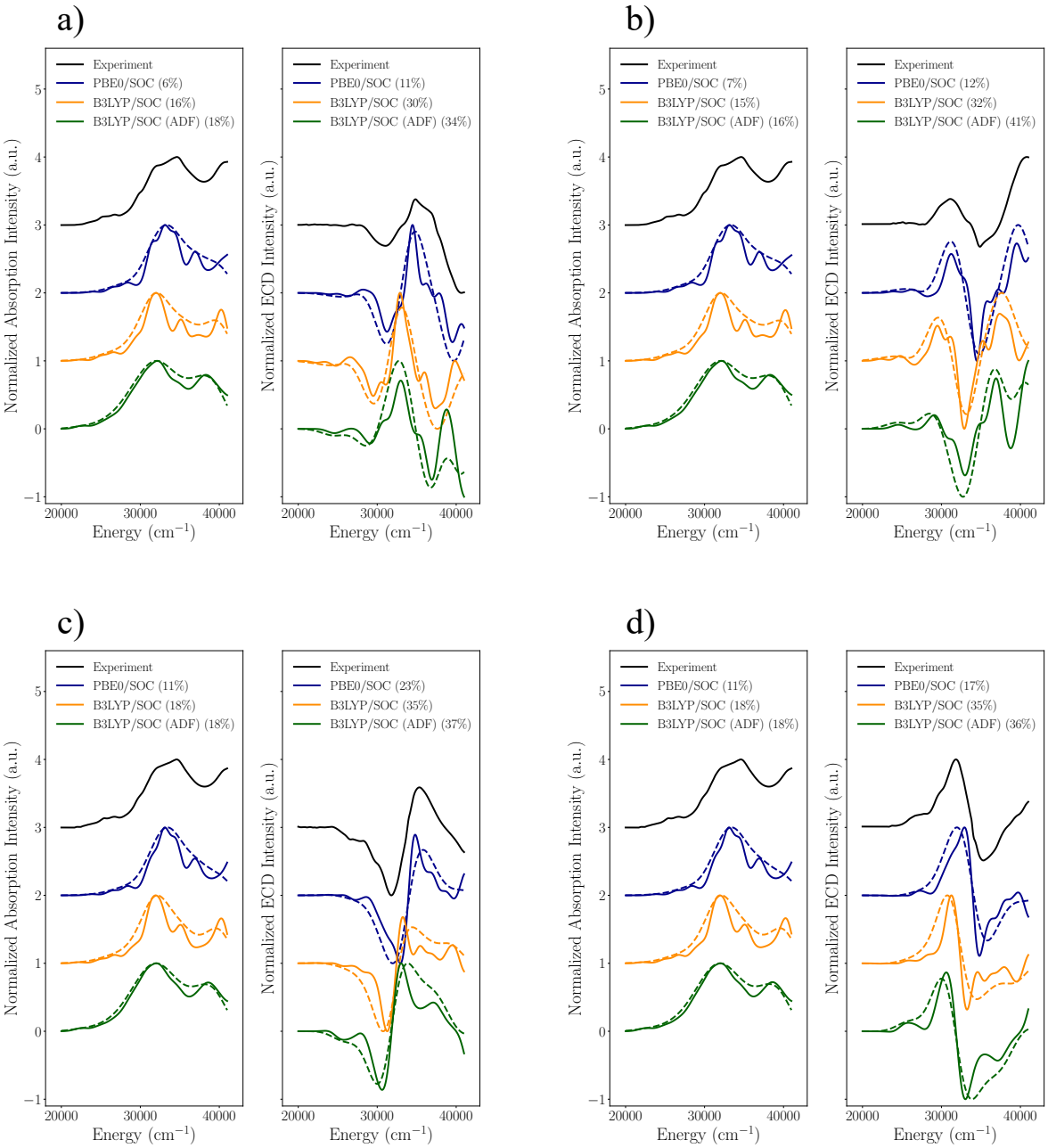

Figure S 10

Experimental (black) versus calculated relativistically corrected Absorption and ECD spectra PBE0/TD-DFT (blue), B3LYP/TD-DFT (orange) B3LYP/TD-DFT (green) of helicene Complex **2** a) M,A-I b) P,C-I c) M,C-I d) P,A-I. %MAE errors in comparison to experiment are provided in parenthesis. Solid lines indicate constant Gaussian broadening of 1500 cm^{-1} while dotted lines indicate constant Gaussian broadening of 3000 cm^{-1}.

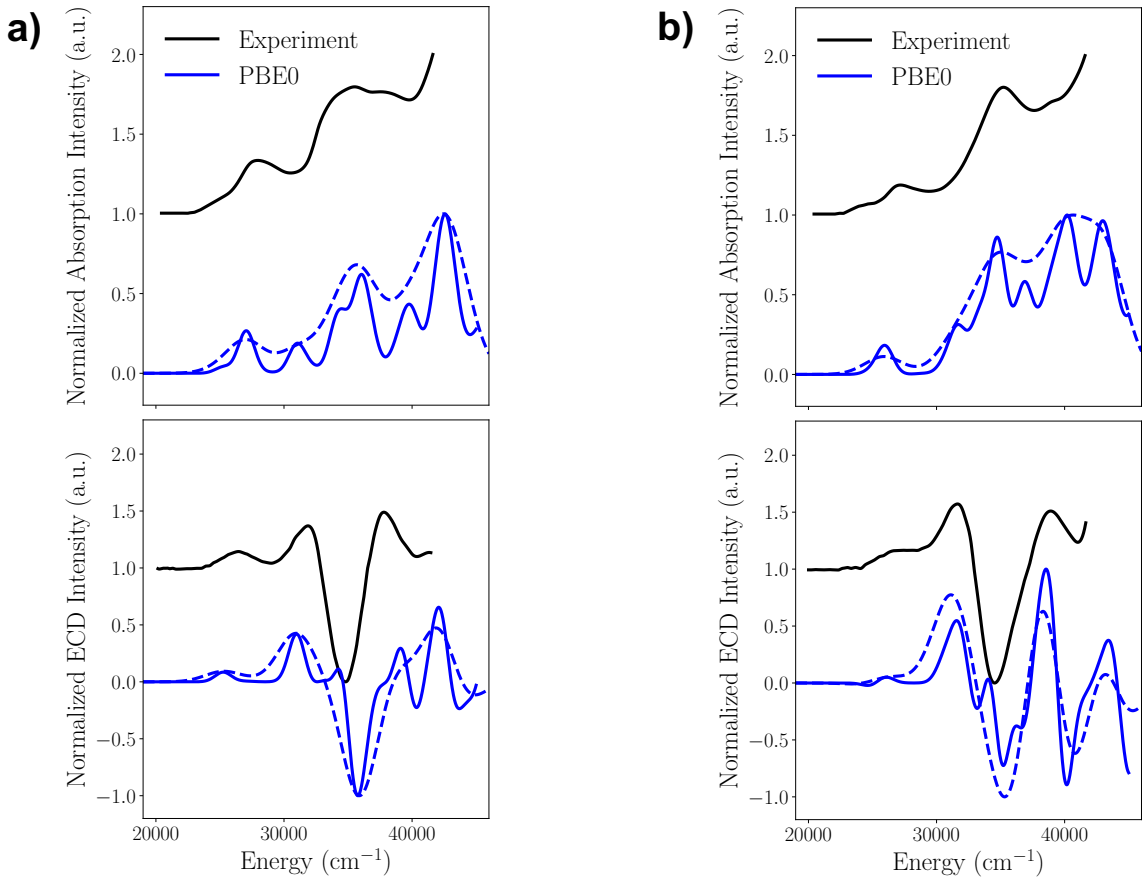

Figure S 11

Experimental (black) PBE0/TD-DFT (blue) of Absorption and ECD spectra of non-helicene enantiomer a) **1** C-Cl and b) **1** C-I. Solid lines indicate constant Gaussian broadening of 1500 cm^{-1} while dotted lines indicate constant Gaussian broadening of 3000 cm^{-1}.

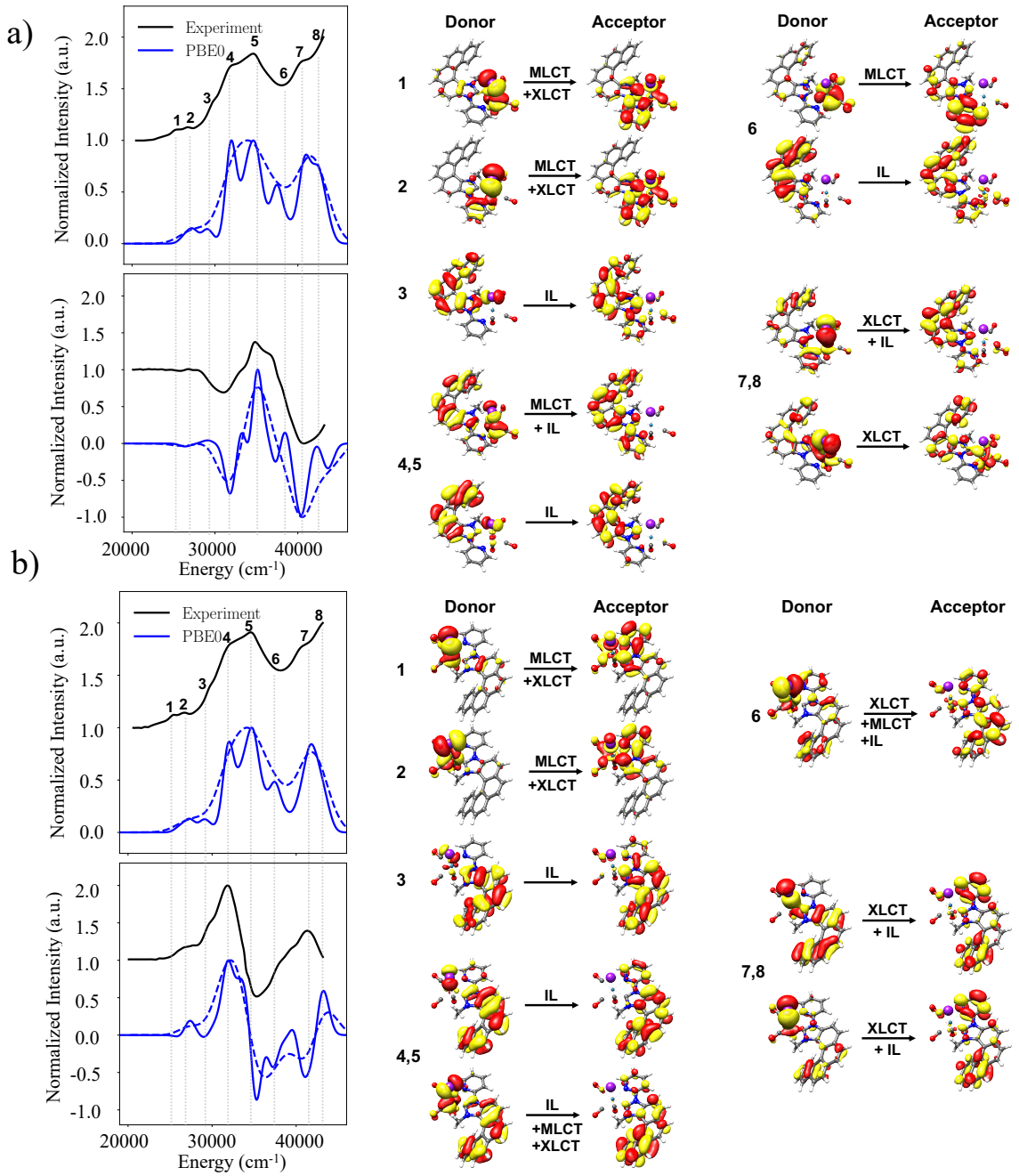

Figure S 12

Experimental (black) PBE0/TD-DFT (blue) of Absorption and ECD spectra of helicene enantiomer a) **2** M,A-I and b) **2** P,A-I. The nature of the most important bands 1-8 is discussed in the framework of NTO analysis. Solid lines indicate constant Gaussian broadening of 1500 cm^{-1} while dotted lines indicate constant Gaussian broadening of 3000 cm^{-1}.

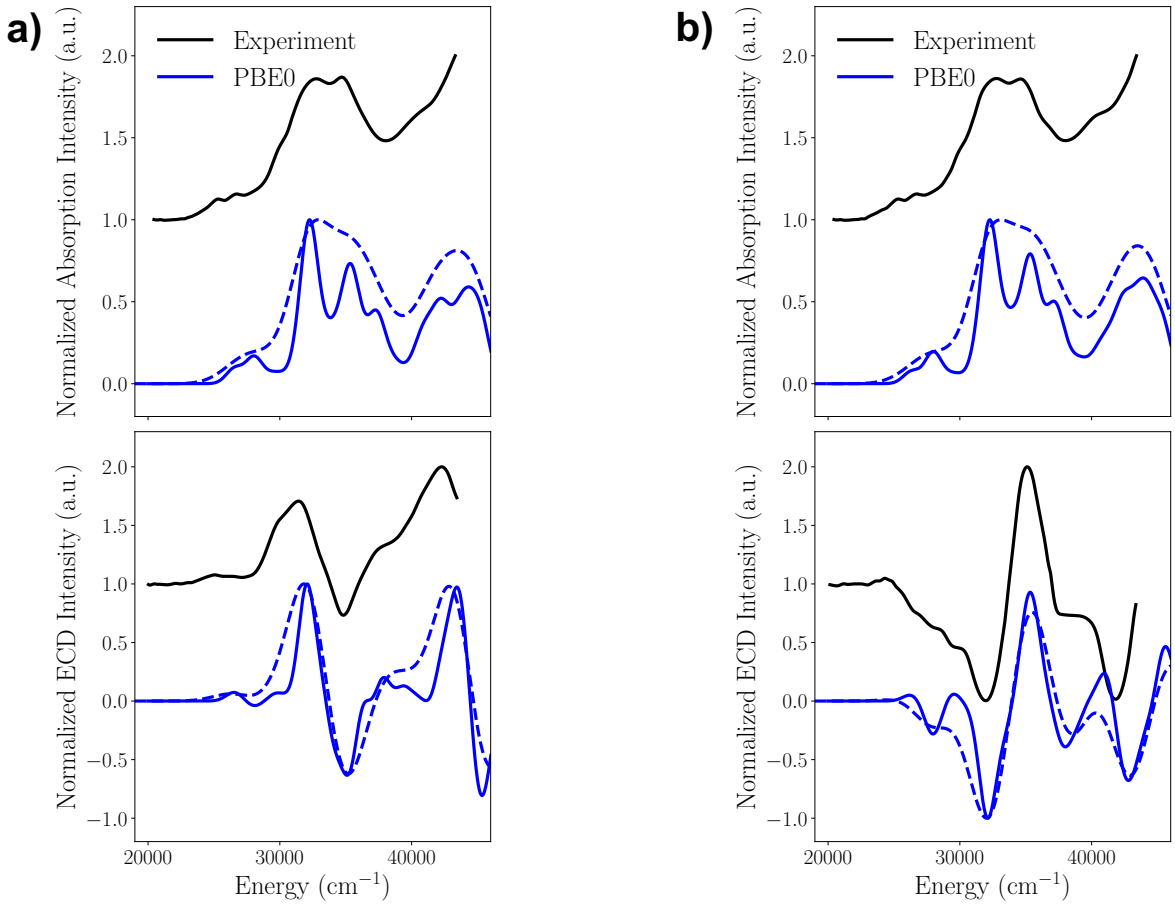

Figure S 13

Experimental (black) PBE0/TD-DFT (blue) of Absorption and ECD spectra of helicene enantiomer a) **2** P,C-Cl and b) **2** M,C-Cl. Solid lines indicate constant Gaussian broadening of 1500 cm^{-1} while dotted lines indicate constant Gaussian broadening of 3000 cm^{-1}.

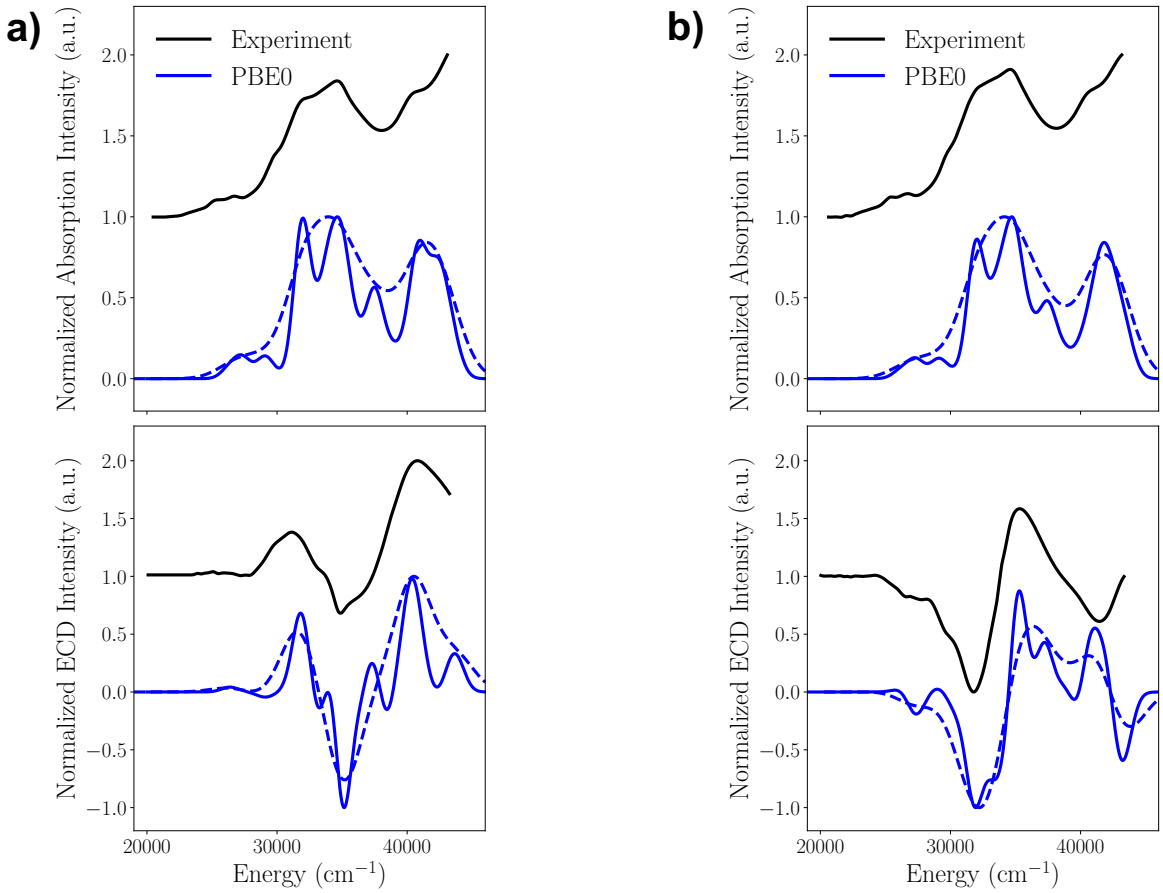

Figure S 14

Experimental (black) PBE0/TD-DFT (blue) of Absorption and ECD spectra of non-helicene enantiomer a) a) **2** P,C-I and b) **2** M,C-I. Solid lines indicate constant Gaussian broadening of 1500 cm^{-1} while dotted lines indicate constant Gaussian broadening of 3000 cm^{-1}.

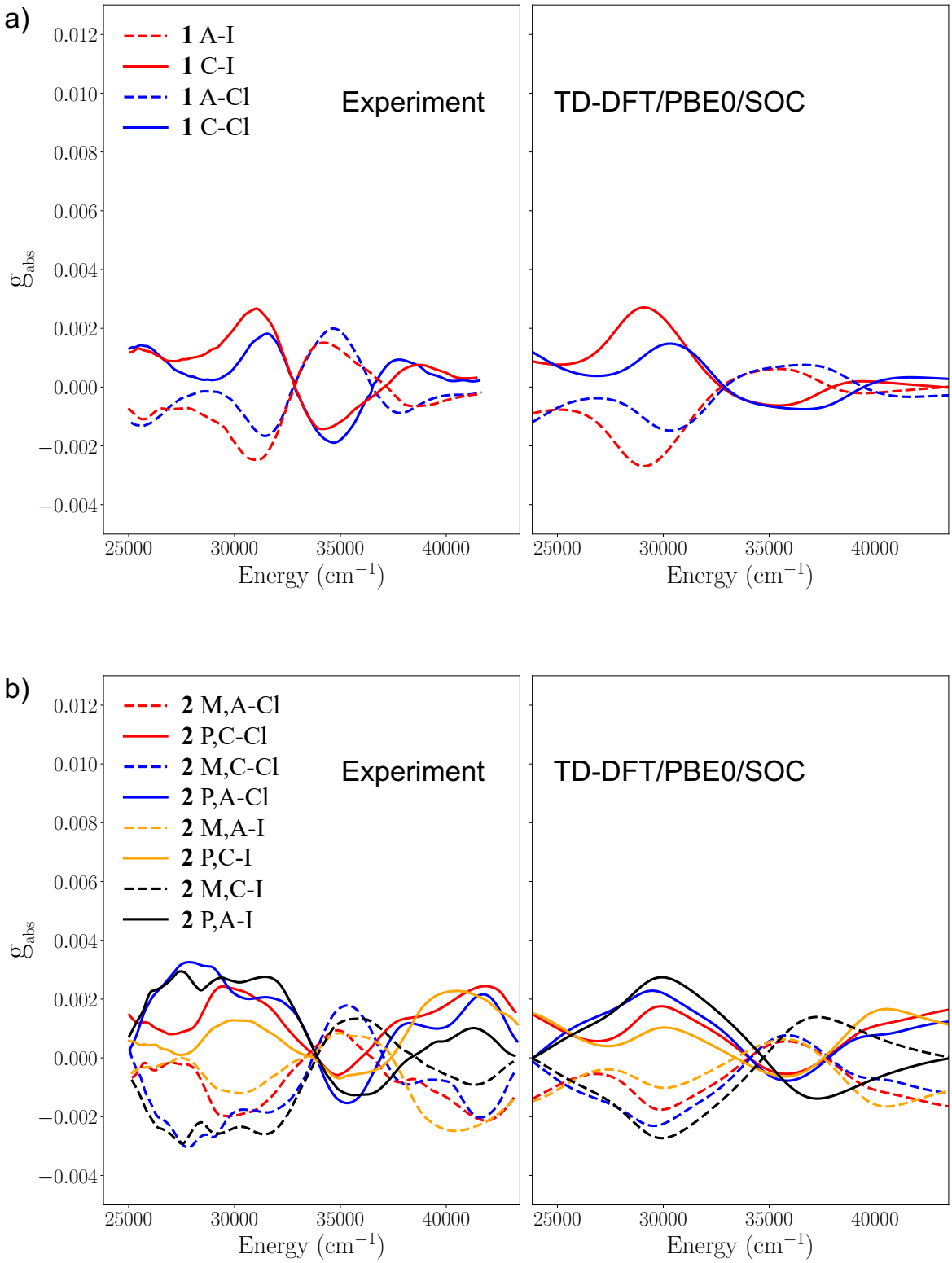

Figure S 15

Experimental (left) versus calculated PBE0/TD-DFT g_{abs} of a) non-helicene diastereomeric structures **1** and b) Helicene diastereomeric structures **2**.

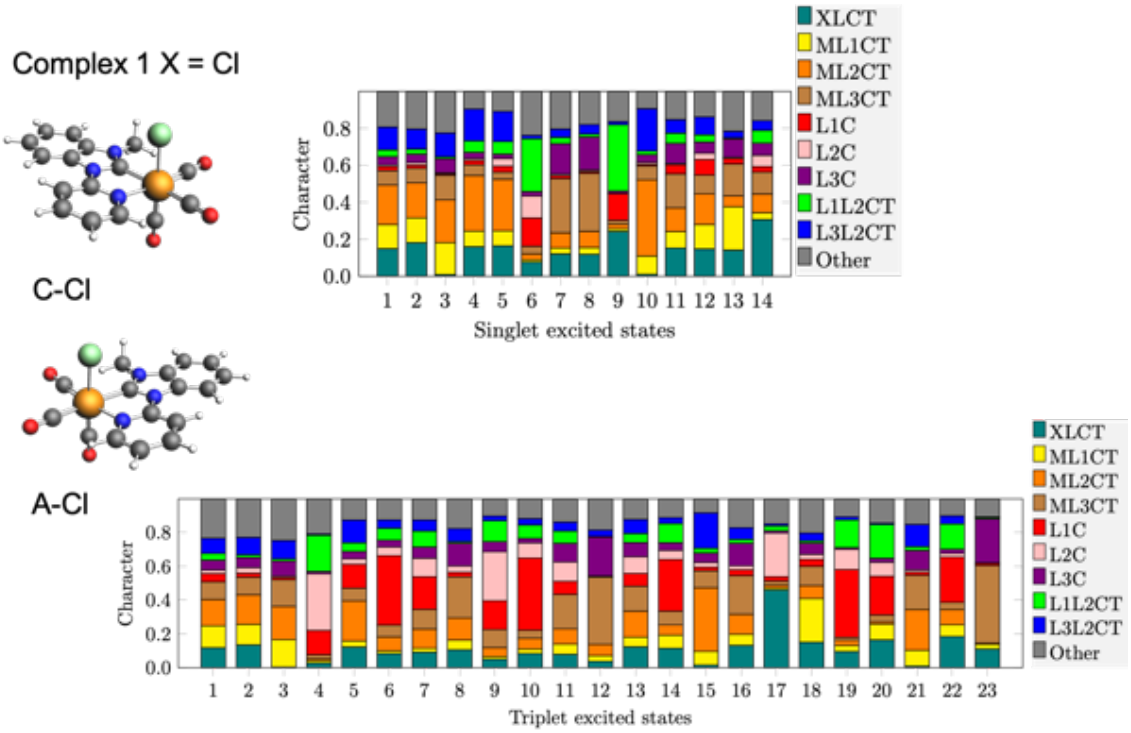

Figure S 16

TheoDore analysis of the low-lying excited states of Complex **1** A-Cl.

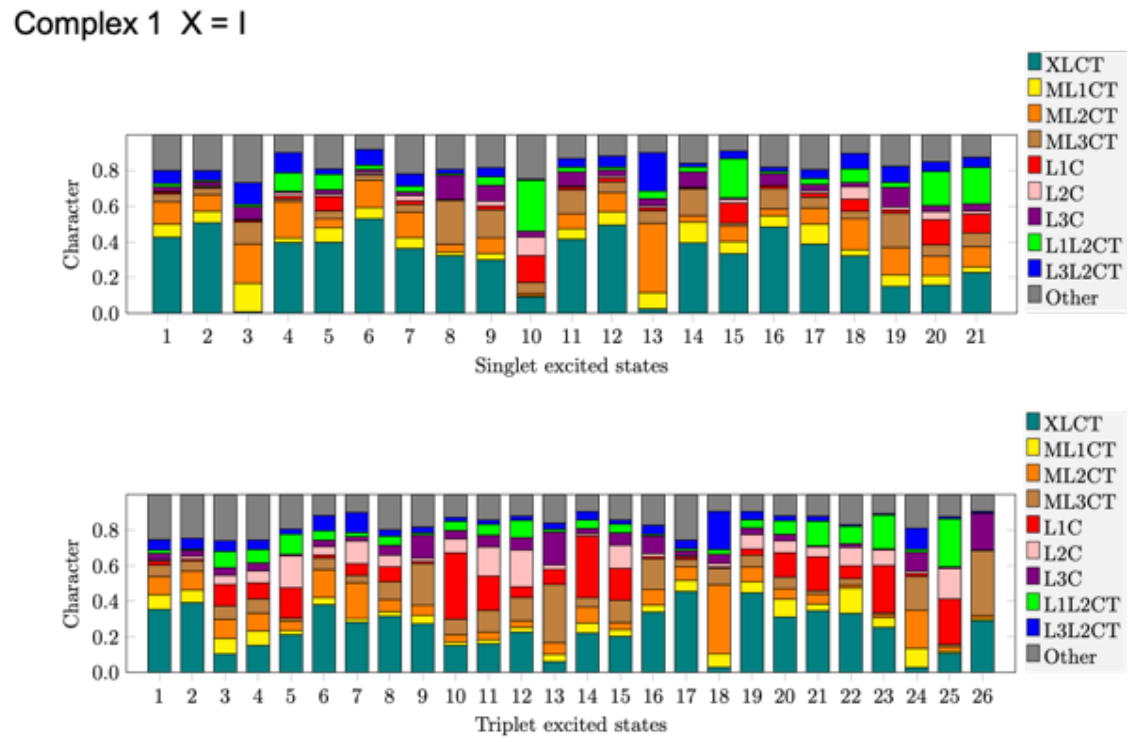

Figure S 17

TheoDore analysis of the low-lying excited states of Complex **1** A-I.

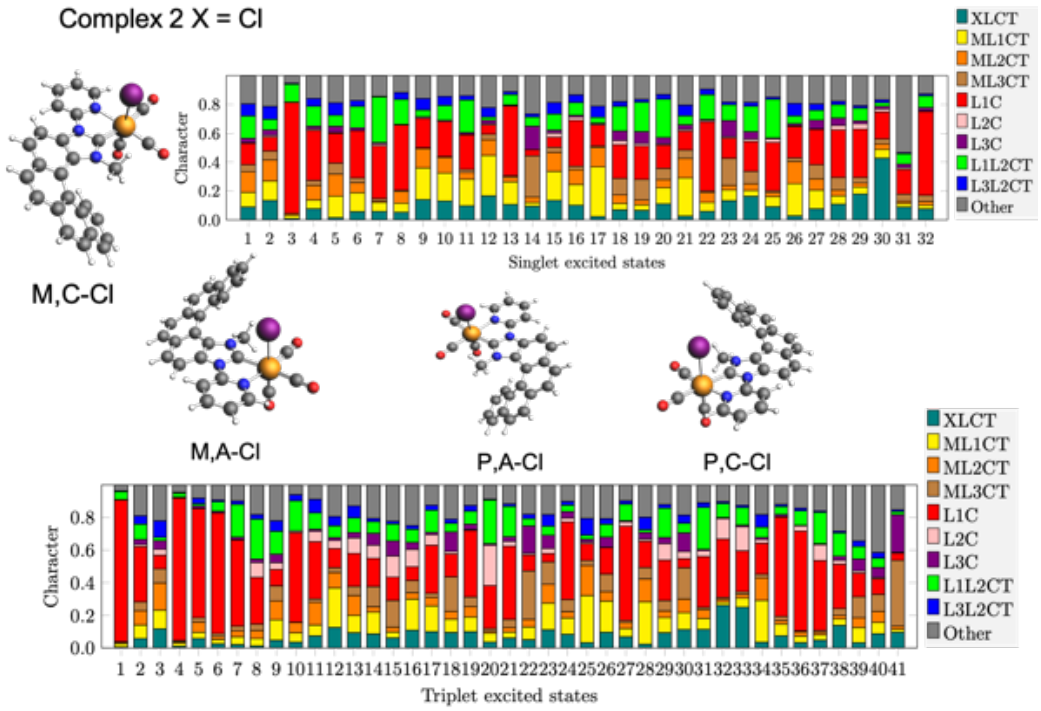

Figure S 18

TheoDore analysis of the low-lying excited states of Complex **2** M,C-Cl.

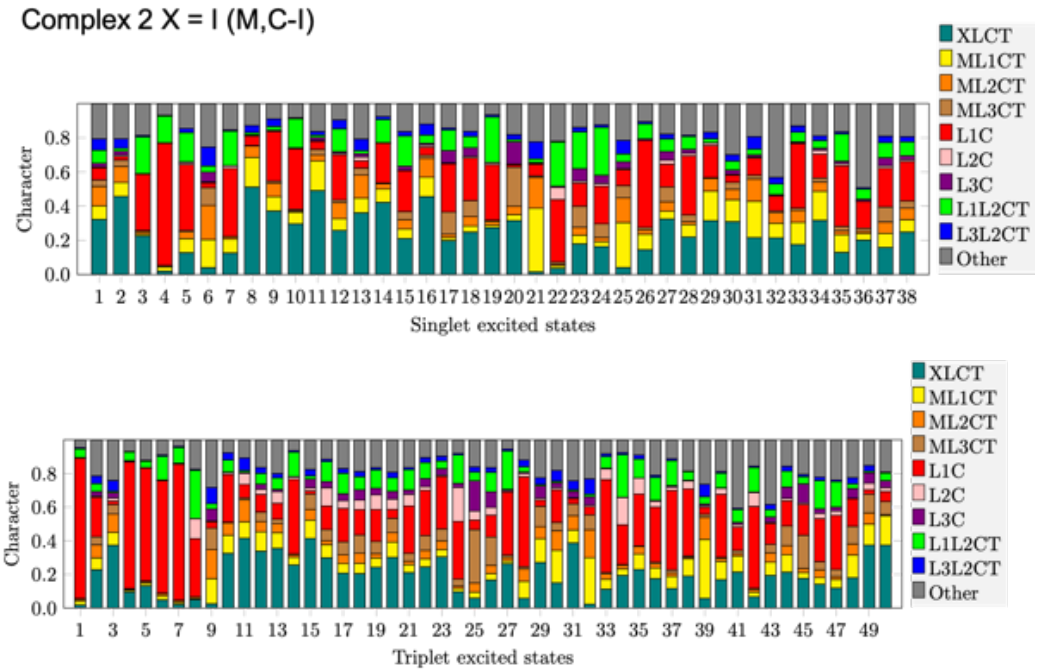

Figure S 19

TheoDore analysis of the low-lying excited states of Complex **2** M,C-I.

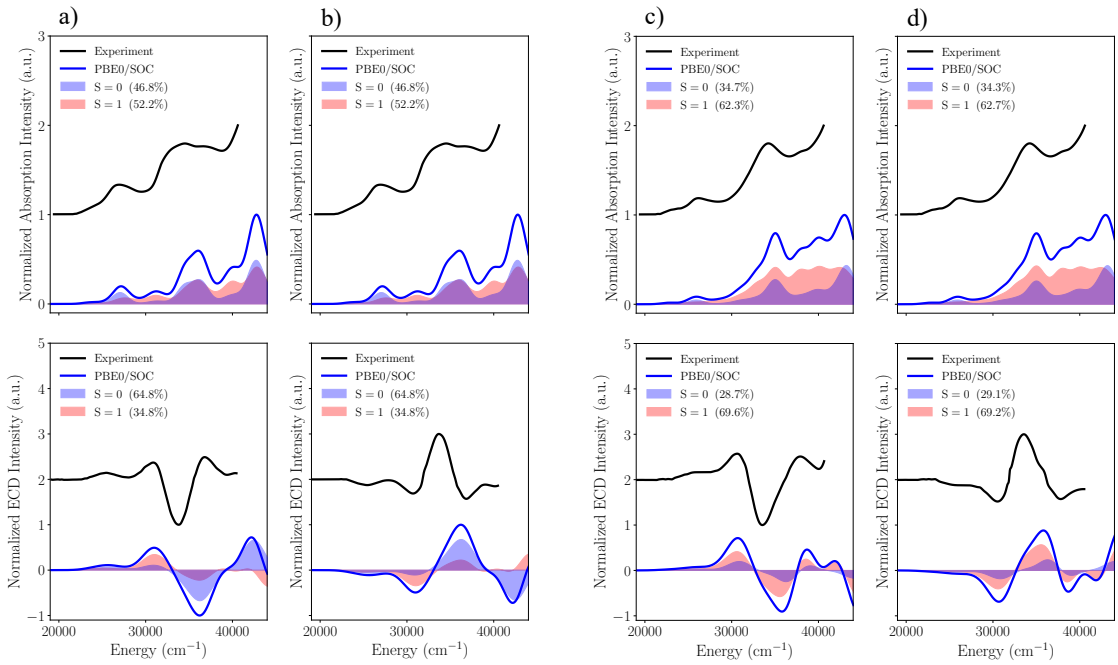

Figure S 20

Experimental and Calculated relativistic absorption and CD spectra [PBE0/TD-DFT/SOC in blue] with singlet and triplet contributions in blue and red fill, respectively of non-helicene complex **1** as a) C-Cl b) A-Cl c) C-I d) A-I.

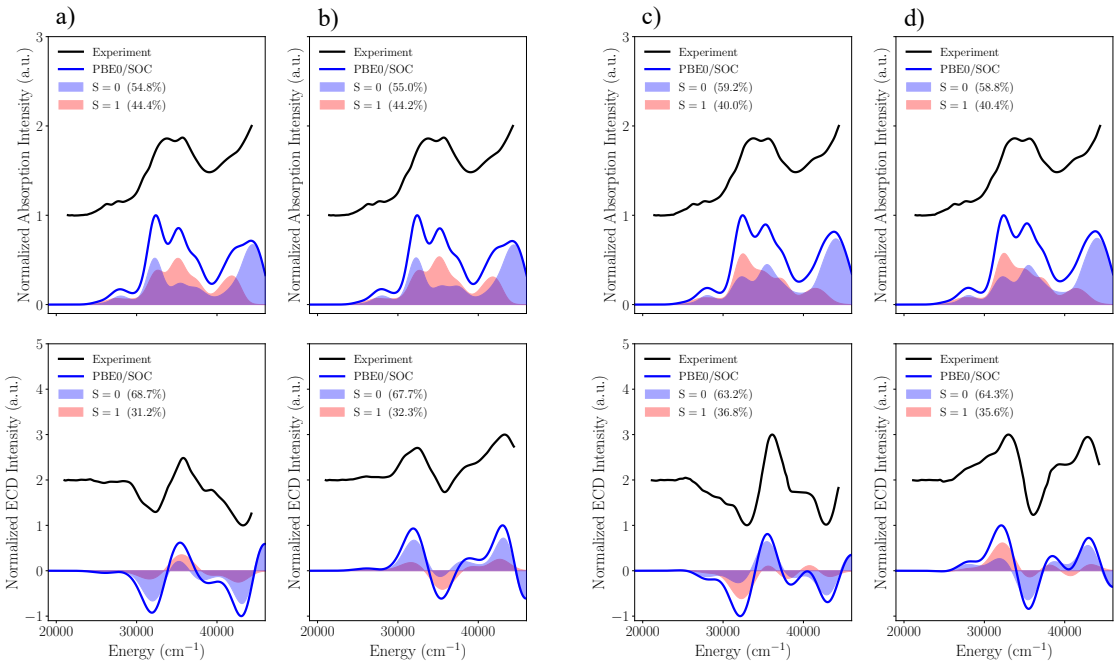

Figure S 21

Experimental and Calculated relativistic absorption and CD spectra [PBE0/TD-DFT/SOC in blue] with singlet and triplet contributions in blue and red fill, respectively of Cl-substituted helicene complex **2** as a) M,A-Cl b) P,C-Cl c) M,C-I d) P,A-Cl.

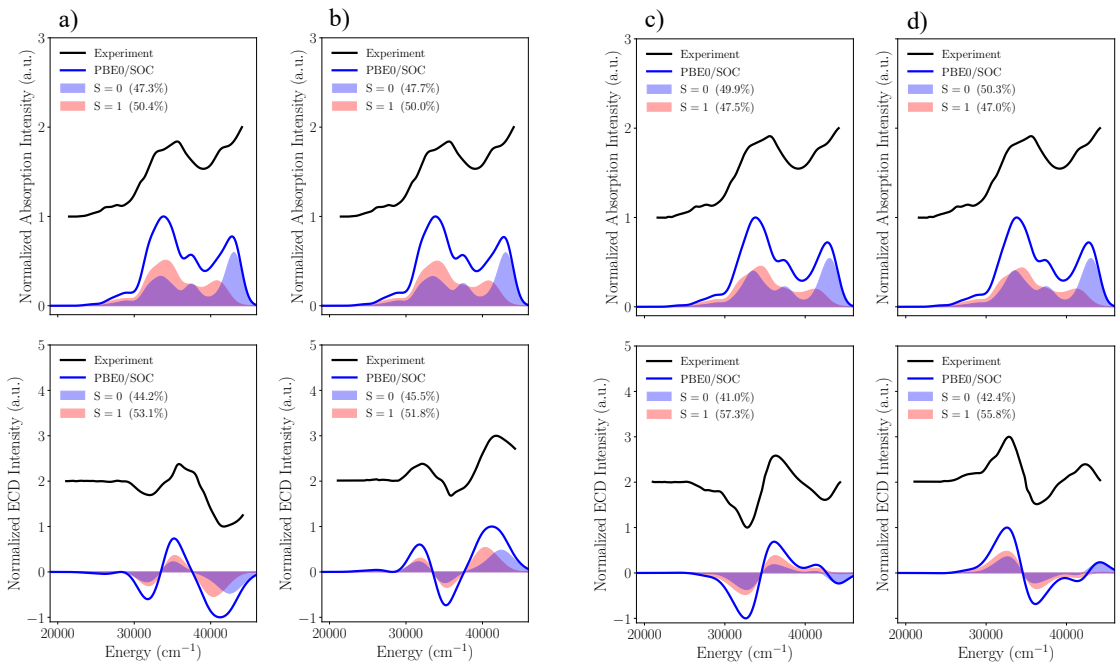

Figure S 22

Experimental and Calculated relativistic absorption and CD spectra [PBE0/TD-DFT/SOC in blue] with singlet and triplet contributions in blue and red fill, respectively of Cl-substituted helicene complex **2** as a) M,A-Cl b) P,C-Cl c) M,C-I d) P,A-Cl.

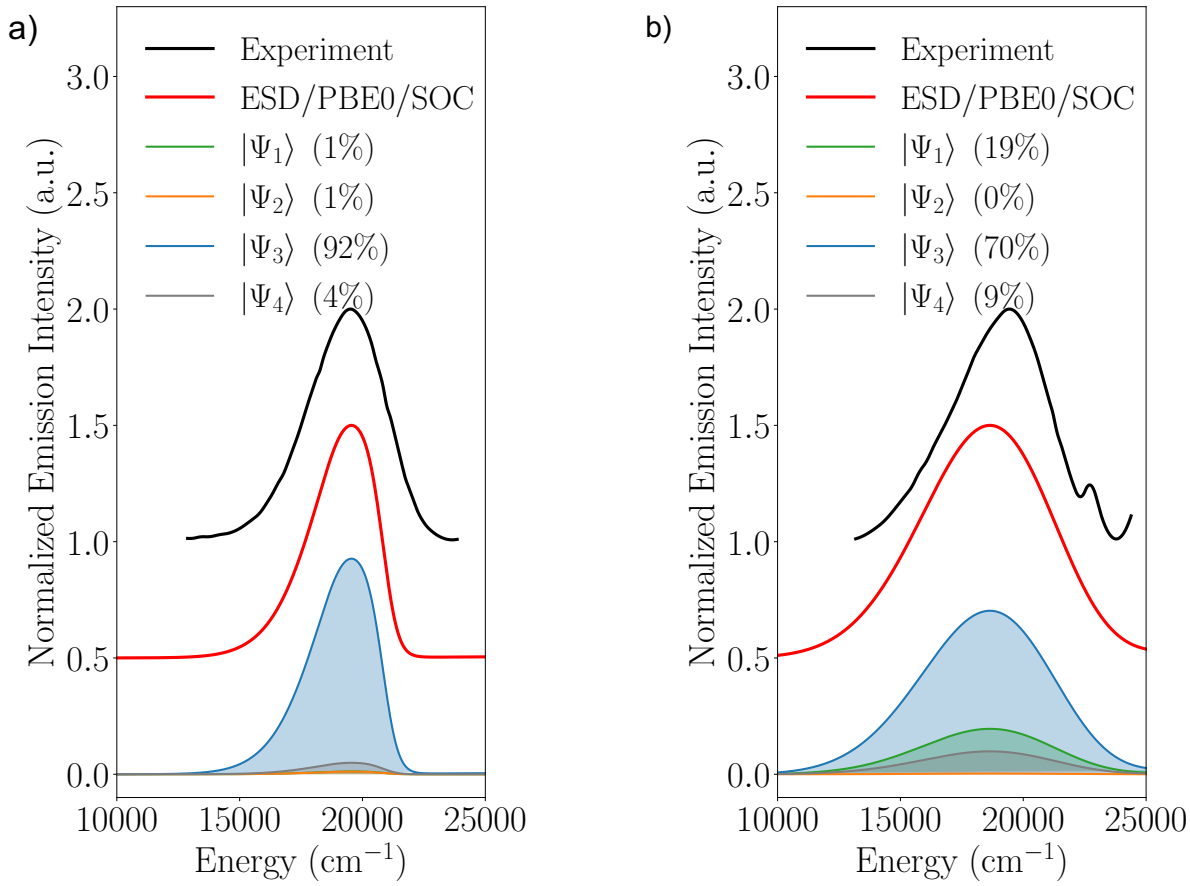

Figure S 23

Experimental and calculated emission spectra (ESD/PBE0/TD-DFT/SOC) of non-helicene complex **1** a) C-Cl b) C-Cl.

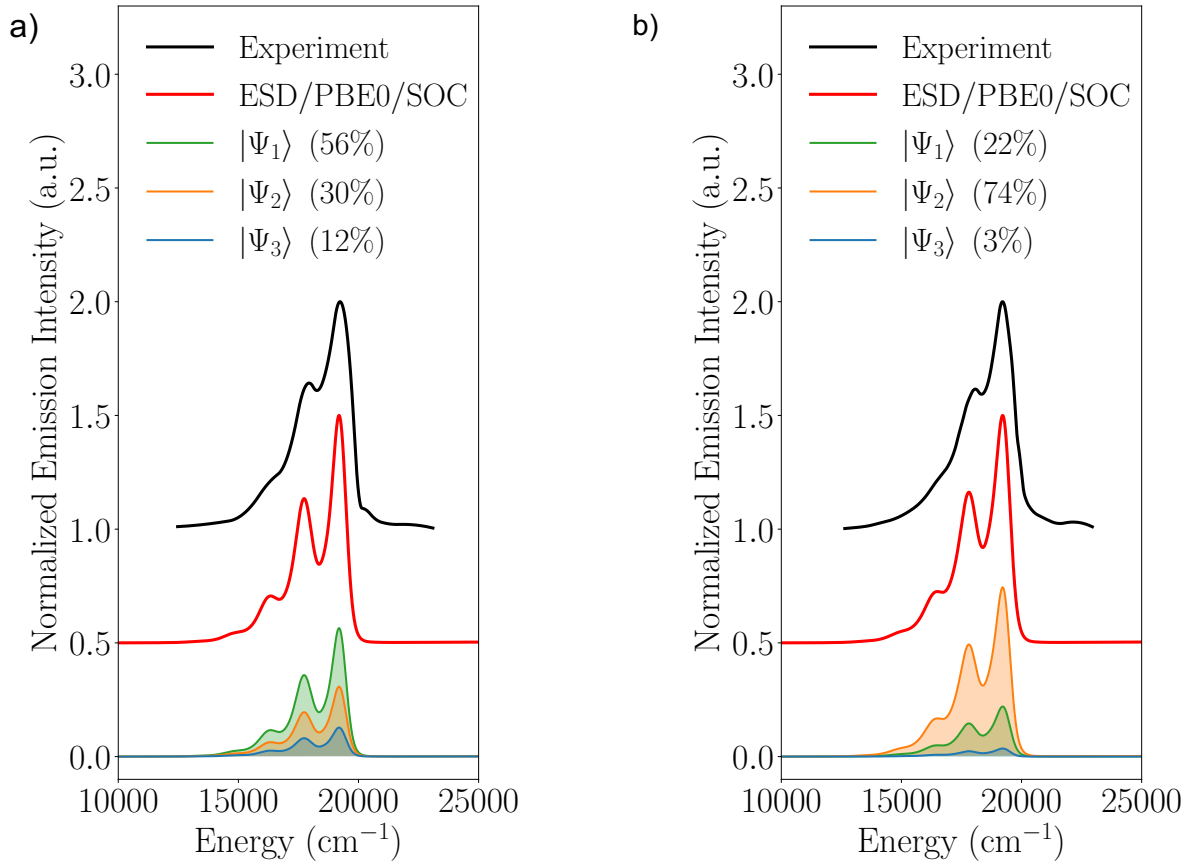

Figure S 24

Experimental and calculated emission spectra (ESD/PBE0/TD-DFT/SOC) of helicene I-substituted complex **2** a) M,A-I b) P,A-I.

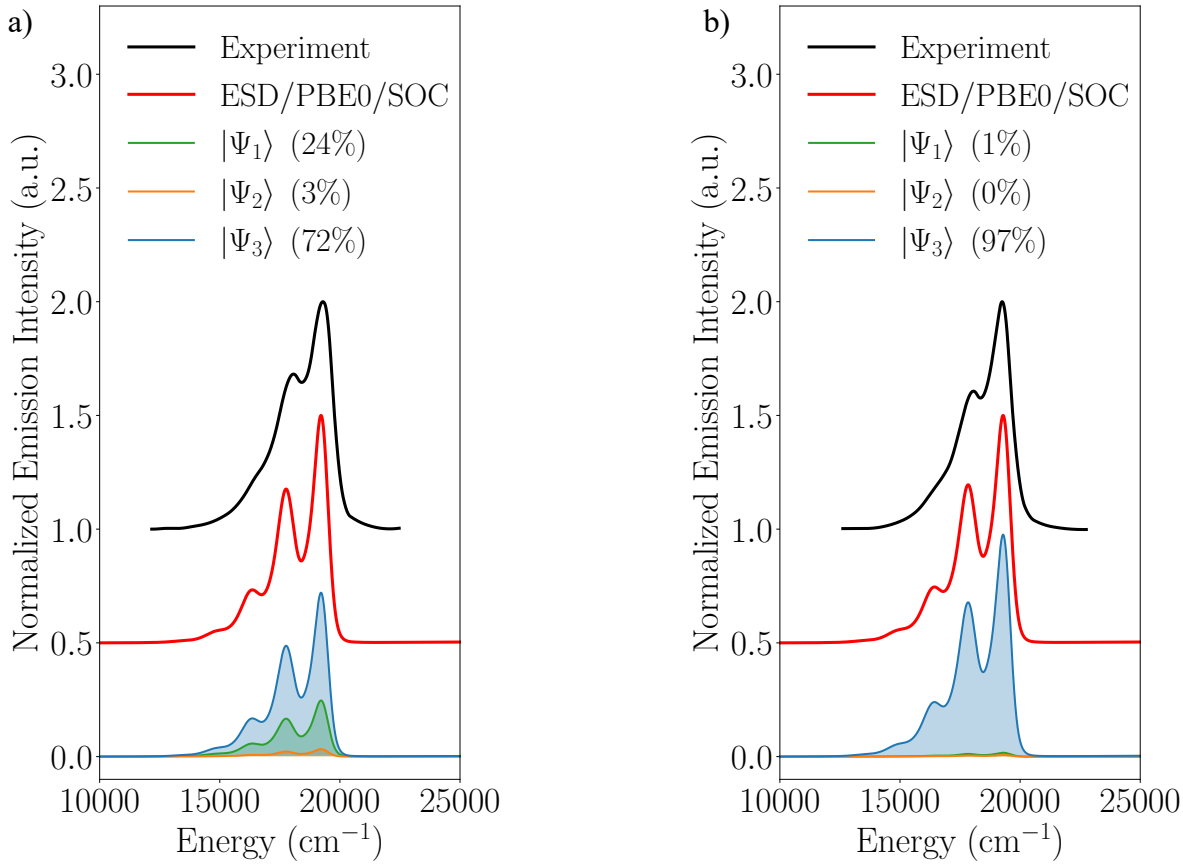

Figure S 25

Experimental and calculated emission spectra (ESD/PBE0/TD-DFT/SOC) of helicene I-substituted complex **2** a) P,C-Cl b) M,C-Cl.

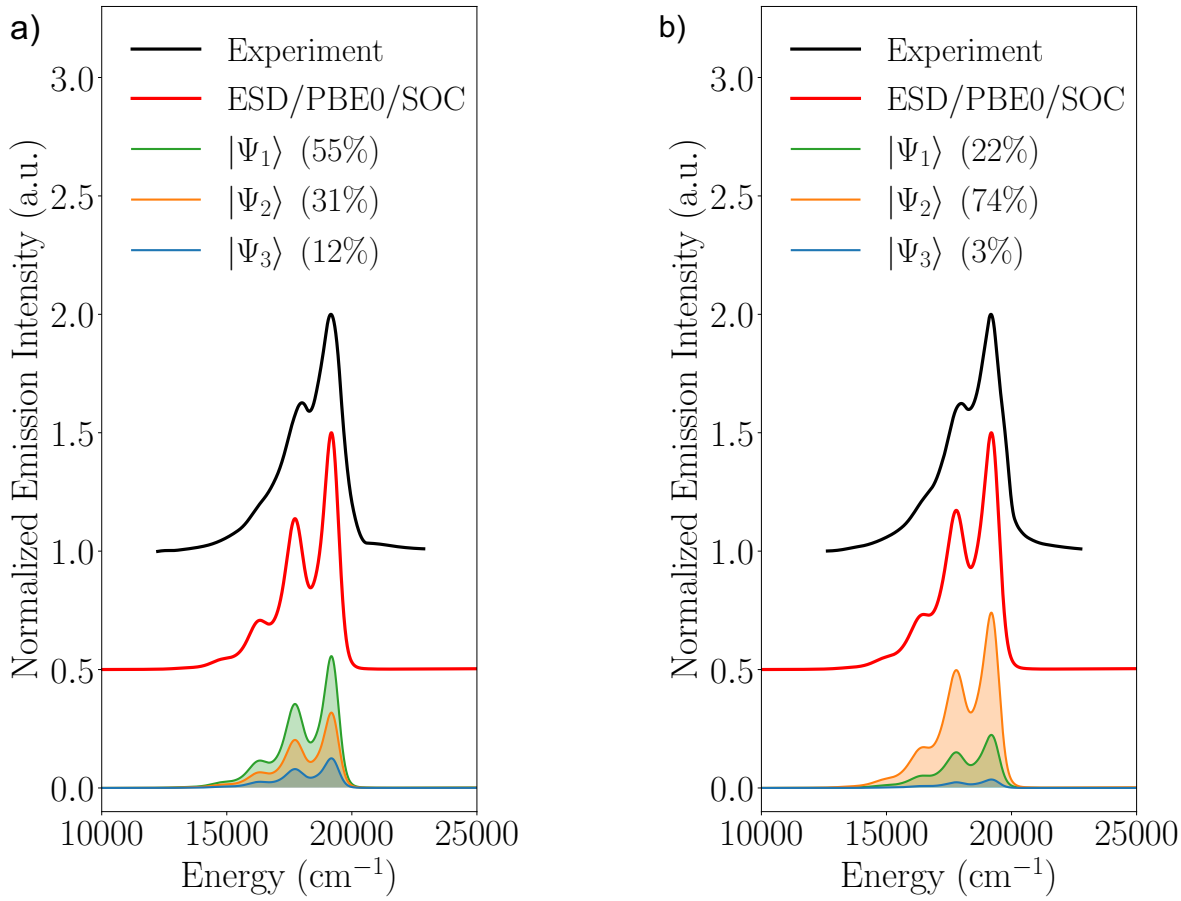

Figure S 26

Experimental and calculated emission spectra (ESD/PBE0/TD-DFT/SOC) of helicene I-substituted complex **2** a) P,C-I b) M,C-I.

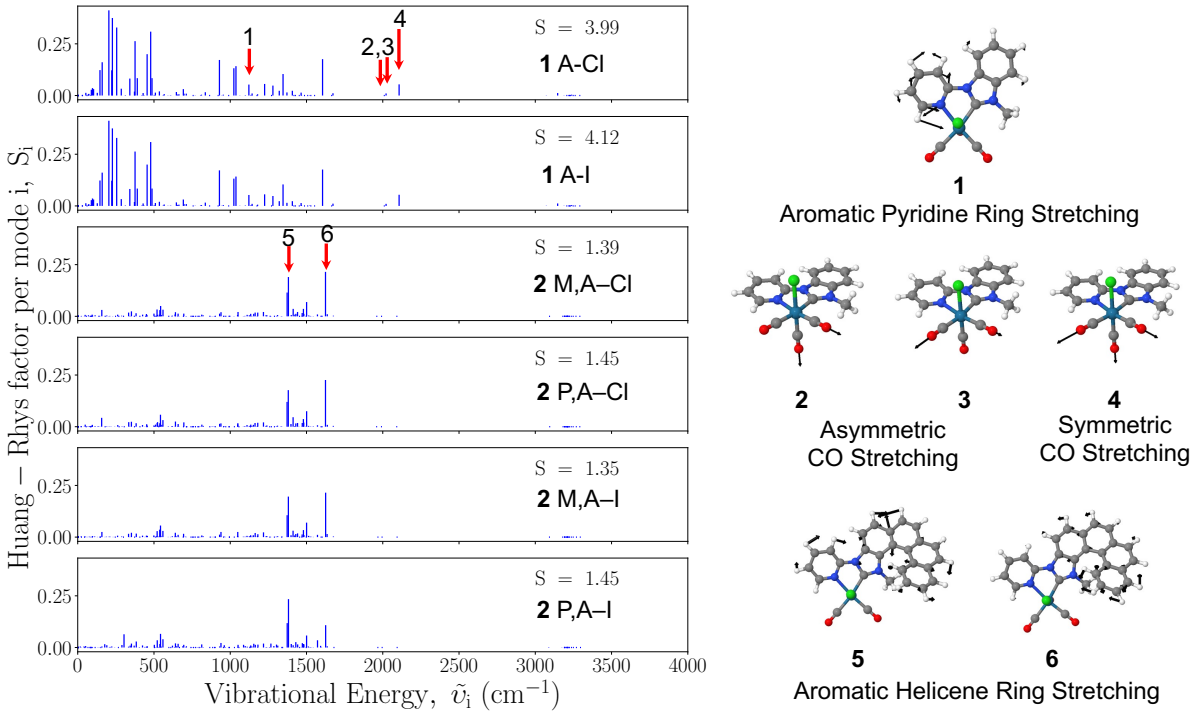

Figure S 27

PBE0/TD-DFT computed Huang-Rhys factor (S_i) distribution over the entire set of the vibrational normal modes with energies ($\tilde{\upsilon}_i$ in wavenumbers, cm^{-1}) for a selected set of diastereomers **1** and **2**. The Huang-Rhys factor (S) of the phosphoresce relaxation transition (defined as $S = \sum_i S_i$) is shown in top right of each case. Red arrows indicate the selected vibrations modes (1-6) for the SA-CASSCF, SA-CASSCF/NEVPT2 and SA-CASSCF/QD-NEVPT2 PES scans. Modes 1-6 are visualized on the right.

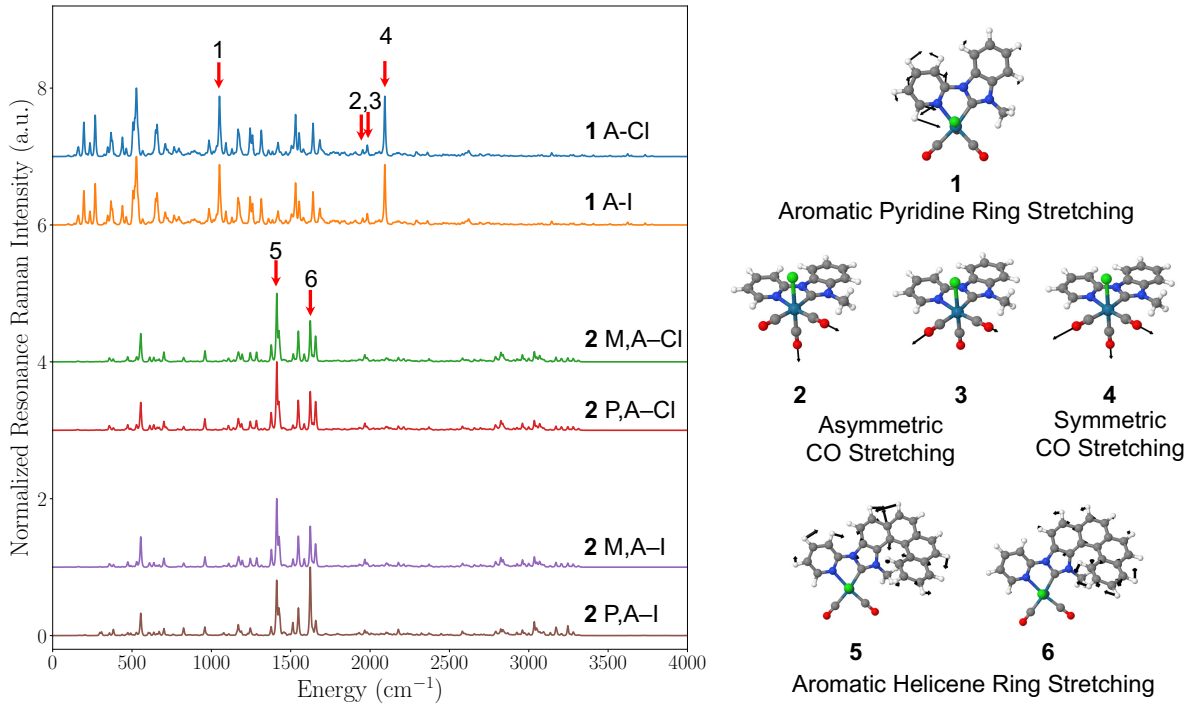

Figure S 28

PBE0/TD-DFT computed resonance Raman (rR) spectra for a selected set of diastereomers **1** and **2**. The laser energy was set to the phosphoresce relaxation transition energies (2.30 eV and 2.65 eV) of diastereomers **1** and **2**, respectively. Red arrows indicate the selected vibrations modes (1-6) for the SA-CASSCF, SA-CASSCF/NEVPT2 and SA-CASSCF/QD-NEVPT2 PES scans. Modes 1-6 are visualized on the right.

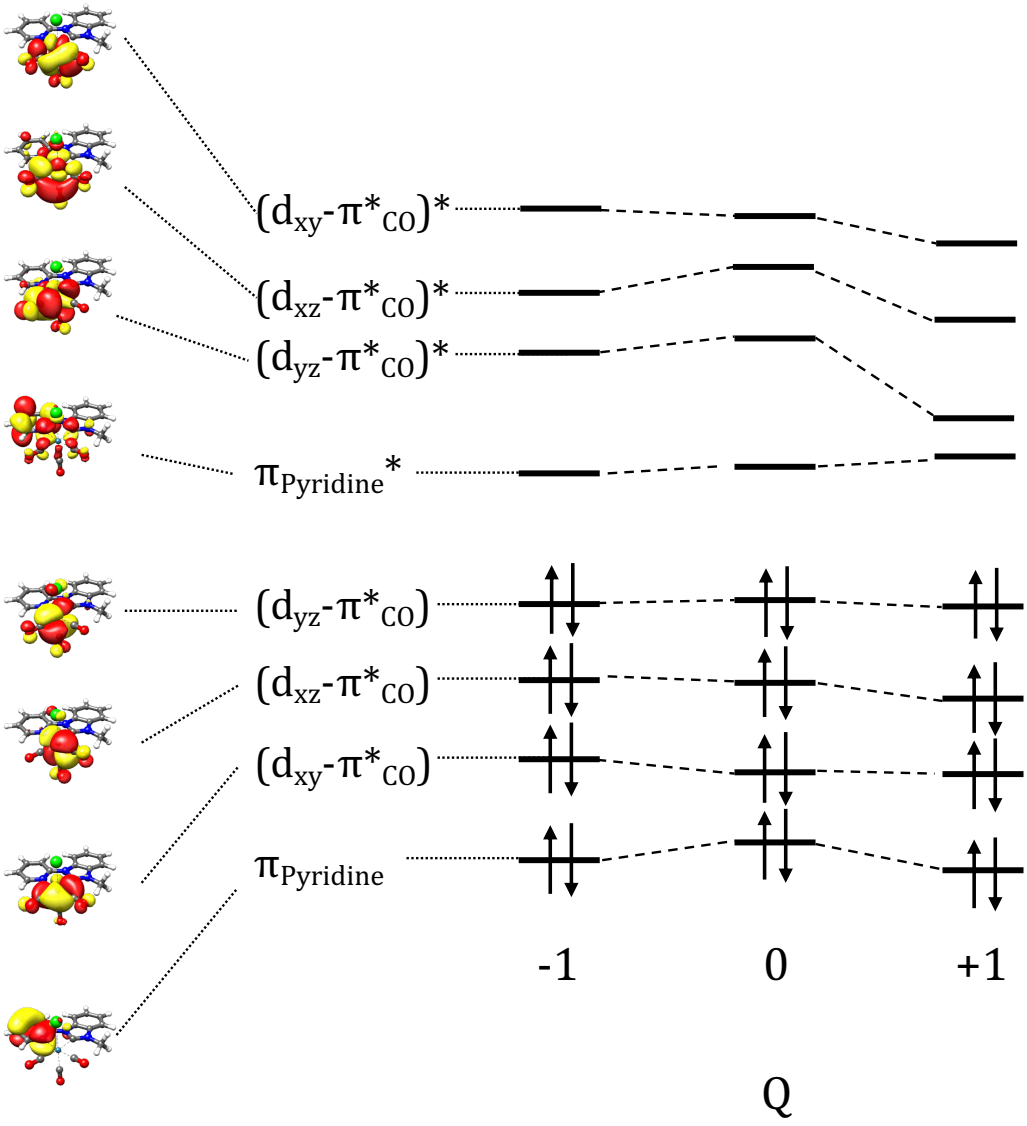

Figure S 29

Molecular orbital diagram of CASSCF(8,8) orbitals along the asymmetric CO stretching mode's normal coordinate at Q=-1, 0, 1 (pointing to a step-before , at, and step-after the equilibrium geometry, respectively) for complex **1** A-Cl of the geometries.

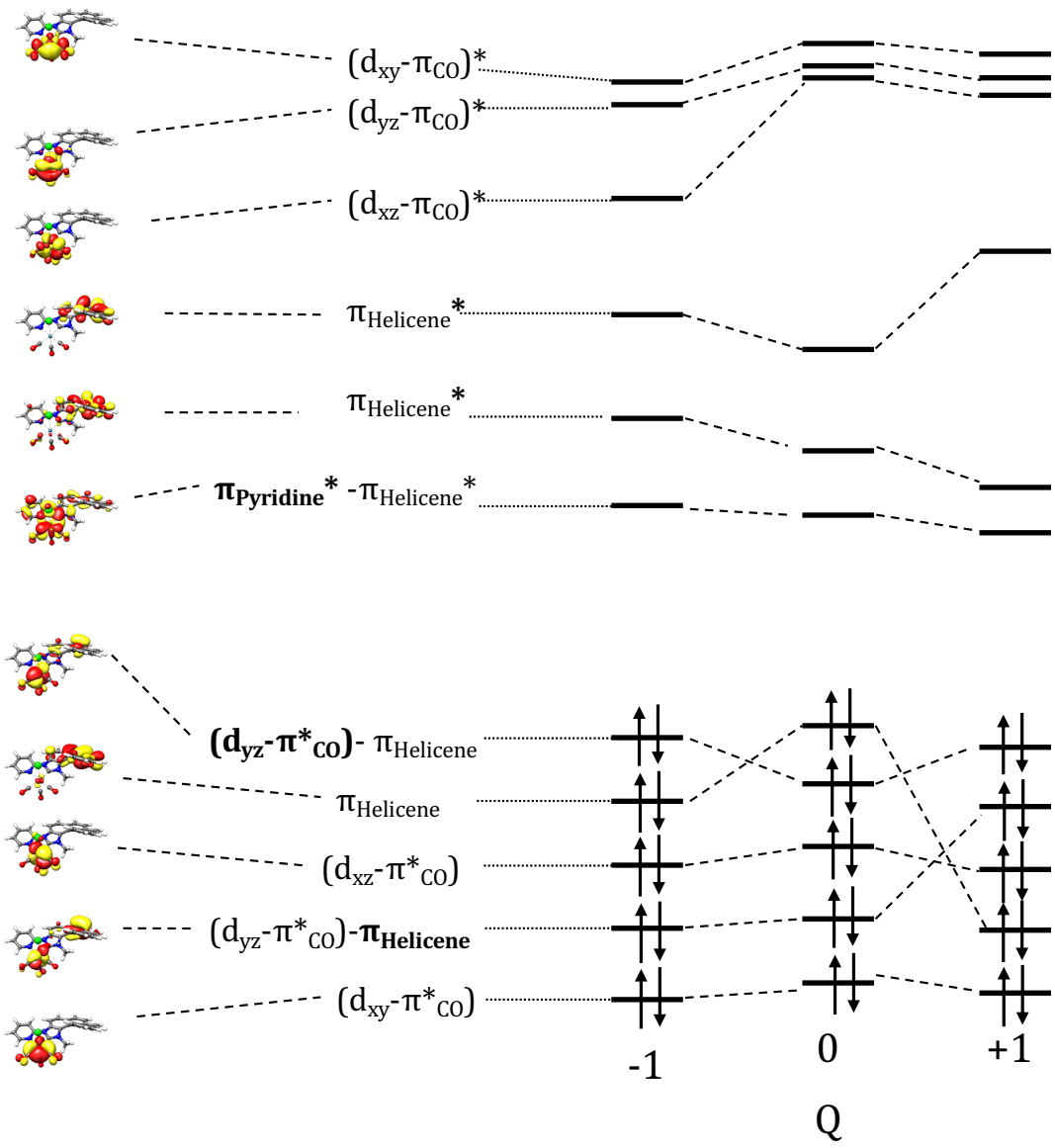

Figure S 30

Molecular orbital diagram of CASSCF(10,11) orbitals along the asymmetric C=C ring stretching mode's normal coordinate at Q=-1, 0, 1 (pointing to a step-before , at, and step-after the equilibrium geometry, respectively) for complex **2** M,A-Cl of the geometries.

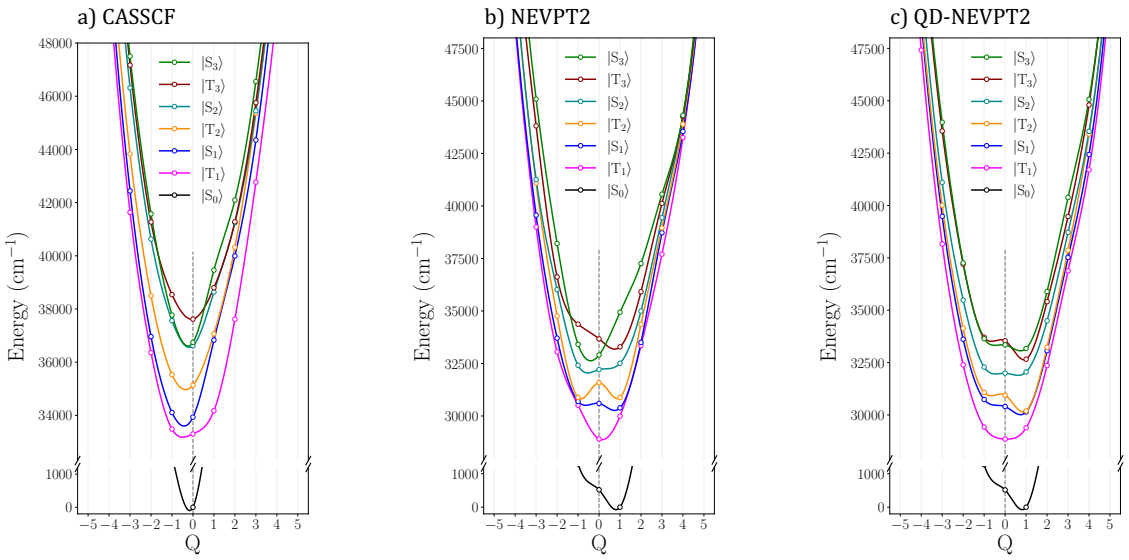

Figure S 31

Computed *non-relativistic* PES complex **1** A-Cl along the asymmetric CO stretching mode's normal coordinate (Q) at different level of theory a) CASSCF(8,8) b) CASSCF/NEVPT2 c) CASSCF/QD-NEVPT2.

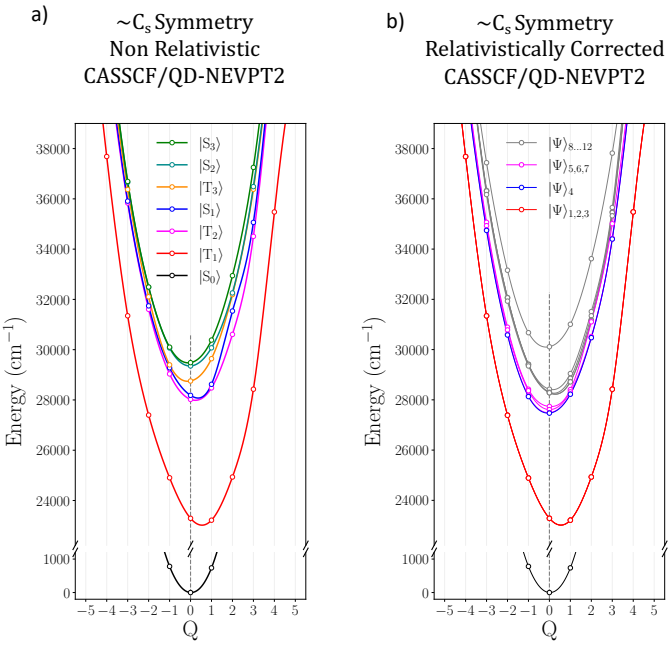

Figure S 32

SA-CASSCF(10,11)/QD-NEVPT2 PES scan along a chosen modes representing antisymmetric stretching helicene vibrations for **2** M,A-I a) for the 'actual' C_s symmetry around Re(I) in the non-relativistic limit and b) for the 'actual' C_s symmetry around Re(I) including relativistic SOC corrections.

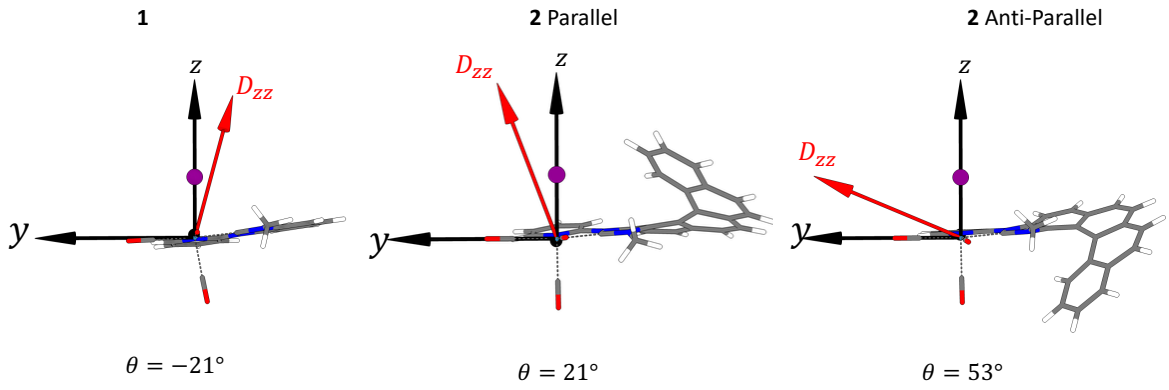

Scheme S 2

SA-CASSCF/QD-NEVPT2 computed D_{zz} magnetic vectors of excited state D tensors, based on the excited ZFS calculated employing the effective Hamiltonian of excited SOC $|\Psi_{1-3}\rangle$ states and its angle from the reference magnetic axis in the ground $|\Psi_0\rangle$ SOC state (aligned with z-axis) for a) complex **1 A-I**, b) 'parallel' complex **2 MA-I** and c) 'anti-parallel' complex **2 PA-I**

Table S 1

Calculated relevant structural parameters [bond distances (A) and angles (º)], for ground, first triplet and first singlet excited states, with available experimental data

Complex	State	Re-X	Re-$C_{carbene}$	Re-N	Re-$C_{ax\text{-}CO}$	Re-$C_{eq\text{-}CO}$	X-Re-$C_{ax\text{-}CO}$	N-$C_{carbene}$-N	Helical angle
	exp.	2.51	2.12	2.20	1.91	1.95/1.92	176.65	106.72	--
1 C-Cl	S_0	2.51	2.13	2.20	1.90	1.96/1.91	177.23	106.15	--
1 A-Cl	T_1	2.45	2.11	2.09	1.95	1.98/1.98	173.00	106.87	--
	S_1	2.41	2.11	2.14	1.95	2.00/1.95	170.50	106.95	--
	exp.	2.83	2.13	2.17	1.94	1.95/1.95	179.08	106.60	--
1 C-I	S_0	2.85	2.13	2.20	1.90	1.96/1.92	178.67	106.20	--
1 A-I	T_1	2.86	2.11	2.10	1.93	1.98/1.97	170.72	106.81	--
	S_1	2.77	2.11	2.15	1.94	2.00/1.94	164.20	106.95	--
2 M,A-Cl **2** P,C-Cl	exp.	Not Available							
	S_0	2.51	2.12	2.20	1.90	1.96/1.91	177.31	106.32	44.26
	T_1	2.51	2.11	2.20	1.90	1.96/1.91	177.67	106.49	44.25
	S_1	2.51	2.12	2.20	1.90	1.96/1.91	177.31	106.32	45.24
2 M,C-Cl **2** P,A–Cl	exp.	2.51	2.08	2.20	1.91	1.98/1.96	176.62	107.21	47.47
	S_0	2.51	2.12	2.20	1.91	1.96/1.91	177.39	106.43	44.09
	T_1	2.51	2.12	2.02	1.90	1.96/1.91	177.39	106.43	44.09
	S_1	2.51	2.13	2.21	1.90	1.96/1.91	176.94	106.25	45.42
	exp.	Not Available							
2 M,A-I	S_0	2.85	2.12	2.20	1.90	1.96/1.92	178.57	106.25	43.90
2 P,C-I	T_1	2.85	2.11	2.20	1.90	1.96/1.92	178.84	106.46	44.88
	S_1	2.78	2.11	2.15	1.94	2.00/1.94	173.54	106.56	44.76
	exp.	2.80	2.12	2.21	1.96	1.97/1.92	176.80	105.77	50.60
2 M,C-I	S_0	2.81	2.12	2.20	1.90	1.96/1.92	178.36	106.21	45.69
2 P,A–I	T_1	2.85	2.11	2.20	1.90	1.97/1.92	178.65	106.44	45.69
	S_1	2.85	2.12	2.20	1.90	1.96/1.92	178.36	106.21	44.55

Table S 2

Calculated MAEs, from the experimental spectra, of all calculated spectra with at different level of theory and also with B3LYP functional on ADF package

Complex	$\mathrm{MAE} = \frac{\lvert \mathrm{Area}_{\mathrm{Exp.}} - \mathrm{Area}_{\mathrm{Calc.}} \rvert}{\mathrm{Area}_{\mathrm{Exp.}}}$							
	STEOM-DLPNO-CCSD/SOC		PBE0/SOC		B3LYP/SOC		B3LYP/SOC (ADF)	
	Absorption	ECD	Absorption	ECD	Absorption	ECD	Absorption	ECD
1 A-Cl	0.10	0.09	0.10	0.19	0.18	0.26	0.19	0.23
1 C-Cl			0.10	0.19	0.18	0.26	0.19	0.23
1 A-I			0.28	0.35	0.32	0.40	0.37	0.59
1 C-I			0.24	0.36	0.31	0.41	0.35	0.56
2 M,A-Cl			0.08	0.15	0.12	0.34	0.14	0.30
2 P,C-Cl			0.08	0.15	0.12	0.33	0.13	0.30
2 M,C-Cl			0.07	0.12	0.11	0.23	0.13	0.24
2 P,A–Cl			0.07	0.09	0.11	0.24	0.13	0.27
2 M,A-I			0.06	0.11	0.16	0.30	0.18	0.34
2 P,C-I			0.07	0.12	0.15	0.32	0.16	0.41
2 M,C-I			0.11	0.23	0.18	0.35	0.18	0.37
2 P,A–I			0.11	0.17	0.18	0.35	0.18	0.36
Average MAE	0.10	0.09	0.12	0.19	0.18	0.31	0.20	0.35

Table S 3

Lowest 5 Singlet and Triplet SO-free States with corresponding transition energies (E in eV), oscillator strength (*f*), rotatory strength (R in 10^{40}cgs) and type of charge transfer as extracted from NTO and TheoDore analysis, for TDDFT-PBE0 (calculated in ORCA) and TDDFT-B3LYP (calculated in ADF), respectively for complex **1** C-Cl

States	PBE0 (ORCA)				B3LYP (ADF)		
	E (eV)	*f*(x10^{-3})	R	NTO Character	E (eV)	*f*(x10^{-3})	TheoDore Character
S_1	3.255	16.40	8.44	MLCT/XLCT	3.275	28.50	$MLCT_{pyr}/MLCT_{NHC}$/XLCT/LLCT
S_2	3.479	111.50	0.49	MLCT/XLCT	3.455	180.10	$MLCT_{pyr}/MLCT_{NHC}$/XLCT/LLCT
S_3	3.707	2.20	-0.01	MLCT	3.654	8.90	$MLCT_{pyr}/MLCT_{NHC}$/ LLCT
S_4	3.969	75.70	35.3	LLCT	3.964	112.30	$MLCT_{pyr}$/ XLCT/LLCT
S_5	4.102	13.30	-4.25	LLCT	4.080	4.90	$MLCT_{pyr}$/ XLCT/LLCT
T_1	3.028	---	---		3.094	---	$MLCT_{pyr}/MLCT_{NH}C/MLCT_{CO}$/XLCT/$LLCT_{pyr}$
T_2	3.149	---	---		3.217	---	$MLCT_{pyr}/MLCT_{NH}C/MLCT_{CO}$/XLCT/$LLCT_{pyr}$
T_3	3.545	---	---		3.566	---	$MLCT_{pyr}/MLCT_{NH}C/MLCT_{CO}/LLCT_{pyr}$
T_4	3.593	---	---		3.669	---	$LC_{pyr}/LLCT_{pyr}/LC_{NHC}$
T_5	3.596	---	---		3.824	---	$MLCT_{pyr}/LC_{NHC}/LLCT_{pyr}$

Table S 4

Lowest 5 Singlet and Triplet SO-free States with corresponding transition energies (E in eV), oscillator strength (*f*), rotatory strength (R in 10^{40}cgs) and type of charge transfer as extracted from NTO and TheoDore analysis, for TDDFT-PBE0 (calculated in ORCA) and TDDFT-B3LYP (calculated in ADF), respectively for complex **1** C-I

States	PBE0 (ORCA)				B3LYP (ADF)		
	E (eV)	*f*(x10^{-3})	R	NTO Character	E (eV)	*f*(x10^{-3})	TheoDore Character
S_1	3.211	6.70	-4.05	MLCT/XLCT	3.123	11.30	$XMLCT_{pyr}/MLCT_{pyr}$
S_2	3.344	55.90	7.37	MLCT/XLCT	3.214	66.30	$XMLCT_{pyr}/MLCT_{pyr}$
S_3	3.709	1.90	-0.02	MLCT	3.633	8.30	$MLCT_{pyr}/MLCT_{NHC}/MLCT_{CO}$
S_4	3.923	16.70	21.47	LLCT/XLCT	3.809	14.50	$XLCT_{pyr}/MLCT_{pyr}/LLCT_{pyr}$
S_5	4.005	21.20	4.19	LLCT/XLCT	3.845	144.40	$XLCT_{pyr}/LLCT_{pyr}$
T_1	3.022	---	---		2.978	---	$XLCT_{pyr}/MLCT_{pyr}/MLCT_{NHC}$
T_2	3.092	---	---		3.044	---	$XLCT_{pyr}/MLCT_{pyr}/MLCT_{NHC}$
T_3	3.481	---	---		3.520	---	$LC_{NHC}/MLCT_{pyr}/LLCT_{pyr}/XLCT_{pyr}$
T_4	3.547	---	---		3.573	---	$LC_{NHC}/MLCT_{pyr}/XLCT_{pyr}/LLCT_{pyr}$
T_5	3.595	---	---		3.643	---	$XLCT_{pyr}/LC_{NHC}/LC_{pyr}$

Table S 5

Lowest 5 Singlet and Triplet SO-free States with corresponding transition energies (E in eV), oscillator strength (*f*), rotatory strength (R in 10^{40}cgs) and type of charge transfer as extracted from NTO and TheoDore analysis, for TDDFT-PBE0 (calculated in ORCA) and TDDFT-B3LYP (calculated in ADF), respectively for complex **2** M,C-Cl

States	PBE0 (ORCA)				B3LYP (ADF)			
	E (eV)	*f*(x10^{-3})	R	NTO Character	E (eV)	*f*(x10^{-3})	R	TheoDore Character
S_1	3.142	44.70	16.69	MLCT/XLCT/ $ILCT_{Helicene}$	3.116	122.10		$MLCT_{pyr,NHC,CO}/LC_{NHC}/LLCT_{pyr}$
S_2	3.346	114.80	-80.0	MLCT/XLCT/ $ILCT_{Helicene}$	3.308	126.70		$MLCT_{pyr,NHC,CO}/LC_{NHC}/LLCT_{pyr}/XLCT_{pyr}$
S_3	3.513	18.20	13.6	$ILCT_{Helicene}$	3.448	24.10		LC_{NHC}
S_4	3.568	16.60	15.94	$ILCT_{Helicene}$	3.472	90.50		$LC_{NHC}/LLCT_{pyr}/MLCT_{pyr,NHC}$
S_5	3.618	2.90	-14.01	$ILCT_{Helicene}$	3.566	27.50		$MLCT_{pyr,NHC,CO}/LC_{NHC}$
T_1	2.333	---	---		2.727	---		LC_{NHC}
T_2	2.878	---	---		2.944	---		$LC_{NHC}/MLCT_{pyr,NHC,CO}/LLCT_{pyr}$
T_3	3.034	---	---		3.115	---		$MLCT_{NHC,pyr,CO}/LLCT_{pyr}/XLCT_{pyr}$
T_4	3.073	---	---		3.137	---		LC_{NHC}
T_5	3.209	---	---		3.249	---		LC_{NHC}

Table S 6

Lowest 5 Singlet and Triplet SO-free States with corresponding transition energies (E in eV), oscillator strength (*f*), rotatory strength (R in 10^{40}cgs) and type of charge transfer as extracted from NTO and TheoDore analysis, for TDDFT-PBE0 (calculated in ORCA) and TDDFT-B3LYP (calculated in ADF), respectively for complex **2** M,C-I

States	PBE0 (ORCA)				B3LYP (ADF)			
	E (eV)	*f*(x10^{-3})	R	NTO Character	E (eV)	*f*(x10^{-3})	R	TheoDore Character
S_1	3.126	29.60	8.65	MLCT/XLCT/ $ILCT_{Helicene}$	3.026	65.40		$XLCT_{pyr}/MLCT_{pyr,NHC}/LC_{NHC}$
S_2	3.267	66.10	-51.37	MLCT/XLCT/ $ILCT_{Helicene}$	3.138	71.50		$XLCT_{pyr}/MLCT_{pyr,NHC}$
S_3	3.477	62.30	9.25	$ILCT_{Helicene}$	3.336	110.20		$LC_{NHC}/XLCT_{pyr}/LLCT_{pyr}$
S_4	3.552	9.50	4.94	$ILCT_{Helicene}$	3.436	25.10		$LC_{NHC}/LLCT_{pyr}$
S_5	3.618	8.80	-23.51	$ILCT_{Helicene}$	3.523	64.90		$LC_{NHC}/LLCT_{pyr}/MLCT_{NHC,pyr}$
T_1	2.331	---	---		2.718			LC_{NHC}
T_2	2.892	---	---		2.892			$LC_{NHC}/XLCT_{pyr}$
T_3	3.02	---	---		2.985			$XLCT_{pyr}/MLCT_{NHC,pyr,CO}$
T_4	3.06	---	---		3.118			LC_{NHC}
T_5	3.174	---	---		3.157			LC_{NHC}

Table S 7

Lowest SOC corrected States (all states with energy ≤ 25000 cm^{-1}) with corresponding energies (E in cm^{-1}), oscillator strength (f), rotatory strength (R in 10^{40}cgs) and composition with respect to Ms characters. Following Tables are for TDDFT-PBE0 (calculated in ORCA) and TDDFT-B3LYP (calculated in ADF), respectively for complex **1** C-Cl

Software	SOC States	E (eV)	*f*(x10^{-3})	R	Composition
ORCA	0	0.000			99% $S_0(0)$
	1	2.991	0.01	-0.00567	37% $T_1(-1)$ + 10% $T_2(-1)$ + 37% $T_1(1)$ + 10% $T_2(1)$
	2	2.993	0.05	-0.07019	37% $T_1(-1)$ + 10% $T_2(-1)$ + 37% $T_1(1)$ + 10% $T_2(1)$
	3	3.016	4.21	-0.30655	87% $T_1(0)$
	4	3.098	5.33	2.98785	27% $S_1(0)$ + 64% $T_2(0)$
	5	3.204	0.01	-0.01922	10% $T_1(-1)$ + 37% $T_2(-1)$ + 10% $T_1(1)$ + 37% $T_2(1)$
	6	3.207	0.30	0.09311	10% $T_1(-1)$ + 38% $T_2(-1)$ + 10% $T_1(1)$ + 38% $T_2(1)$
	7	3.312	10.73	5.4157	65% $S_1(0)$ + 30% $T_2(0)$
	8	3.483	82.38	1.83379	71% $S_2(0)$ + 6% $T_1(0)$ + 5% $T_3(0)$ + 6% $T_4(-1)$ + 6% $T_4(1)$
	9	3.564	0.00	0.00078	7% $T_3(0)$ + 6% $T_4(0)$ + 40% $T_3(-1)$ + 40% $T_3(1)$
	10	3.568	0.06	-0.05746	7% $T_3(0)$ + 44% $T_3(-1)$ + 44% $T_3(1)$
	11	3.573	7.16	-0.47547	7% $S_2(0)$ + 76% $T_3(0)$ + 7% $T_3(-1)$ + 7% $T_3(1)$
	12	3.605	0.08	0.04653	19% $T_4(0)$ + 5% $T_5(0)$ + 29% $T_5(-1)$ + 29% $T_5(1)$
	13	3.608	2.67	0.79317	65% $T_5(0)$ + 7% $T_4(-1)$ + 7% $T_4(1)$
	14	3.614	0.28	0.07554	42% $T_5(-1)$ + 42% $T_5(1)$
	15	3.648	1.34	0.22303	43% $T_4(0)$ + 14% $T_4(-1)$ + 9% $T_5(-1)$ + 14% $T_4(1)$ + 9% $T_5(1)$
	16	3.653	1.10	-0.22302	21% $T_4(0)$ + 9% $T_5(0)$ + 25% $T_4(-1)$ + 7% $T_5(-1)$ + 25% $T_4(1)$ + 7% $T_5(1)$
	17	3.658	8.69	-0.48791	10% $S_2(0)$ + 10% $T_5(0)$ + 35% $T_4(-1)$ + 35% $T_4(1)$
	18	3.743	0.85	-0.24827	55% $S_3(0)$ + 12% $T_6(-1)$ + 7% $T_7(-1)$ + 12% $T_6(1)$ + 7% $T_7(1)$
	19	3.751	0.75	-0.00221	10% $T_6(0)$ + 26% $T_6(-1)$ + 13% $T_7(-1)$ + 26% $T_6(1)$ + 13% $T_7(1)$
	20	3.760	0.81	0.37078	35% $S_3(0)$ + 21% $T_6(-1)$ + 7% $T_7(-1)$ + 21% $T_6(1)$ + 7% $T_7(1)$
ADF	1	3.019	0.04		71%T_1 + 20%T_2
	2	3.023	0.43		66%T_1 + 22%T_2
	3	3.046	10.36		77%T_1
	4	3.117	10.24		50%T_2 + 35%S_1
	5	3.252	0.07		66%T_2 + 24%T_1
	6	3.253	0.09		
	7	3.326	16.60		57%S_1 + 35%T_2
	8	3.448	138.50		77%S_2
	9	3.584	0.04		
	10	3.594	7.44		
	11	3.602	24.26		80%T_3 + 13%S_2
	12	3.654	2.94		
	13	3.666	0.58		
	14	3.667	0.27		
	15	3.680	5.53		
	16	3.753	0.16		
	17	3.759	2.02		
	18	3.776	2.99		
	19	3.809	25.52		32% T_6 + 23%S_4 + 16% T_7
	20	3.846	0.34		

Table S 8

Lowest SOC corrected States (all states with energy ≤ 25000 cm^{-1}) with corresponding energies (E in cm^{-1}), oscillator strength (f), rotatory strength (R in 10^{40}cgs) and composition with respect to Ms characters. Following Tables are for TDDFT-PBE0 (calculated in ORCA) and TDDFT-B3LYP (calculated in ADF), respectively for complex **1** C-I

Software	SOC States	E (eV)	*f*(x10^{-3})	R	Composition
ORCA	0	0.000			99% $S_0(0)$
	1	2.893	0.06	0.07239	30% $T_1(-1)$ + 18% $T_2(-1)$ + 30% $T_1(1)$ + 18% $T_2(1)$
	2	2.894	0.13	-0.04936	29% $T_1(-1)$ + 19% $T_2(-1)$ + 29% $T_1(1)$ + 19% $T_2(1)$
	3	2.937	4.20	1.22106	16% $S_2(0)$ + 78% $T_1(0)$
	4	2.962	2.17	0.0346	34% $S_1(0)$ + 60% $T_2(0)$
	5	3.178	0.00	0.00794	18% $T_1(-1)$ + 29% $T_2(-1)$ + 18% $T_1(1)$ + 29% $T_2(1)$
	6	3.192	3.95	2.31008	18% $T_1(-1)$ + 29% $T_2(-1)$ + 18% $T_1(1)$ + 29% $T_2(1)$
	7	3.276	4.46	-1.52173	54% $S_1(0)$ + 33% $T_2(0)$
	8	3.344	24.90	4.72195	65% $S_2(0)$ + 13% $T_1(0)$ + 8% $T_3(0)$
	9	3.479	0.16	-0.02527	7% $T_4(0)$ + 38% $T_3(-1)$ + 38% $T_3(1)$
	10	3.480	0.43	-0.07257	27% $T_3(0)$ + 24% $T_3(-1)$ + 9% $T_4(-1)$ + 24% $T_3(1)$ + 9% $T_4(1)$
	11	3.509	5.32	-0.07696	6% $S_2(0)$ + 52% $T_3(0)$ + 17% $T_3(-1)$ + 17% $T_3(1)$
	12	3.554	0.66	1.63165	45% $T_4(0)$ + 17% $T_4(-1)$ + 17% $T_4(1)$
	13	3.566	0.06	-0.17033	20% $T_4(0)$ + 6% $T_5(0)$ + 7% $T_3(-1)$ + 22% $T_4(-1)$ + 7% $T_3(1)$ + 22% $T_4(1)$
	14	3.577	2.62	-0.79556	7% $T_4(0)$ + 7% $T_3(-1)$ + 30% $T_4(-1)$ + 7% $T_3(1)$ + 30% $T_4(1)$
	15	3.619	2.86	0.43404	41% $T_5(-1)$ + 41% $T_5(1)$
	16	3.621	0.94	-0.28811	49% $T_5(0)$ + 15% $T_5(-1)$ + 15% $T_5(1)$
	17	3.626	0.11	0.4212	7% $T_4(0)$ + 22% $T_5(0)$ + 23% $T_5(-1)$ + 23% $T_5(1)$
	18	3.679	0.14	-0.2972	16% $T_6(-1)$ + 18% $T_7(-1)$ + 16% $T_6(1)$ + 18% $T_7(1)$
	19	3.684	0.65	0.22927	11% $T_6(-1)$ + 22% $T_7(-1)$ + 5% T8(-1) + 11% $T_6(1)$ + 22% $T_7(1)$ + 5% T8(1)
	20	3.704	3.19	1.86317	6% $S_3(0)$ + 8% $S_5(0)$ + 27% $T_6(0)$ + 22% $T_7(0)$ + 6% T8(0)
ADF	1	2.794	0.06		58%T_1 + 40% T_2
	2	2.796	0.15		58%T_1 + 40% T_2
	3	2.839	14.05		73%T_1+ 20%S_2
	4	2.861	5.44		57%T_2 + 36%S_1
	5	3.109	0.06		54%T_2 + 36%T_1
	6	3.128	4.03		56%T_2 + 36%T_1
	7	3.177	5.97		52%S_1 + 34%T_2
	8	3.214	44.67		67%S_2 + 17%T_1
	9	3.445	0.43		
	10	3.458	2.37		
	11	3.473	9.73		
	12	3.503	9.61		
	13	3.559	0.76		
	14	3.562	1.22		
	15	3.565	0.73		
	16	3.574	1.41		
	17	3.586	8.65		
	18	3.600	16.19		28%S_4 + 21%T_7 + 15%T_6
	19	3.626	8.75		
	20	3.655	14.36		T_5

Table S 9

Lowest SOC corrected States (all states with energy ≤ 25000 cm^{-1}) with corresponding energies (E in cm^{-1}), oscillator strength (f), rotatory strength (R in 10^{40}cgs) and composition with respect to Ms characters. Following Tables are for TDDFT-PBE0 (calculated in ORCA) and TDDFT-B3LYP (calculated in ADF), respectively for complex **2** M,C-Cl

Software	SO-States	E (eV)	*f*(x10^{-3})	R	Composition
ORCA	0	0.000			100% $S_0(0)$
	1	2.343	0.001	0.00085	24% $T_1(0)$ + 38% $T_1(-1)$ + 38% $T_1(1)$
	2	2.343	0.001	-0.00028	75% $T_1(0)$ + 12% $T_1(-1)$ + 12% $T_1(1)$
	3	2.343	0.01	-0.00167	50% $T_1(-1)$ + 50% $T_1(1)$
	4	2.858	0.01	-0.02337	42% $T_2(-1)$ + 42% $T_2(1)$
	5	2.859	0.04	-0.14687	43% $T_2(-1)$ + 43% $T_2(1)$
	6	2.869	1.35	-0.72987	92% $T_2(0)$
	7	2.988	9.95	4.01739	23% $S_1(0)$ + 59% $T_3(0)$ + 9% $T_4(0)$
	8	3.022	0.12	0.05051	33% $T_3(-1)$ + 9% $T_4(-1)$ + 33% $T_3(1)$ + 9% $T_4(1)$
	9	3.023	0.07	-0.13635	34% $T_3(-1)$ + 8% $T_4(-1)$ + 34% $T_3(1)$ + 8% $T_4(1)$
	10	3.060	1.45	-0.24603	6% $S_1(0)$ + 23% $T_3(0)$ + 63% $T_4(0)$
	11	3.096	0.00	-0.00801	8% $T_3(-1)$ + 39% $T_4(-1)$ + 8% $T_3(1)$ + 39% $T_4(1)$
	12	3.098	0.26	0.02747	9% $T_3(-1)$ + 38% $T_4(-1)$ + 9% $T_3(1)$ + 38% $T_4(1)$
	13	3.155	11.65	4.2646	39% $S_1(0)$ + 7% $T_3(0)$ + 22% $T_4(0)$ + 25% $T_5(0)$
	14	3.223	10.26	1.36976	8% $S_1(0)$ + 39% $T_5(0)$ + 21% $T_5(-1)$ + 21% $T_5(1)$
	15	3.226	0.25	-0.01313	46% $T_5(-1)$ + 46% $T_5(1)$
	16	3.229	18.91	1.49625	19% $S_1(0)$ + 24% $T_5(0)$ + 24% $T_5(-1)$ + 24% $T_5(1)$
	17	3.301	4.67	-1.93373	91% $T_6(0)$
	18	3.302	0.01	-0.00067	47% $T_6(-1)$ + 47% $T_6(1)$
	19	3.302	0.26	-0.0516	50% $T_6(-1)$ + 50% $T_6(1)$
	20	3.351	78.41	-55.9888	71% $S_2(0)$ + 8% $T_5(0)$
ADF	1	2.724	0.00		T_1
	2	2.725	0.07		T_1
	3	2.725	0.27		T_1
	4	2.904	0.03		T_2
	5	2.906	1.18		T_2
	6	2.917	4.36		T_2
	7	3.011	55.75		45%S_1 + 34%T_3
	8	3.101	0.03		
	9	3.102	1.00		
	10	3.133	1.23		
	11	3.140	0.07		
	12	3.140	0.06		
	13	3.164	51.51		40%S_1 + 34%T_3
	14	3.225	41.93		56%T_5 + 22%S_2 + 12%S_1
	15	3.259	0.28		
	16	3.259	0.05		
	17	3.303	53.58		42%S_2 + 18%T_5 + 12%T_6
	18				
	19				
	20	3.360	18.63		75%T_6 + 14%S_2

Table S 10

Lowest SOC corrected States (all states with energy ≤ 25000 cm^{-1}) with corresponding energies (E in cm^{-1}), oscillator strength (f), rotatory strength (R in 10^{40}cgs) and composition with respect to Ms characters. Following Tables are for TDDFT-PBE0 (calculated in ORCA) and TDDFT-B3LYP (calculated in ADF), respectively for complex **2** M,C-I

Software	SOC States	E (eV)	*f*(x10^{-3})	R	Composition
ORCA	0	0.000			100% $S_0(0)$
	1	2.347	0.001	0.00182	50% $T_1(-1)$ + 50% $T_1(1)$
	2	2.347	0.03	0.00836	8% $T_1(0)$ + 46% $T_1(-1)$ + 46% $T_1(1)$
	3	2.347	0.00	-0.00474	92% $T_1(0)$
	4	2.818	0.08	-0.01383	30% $T_2(-1)$ + 12% $T_3(-1)$ + 30% $T_2(1)$ + 12% $T_3(1)$
	5	2.818	0.06	-0.05205	30% $T_2(-1)$ + 13% $T_3(-1)$ + 30% $T_2(1)$ + 13% $T_3(1)$
	6	2.845	2.04	0.10281	10% $S_2(0)$ + 79% $T_2(0)$
	7	2.894	7.62	2.66297	34% $S_1(0)$ + 50% $T_3(0)$ + 9% $T_4(0)$
	8	2.988	0.00	-0.00265	17% $T_2(-1)$ + 19% $T_3(-1)$ + 9% $T_4(-1)$ + 17% $T_2(1)$ + 19% $T_3(1)$ + 9% $T_4(1)$
	9	2.990	0.77	0.00939	17% $T_2(-1)$ + 18% $T_3(-1)$ + 11% $T_4(-1)$ + 17% $T_2(1)$ + 18% $T_3(1)$ + 11% $T_4(1)$
	10	3.020	1.12	-0.66316	8% $S_2(0)$ + 13% $T_2(0)$ + 20% $T_3(0)$ + 43% $T_4(0)$ + 7% $T_5(0)$
	11	3.100	0.01	-0.02936	9% $T_3(-1)$ + 32% $T_4(-1)$ + 9% $T_3(1)$ + 32% $T_4(1)$
	12	3.105	0.92	0.1013	9% $T_3(-1)$ + 33% $T_4(-1)$ + 6% $T_5(-1)$ + 9% $T_3(1)$ + 33% $T_4(1)$ + 6% $T_5(1)$
	13	3.132	1.18	0.1671	10% $S_1(0)$ + 33% $T_4(0)$ + 37% $T_5(0)$
	14	3.181	12.50	4.21576	20% $S_1(0)$ + 6% $S_2(0)$ + 8% $T_3(0)$ + 15% $T_5(0)$ + 16% $T_5(-1)$ + 16% $T_5(1)$
	15	3.196	0.11	-0.04924	7% $T_5(0)$ + 7% $T_3(-1)$ + 35% $T_5(-1)$ + 7% $T_3(1)$ + 35% $T_5(1)$
	16	3.222	17.25	-1.03966	22% $S_1(0)$ + 5% $S_2(0)$ + 11% $T_3(0)$ + 21% $T_5(-1)$ + 21% $T_5(1)$
	17	3.286	12.60	-11.82175	36% $S_2(0)$ + 17% $T_5(0)$ + 15% $T_6(0)$ + 6% $T_6(-1)$ + 6% $T_6(1)$
	18	3.305	0.00	-0.00045	38% $T_6(0)$ + 30% $T_6(-1)$ + 30% $T_6(1)$
	19	3.305	0.62	-0.11969	49% $T_6(-1)$ + 49% $T_6(1)$
	20	3.313	4.07	-4.48478	14% $S_2(0)$ + 45% $T_6(0)$ + 14% $T_6(-1)$ + 14% $T_6(1)$
ADF	1	2.695	0.07		T_1
	2	2.695	0.17		T_1
	3	2.704	2.79		T_1
	4	2.762	0.13		42%T_2 26%T_1 22%T_3
	5	2.763	0.19		44%T_2 + 26%T_1 + 22%T_3
	6	2.790	13.17		60%T_2 + 15%S_2
	7	2.801	27.35		46%T_3 + 37%S_1
	8	2.998	0.02		
	9	3.007	2.59		
	10	3.045	20.57		36%T_3 + 34%T_2
	11	3.084	30.60		36%S_1 + 21%T_3
	12	3.123	0.06		
	13	3.128	1.54		
	14	3.133	4.29		
	15	3.163	0.28		
	16	3.179	8.30		
	17	3.203	26.16		35%S_2 + 25%T_5
	18	3.297	21.97		70%T_6 + 19%S_3
	19	3.300	0.97		
	20	3.305	4.97		

Table S 11

Experimental and ESD/TD-DFT/PBE0+SOC calculated radiative and non-radiative relaxation rates and phosphorescence times (μs) at 295K. Relativistic ground and lowest excited SOC states with corresponding energies and composition with respect to M_S characters.

Complex	SOC State	SOC State Composition	Energy (cm^{-1})	k_r (s^{-1})	k_r (s^{-1})	t (μs)	k_r (s^{-1})	k_r (s^{-1})	k_{nr} (s^{-1})	k_{nr} (s^{-1})	Φ ($\times 10^2$)	t (μs)
				77K			295K					
2 M,A-I	$\|\Psi_0\rangle$	99% $S_0(0)$	0									
	$\|\Psi_1\rangle$	98% $T_1(\pm1)$	18880	202			277		34306			
	$\|\Psi_2\rangle$	17% $T_1(0)$ + 82% $T_1(\pm1)$	18880	110	119	8395	151	163	18681	20245	0.8	49
	$\|\Psi_3\rangle$	82% $T_1(0)$ + 16% $T_1(\pm1)$	18880	46			62		7747			
2 P,A-I	$\|\Psi_0\rangle$	99% $S_0(0)$	0									
	$\|\Psi_1\rangle$	98% $T_1(\pm1)$	18924	110			117		14559			
	$\|\Psi_2\rangle$	6% $T_1(0)$ + 92% $T_1(\pm1)$	18924	372	166	6010	397	178	49223	22044	0.8	45
	$\|\Psi_3\rangle$	92% $T_1(0)$	18924	18			19		2352			
2 M,A-Cl	$\|\Psi_0\rangle$	99% $S_0(0)$	0									
	$\|\Psi_1\rangle$	73% $T_1(0)$ + 26% $T_1(\pm1)$	18853	108			102		915			
	$\|\Psi_2\rangle$	6% $T_1(0)$ + 92% $T_1(\pm1)$	18853	15	151	6626	14	143	126	1284	10.0	701
	$\|\Psi_3\rangle$	20% $T_1(0)$ + 78% $T_1(\pm1)$	18853	330			312		2811			
2 P,A-Cl	$\|\Psi_0\rangle$	99% $S_0(0)$	0									
	$\|\Psi_1\rangle$	26% $T_1(0)$ + 72% $T_1(\pm1)$	18881	9			13		200			
	$\|\Psi_2\rangle$	73% $T_1(0)$ + 26% $T_1(\pm1)$	18881	4	184	5427	5	139	81	2171	6.0	433
	$\|\Psi_3\rangle$	98% $T_1(\pm1)$	18881	541			398		6231			

	$\|\Psi_0\rangle$	99% $S_0(0)$	0									
	$\|\Psi_1\rangle$	58% $T_1(\pm1)$ + 34% $T_2(\pm1)$	23324	394898			3629		2588374			
1 A-I	$\|\Psi_2\rangle$	58% $T_1(\pm1)$ + 36% $T_2(\pm1)$	23336	6543	227276	4.4	60	7368	42885	5.5×10^6	0.14	0.19
	$\|\Psi_3\rangle$	15% $S_2(0)$ + 77% $T_1(0)$	23676	6532046			60025		42814694			
	$\|\Psi_4\rangle$	33% $S_1(0)$ + 59% $T_2(0)$	23887				25643		18290541			
	$\|\Psi_0\rangle$	99% $S_0(0)$	0									
	$\|\Psi_1\rangle$	72% $T_1(\pm1)$ + 18% $T_2(\pm1)$	24123	88154			8314		407385			
1 A-Cl	$\|\Psi_2\rangle$	74% $T_1(\pm1)$ + 18% $T_2(\pm1)$	24143	80698	312500	3.2	7611	285714	372930	1.4×10^7	2.00	0.07
	$\|\Psi_3\rangle$	10% $S_2(0)$ + 87% $T_1(0)$	24326	17354432			1636738		80200153			
	$\|\Psi_4\rangle$	26% $S_1(0)$ + 63% $T_2(0)$	24990				2185367		107083000			

Table S 12

Calculated versus available experimental normalized dissymmetry factors (g_{lum}) of CPL for complexes 2 and 1. Electronic transition properties are given, in terms of transition electric dipole ($D = |\mu|^2$), magnetic dipole ($M = |m|^2$) and rotatory ($R = -|\mu||m|cos\theta$) strengths. $\mu, m, \theta°$ are transition electric and magnetic dipole moments and angle between them, respectively.

Complex	$D = \|\mu\|^2$ $/10^{-40}$ $esu^2.cm^2$	$M = \|m\|^2$ $/10^{-40}$ $erg^2.G^{-2}$	$R = -\|\mu\|\|m\|cos\theta$ $/10^{-40}$ $esu.cm.erg.G^{-1}$	$\theta°$	Calc. $/10^{-2}$ $g_{lum} = -4R/D \cdot M$	Exp. $/10^{-2}$ g_{lum}	Normalized Calc. g_{lum}	Normalized Exp. g_{lum}
2 M,A-I	212	0.0001	-0.0022	79	0.4	0.1	0.03	0.02
2 P,C-I	214	0.0001	0.0014	79	-0.3	-0.1	-0.02	-0.02
2 M,C-I	212	0.0002	0.1502	36	13.0	-4.5	-0.84	-0.90
2 P,A-I	216	0.0002	-0.1484	39	-12.9	4.5	0.83	0.90
2 M,A-Cl	102	0.0001	-0.0150	60	5.7	2	0.34	0.40
2 P,C-Cl	102	0.0001	0.0150	57	-5.7	-2	-0.35	-0.40
2 M,C-Cl	129	0.0001	0.0740	34	15.8	-5	-1.00	-1.00
2 P,A-Cl	137	0.0002	-0.0801	42	-15.5	5	1.00	1.00
1 A-Cl	45847	0.0252	3.2293	54	0.01	0.1	-0.001	-0.20
1 C-Cl	45847	0.0252	-3.2270	54	-0.01	-0.1	0.001	0.20

Table S 13

SA-CASSCF/QD-NEVPT2 computed axial and rhombic excited state multiplet ZFS parameters (D (cm^{-1}) and E/D) at equilibrium and minimum energy geometries together with the respective axial and rhombic spin-vibronic coupling constants ξ_D (cm^{-1}) and ξ_E along a selected set of vibrational normal modes for A-Cl/I diastereomers **1** and **2**.

Complex	CAS (m,n)	Mode†	ZFS				Spin-Vibronic Coupling	
			$Q_{eq.}$		$Q_{min.}$			
			D	E/D	D	E/D	Axial coupling ξ_D	Rhombic Coupling ξ_E
1 A-Cl	(8,8)	1	-83.14	0.07	-248.29	0.10	-83.99	-7.56
		2	-85.14	0.01	-350.15	0.05	-121.83	-9.75
		3	-85.14	0.04	-319.15	0.08	-119.83	-9.59
		4	-86.75	0.08	-84.59	0.20	-119.04	-8.33
Total/Average			-84.72	0.05	-250.25	0.09	-110.63	-7.74
1 A-I	(8,8)	1	-318.01	0.01	-215.78	0.01	-95.27	-0.95
		2	-330.01	0.01	-354.23	0.01	-107.24	-1.07
		3	-324.01	0.01	-229.51	0.06	-102.62	-1.03
		4	-330.01	0.01	-312.94	0.02	-105.23	-1.05
Total/Average			-325.52	0.02	-277.52	0.02	-102.25	-1.02

2 M,A-Cl	(10,11)	5	-5.54	0.27	-3.86	0.30	-20.05	-2.41
		6	-5.53	0.25	-4.40	0.23	-20.58	-2.12
Total/Average			-5.53	0.25	-4.13	0.25	-20.27	-2.23
2 P,A-Cl	(10,11)	5	-6.96	0.28	-4.32	0.29	-20.38	-4.89
		6	-4.97	0.21	-5.38	0.20	-30.90	-5.43
Total/Average			-4.96	0.24	-4.85	0.23	-30.14	-5.04
2 M,A-I	(10,11)	5	-4.92	0.18	-4.92	0.18	~0	0.00
		6	-3.56	0.24	-4.47	0.29	-1.35	-0.16
Total/Average			-4.24	0.21	-4.69	0.21	-1.35	-0.16
2 P,A-I	(10,11)	5	-5.92	0.16	-6.01	0.21	-0.22	-0.05
		6	-4.05	0.27	-4.24	0.23	-0.37	-0.08
Total/Average			-4.98	0.23	-5.12	0.22	-0.27	-0.06

[†]The modes are visualized in Figures S25 and S26

VI. Inputs

1. Geometry Optimization and Hessian of Ground State

```
! PBE0 D3BJ RIJCOSX PAL8
! def2-TZVP def2/J def2-TZVP/C
! TightSCF DefGrid3 SmallPrint
! Opt TightOpt Freq
! CPCM(CH2Cl2)
%MaxCore 10000

%SCF    MaxIter   500
        End

%Geom   MaxIter   500
        End



* xyzfile 0 1 B1_MA_opt_PBE0_S0.xyz
```

2. Geometry Optimization and Hessian of 1st Triplet Excited State

```
! PBE0 D3BJ RIJCOSX PAL16
! def2-TZVP def2/J def2-TZVP/C
! TightSCF DefGrid3 SmallPrint
! Opt TightOpt Freq
! CPCM(CH2Cl2)
%MaxCore 5000

%SCF    MaxIter   500
        End

%Geom   MaxIter   500
        End

%TDDFT  IRoot     1
        IRootMult Triplet
        End



* xyzfile 0 1 B1_MA_opt_PBE0_T1.xyz
```

3. Calculation of Absorption and CD Spectra (TDDFT PBE0/SOC)

```
! PBE0 D3BJ RIJCOSX PAL16
! DKH2 DKH-def2-TZVP SARC/J def2-TZVP/C
! TightSCF DefGrid3 NormalPrint
! CPCM(CH2Cl2)
%MaxCore 5000

%Basis  NewGTO Re "SARC-DKH-TZVP" End
        NewGTO I  "SARC-DKH-TZVP" End
        End

%Method FrozenCore FC_None
        End

%SCF    MaxIter    500
        End

%TDDFT  NRoots     50
        MaxDim     10
        TDA        False
        Triplets   True
        DoSOC      True
        DoNTO      True
        DoQuad     True
        DoLength   True
        DoVelocity True
        PrintLevel 3
        MaxIter    500
        MaxCore    10000
        End

* xyzfile 0 1 B1_MA_opt_PBE0_S0.xyz
```

4. Absorption and CD Spectra (STEOM-DLPNO-CCSD/SOC)

```
! RHF STEOM-DLPNO-CCSD RIJCOSX PAL16
! DKH2 DKH-def2-TZVP SARC/J def2-TZVP/C
! TightSCF TightPNO
! CPCM(CH2Cl2)
%MaxCore 10000

%Basis  NewGTO Re "SARC-DKH-TZVP" End
        NewGTO I  "SARC-DKH-TZVP" End
        End

%Method FrozenCore FC_None
        End

%MDCI NRoots        25
      NDav          50
      NRootsCISNAT  50
      STEOMSOC     True
      DTol         1e-4
      DLPNOLINEAR  True
      NEWDOMAINS   True
      DoEOMMP2     True
      DoRECAN      True
      DoLeft       True
      DoTDM        True
      DoSolv       True
      DoRootWise   True
      DoDbFilter   True
      MaxCore      10000
      MaxIter      250
      PrintLevel   3
      DosimpleDens False
      End

* xyzfile 0 1 B1_MA_opt_PBE0_S0.xyz
```

5. Calculation of Phosphorescence Spectra and Relaxation Rates (FC|HT)

```
! PBE0 D3BJ RIJCOSX PAL16
! DKH2 DKH-def2-TZVP SARC/J def2-TZVP/C
! TightSCF DefGrid3 NormalPrint
! CPCM(CH2Cl2)
! MoRead
%MaxCore 5000

%Basis  NewGTO Re "SARC-DKH-TZVP" End
        NewGTO I  "SARC-DKH-TZVP" End
        End

%Method FrozenCore FC_None
        End

%MOInp “B1_MA_tddft_PBE0_S0.gbw”

%TDDFT  NRoots     10
        MaxDim     10
        DoSOC      True
        TDA        False
        MaxIter    250
        IROOT      1
        End

%ESD    ESDFLAG      PHOSP
        GSHESSIAN   "B1_MA_opt_PBE0_S0.hess"
        TSHESSIAN   "B1_MA_opt_PBE0_T1.hess"
        DELE         19849.86
        DOHT         True
        LINES        GAUSS
        LINEW        10
        PrintLevel   4
        TEMP         295
        End

* xyzfile 0 1 B1_MA_opt_PBE0_S0.xyz
```

6. Calculation of Non-radiative rate ($T_1 \rightsquigarrow S_0$ *ISC Rate*)

```
! ESD(ISC)
! PBE0 D3BJ RIJCOSX PAL16
! DKH2 DKH-def2-TZVP SARC/J def2-TZVP/C
! TightSCF DefGrid3 NormalPrint
! CPCM(CH2Cl2)
! MoRead
%MaxCore 5000

%Basis  NewGTO Re "SARC-DKH-TZVP" End
        NewGTO I  "SARC-DKH-TZVP" End
        End

%Method FrozenCore FC_None
        End

%MOInp “B1_MA_tddft_PBE0_S0.gbw”

%TDDFT  NRoots     10
        MaxDim     10
        DoSOC      True
        TDA        False
        MaxIter    250
        SROOT      0
        TROOT      1
        TROOTSSL   1
        End

%ESD
        ISCISHESS   "B1_MA_opt_PBE0_T1.hess"
        ISCFSHESS   "B1_MA_opt_PBE0_S0.hess"
        DELE         19849.86
        DOHT         FALSE
        USEJ         FALSE
        LINES        LORENTZ
        LINEW        10
        MAXTIME      20671
        NPOINTS      500000
        PrintLevel   5
        TEMP         295
        End


* xyzfile 0 1 B1_MA_opt_PBE0_S0.xyz
```

7. CASSCF/NEVPT2/SOC

```
! DKH2 DKH-def2-TZVP SARC/J def2-TZVP/C PAL16
! TightSCF RIJCOSX
! CPCM(CH2Cl2)
! MoRead
%MaxCore 5000
%Basis  NewGTO Re "SARC-DKH-TZVP" End
        NewGTO I  "SARC-DKH-TZVP" End
        End
%Method FrozenCore FC_None
        End

%MOInp “B1_MA_CAS1011_0505.gbw”

%CASSCF Nel       10
        NOrb      11
        Mult       3, 1
        NRoots    10,11
        TrafoStep RI
        MaxIter   500
        CI
          NGuessMat 1024
          MaxIter   500
          End
        Rel
          DoSOC        True
          DoQuadrupole True
          PrintLevel   3
          End
        NEVPT2    True
        End

* xyzfile 0 1 B1_MA_opt_PBE0_S0.xyz
```

8. Normal Mode SCAN and ZFS (CASSCF/NEVPT2/QD-NEVPT2/SOC)

```
! DKH2 DKH-def2-TZVP SARC/J def2-TZVP/C PAL16
! TightSCF RIJCOSX
! MTR
! CPCM(CH2Cl2)
! MoRead
%MaxCore 5000
%Basis  NewGTO Re "SARC-DKH-TZVP" End
        NewGTO I  "SARC-DKH-TZVP" End
        End
%Method FrozenCore FC_None
        End
%MOInp “B1_MA_CAS1011_1011.gbw”
%CASSCF Nel       10
        NOrb      11
        Mult       3, 1
        NRoots    10,11
        TrafoStep RI
        MaxIter   500
        CI
          NGuessMat 1024
          MaxIter   500
          End
        Rel
          DoSOC    True
          GTensor  True
          NStates  3
          IStates  1,2,3
          Printlevel   3
          DoQuadrupole True
          End
        PTMethod             SC_NEVPT2
        PTSettings
          QDType             QD_VanVleck
          CASCI_Approx     = True
          End
        End
%MTR    HessName "B1_MA_opt_PBE0_S0.hess"
        ModeType  Normal
        MList     87
        RSteps     5
        LSteps     5
        ddnc       1.0
        End
* xyzfile 0 1 B1_MA_opt_PBE0_S0.xyz
```

VII. Ground State (DFT/PBE0) Optimized Coordinates

Complex **1** A-I				Complex **1** C-I			
Re	-0.017884	-0.015798	0.001433	Re	-0.021479	0.010320	0.002388
I	0.200768	-0.146957	2.836449	I	0.150694	0.218683	2.836171
C	-1.799435	-0.713177	0.074463	C	-1.928735	0.157092	0.080684
O	-2.872861	-1.128344	0.122420	O	-3.076422	0.240645	0.132722
C	-0.775831	1.782875	0.143426	C	-0.219913	-1.930505	0.155623
O	-1.211716	2.840403	0.225289	O	-0.323983	-3.069072	0.244667
C	-0.130671	0.042927	-1.894924	C	-0.116388	-0.088244	-1.893283
O	-0.219675	0.074960	-3.045185	O	-0.194574	-0.150961	-3.043066
N	2.095931	0.586690	0.052722	N	2.175751	0.050194	0.047645
C	2.509219	1.859437	0.015463	C	2.941845	-1.046793	0.005460
H	1.733281	2.610230	-0.039366	H	2.418250	-1.990811	-0.053706
C	3.839532	2.214044	0.041386	C	4.317781	-0.998418	0.032357
H	4.118478	3.258555	0.011581	H	4.888991	-1.916138	-0.001761
C	4.787249	1.204550	0.095887	C	4.930139	0.243107	0.094360
H	5.845331	1.435820	0.104893	H	6.009674	0.330053	0.105888
C	4.376072	-0.113559	0.134430	C	4.152720	1.384093	0.136842
H	5.104552	-0.904973	0.157518	H	4.618839	2.353430	0.165285
C	3.017182	-0.386788	0.123296	C	2.773331	1.249635	0.121851
N	2.481776	-1.672123	0.163192	N	1.886651	2.323179	0.161029
C	3.095011	-2.920214	0.316236	C	2.109369	3.695458	0.315907
C	4.397933	-3.355487	0.514723	C	3.228720	4.490797	0.517905
H	5.242405	-2.689661	0.591136	H	4.230392	4.099036	0.593679
C	4.604463	-4.722290	0.637581	C	3.027808	5.857997	0.645769
H	5.613962	-5.082388	0.794488	H	3.888251	6.496061	0.806585
C	3.553704	-5.635252	0.570929	C	1.756615	6.425279	0.579920
H	3.757393	-6.694089	0.673727	H	1.642790	7.496998	0.687785
C	2.249485	-5.206611	0.385143	C	0.634192	5.636044	0.388366
H	1.424601	-5.906353	0.346947	H	-0.358890	6.064999	0.350980
C	2.047325	-3.843708	0.261432	C	0.838270	4.273874	0.259753
N	0.875231	-3.123307	0.085036	N	-0.072759	3.243641	0.079054
C	1.118176	-1.813006	0.047962	C	0.541352	2.060885	0.042760
C	-0.432821	-3.732840	0.006260	C	-1.501229	3.446295	-0.005142
H	-1.098033	-3.070034	-0.537436	H	-1.944485	2.609808	-0.535450
H	-0.354761	-4.675783	-0.532512	H	-1.698960	4.362293	-0.559897
H	-0.828123	-3.915979	1.006625	H	-1.934118	3.523715	0.993431

Complex **1** A-Cl				Complex **1** C-Cl			
Re	0.017262	-0.000430	-0.130549	Re	0.017257	0.000376	-0.130538
Cl	0.070643	0.343154	2.353055	Cl	0.069460	-0.343012	2.353122
C	-0.160602	1.921474	-0.450090	C	-0.167601	-1.920960	-0.449566
O	-0.256838	3.045622	-0.657465	O	-0.267922	-3.044822	-0.656545
C	0.050691	-0.315104	-2.004688	C	0.051763	0.314529	-2.004748
O	0.058655	-0.508105	-3.143785	O	0.060370	0.507247	-3.143889
C	-1.891797	-0.116547	-0.169189	C	-1.891358	0.123554	-0.169146
O	-3.042469	-0.179998	-0.192630	O	-3.041782	0.191356	-0.192563
N	2.202877	-0.023361	0.111215	N	2.202951	0.015504	0.111150
C	2.975115	1.061785	-0.014381	C	2.971323	-1.072390	-0.014405
H	2.480748	1.961186	-0.354405	H	2.473758	-1.970058	-0.354339
C	4.322878	1.056570	0.270703	C	4.319109	-1.071948	0.270615
H	4.902588	1.961428	0.149116	H	4.895576	-1.978885	0.149104
C	4.892351	-0.122274	0.723443	C	4.892810	0.104913	0.723181
H	5.944046	-0.168898	0.978235	H	5.944682	0.147825	0.977893
C	4.107305	-1.251648	0.855505	C	4.111793	1.237085	0.855173
H	4.536895	-2.166360	1.224659	H	4.544620	2.150334	1.224167
C	2.764130	-1.169036	0.525122	C	2.768300	1.159201	0.524939
N	1.878291	-2.243555	0.597616	N	1.886299	2.236867	0.597460
C	2.097402	-3.593308	0.893729	C	2.110201	3.585798	0.893707
C	3.210614	-4.366728	1.193507	C	3.226144	4.355179	1.193718
H	4.213110	-3.973394	1.243349	H	4.227203	3.958200	1.243660
C	3.006109	-5.719701	1.425076	C	3.026471	5.708853	1.425395
H	3.861843	-6.340047	1.662366	H	3.884394	6.326097	1.662867
C	1.739081	-6.296746	1.359199	C	1.761527	6.290445	1.359413
H	1.623143	-7.356590	1.550155	H	1.649369	7.350678	1.550466
C	0.626192	-5.533598	1.046084	C	0.645941	5.531326	1.046095
H	-0.362433	-5.970286	0.984696	H	-0.341107	5.971560	0.984668
C	0.835048	-4.186080	0.813662	C	0.849983	4.183090	0.813562
N	-0.064017	-3.190280	0.462763	N	-0.052608	3.190532	0.462510
C	0.548653	-2.014014	0.331654	C	0.555869	2.012092	0.331412
C	-1.474684	-3.437913	0.273231	C	-1.462394	3.443120	0.272960
H	-1.917117	-2.583491	-0.226149	H	-1.907589	2.590741	-0.227469
H	-1.603245	-4.323287	-0.349242	H	-1.587820	4.329584	-0.348587
H	-1.961839	-3.597090	1.236283	H	-1.949243	3.602900	1.236067

Complex **2** M,A-I			
Re	-0.045731	-0.109330	-0.061129
I	0.302817	-0.587744	2.726521
C	-0.260572	0.166694	-1.928987
O	-0.411872	0.333228	-3.061146
C	-0.399131	1.783585	0.297592
O	-0.596943	2.893948	0.505496
C	-1.921893	-0.457154	0.096107
O	-3.048529	-0.673884	0.193343
N	2.152028	0.031481	-0.104188
C	2.832910	1.175260	0.036122
H	2.241666	2.079801	0.070445
C	4.205590	1.218361	0.142840
H	4.706508	2.170730	0.251266
C	4.904862	0.021767	0.131728
H	5.981894	0.007293	0.245200
C	4.216475	-1.167130	-0.015100
H	4.742416	-2.107016	0.011156
C	2.838921	-1.120406	-0.155878
N	2.037023	-2.247494	-0.317291
C	0.677617	-2.090107	-0.277427
N	0.156259	-3.316733	-0.373549
C	-1.250351	-3.530192	-0.670798
H	-1.571972	-2.749185	-1.355759
H	-1.365315	-4.496637	-1.153543
H	-1.854247	-3.503277	0.233610
C	1.162674	-4.280065	-0.444231
C	2.367728	-3.589399	-0.507322
C	3.553243	-4.228726	-0.887544
H	4.489493	-3.705703	-1.003083
C	3.465406	-5.554327	-1.223890
H	4.338765	-6.064945	-1.612738
C	2.270387	-6.292676	-1.082486
C	2.199339	-7.639501	-1.529620
H	3.081478	-8.080237	-1.980470
C	1.035023	-8.332060	-1.451031
H	0.954594	-9.330896	-1.865667
C	-0.074927	-7.806493	-0.735461
C	-1.245515	-8.594134	-0.551522
H	-1.310309	-9.544458	-1.070281
C	-2.253730	-8.170567	0.250135
H	-3.155721	-8.761236	0.368115
C	-2.104830	-6.991341	1.031048
C	-3.055306	-6.655270	2.014298
H	-3.950420	-7.262804	2.096240
C	-2.838382	-5.611650	2.877807
H	-3.571240	-5.369149	3.638485
C	-1.639824	-4.887895	2.800994
H	-1.433682	-4.101077	3.517560
C	-0.718150	-5.170661	1.824008
H	0.207468	-4.610983	1.803373
C	-0.943685	-6.190014	0.876341
C	0.005213	-6.528973	-0.153673
C	1.105011	-5.688329	-0.536618

Complex **2** P,C-I			
Re	0.052521	-0.102696	-0.060554
I	-0.263203	-0.596836	2.728906
C	0.248546	0.182060	-1.929166
O	0.388970	0.355162	-3.061741
C	0.252612	1.814369	0.290276
O	0.363441	2.937738	0.492744
C	1.949941	-0.298906	0.100445
O	3.090850	-0.417643	0.200415
N	-2.149232	-0.140753	-0.107324
C	-2.921909	0.943665	0.029402
H	-2.407176	1.894094	0.057254
C	-4.293252	0.873543	0.139745
H	-4.870905	1.781815	0.244976
C	-4.891483	-0.376793	0.137131
H	-5.963234	-0.479463	0.254716
C	-4.107507	-1.505282	-0.006625
H	-4.551707	-2.486305	0.025917
C	-2.739217	-1.345263	-0.152775
N	-1.848641	-2.403722	-0.313173
C	-0.506645	-2.137114	-0.272590
N	0.112025	-3.317679	-0.369575
C	1.531511	-3.416149	-0.666120
H	1.788467	-2.613473	-1.353379
H	1.725593	-4.371120	-1.146273
H	2.130769	-3.337306	0.238329
C	-0.813503	-4.359024	-0.442439
C	-2.070237	-3.767526	-0.505491
C	-3.200578	-4.498986	-0.887802
H	-4.175707	-4.052178	-1.003238
C	-3.006361	-5.812818	-1.225784
H	-3.835876	-6.391229	-1.615756
C	-1.756056	-6.453169	-1.084159
C	-1.577123	-7.789606	-1.532373
H	-2.420759	-8.299513	-1.984039
C	-0.361196	-8.386828	-1.453761
H	-0.201052	-9.375629	-1.869290
C	0.702920	-7.774694	-0.737479
C	1.933043	-8.465990	-0.554793
H	2.074120	-9.407351	-1.074811
C	2.904251	-7.963647	0.246958
H	3.850784	-8.480175	0.363782
C	2.661380	-6.801214	1.029366
C	3.582099	-6.391302	2.012897
H	4.523165	-6.925065	2.093967
C	3.282347	-5.369532	2.877762
H	3.993596	-5.069954	3.638619
C	2.029561	-4.744085	2.802013
H	1.761147	-3.977384	3.519763
C	1.133356	-5.098571	1.824749
H	0.165751	-4.615081	1.805010
C	1.439591	-6.095497	0.875912
C	0.520529	-6.508372	-0.154284
C	-0.642978	-5.758066	-0.536871

Complex **2** M,C-I

Re	-0.069426	0.077392	-0.029365
I	0.003934	0.133838	2.814964
C	-0.098739	0.091948	-1.929024
O	-0.138119	0.101204	-3.082581
C	-0.092026	-1.880545	-0.003905
O	-0.092261	-3.027347	0.009398
C	-1.983400	0.070097	-0.038608
O	-3.134939	0.069639	-0.054364
N	2.119943	0.319063	0.044869
C	2.991499	-0.692702	-0.044715
H	2.566057	-1.686389	-0.069870
C	4.354110	-0.499981	-0.110301
H	5.014726	-1.353680	-0.177418
C	4.836670	0.799344	-0.113061
H	5.898256	0.996900	-0.196984
C	3.949232	1.854074	-0.018222
H	4.303142	2.870949	-0.057918
C	2.596929	1.572346	0.088073
N	1.609794	2.548152	0.204088
C	0.298780	2.162993	0.123203
N	-0.426240	3.279736	0.242117
C	-1.850234	3.232248	0.532779
H	-2.019323	2.432110	1.250694
H	-2.152148	4.175222	0.977959
H	-2.430608	3.056179	-0.370359
C	0.398683	4.396581	0.380436
C	1.702291	3.917576	0.452677
C	2.755570	4.730921	0.885497
H	3.764274	4.368595	1.007429
C	2.438248	6.008813	1.264039
H	3.204703	6.644312	1.692265
C	1.138495	6.540171	1.118253
C	0.836920	7.837925	1.611488
H	1.626691	8.401558	2.095408
C	-0.425372	8.329067	1.534939
H	-0.678073	9.283400	1.983697
C	-1.422034	7.652000	0.781509
C	-2.707357	8.237868	0.611032
H	-2.935366	9.142226	1.164629
C	-3.624447	7.681910	-0.218191
H	-4.612672	8.115812	-0.325247
C	-3.272749	6.576071	-1.039998
C	-4.147166	6.122768	-2.046358
H	-5.131860	6.572819	-2.116243
C	-3.752090	5.165407	-2.945693
H	-4.428902	4.832689	-3.723980
C	-2.448616	4.652610	-2.881197
H	-2.108476	3.943598	-3.627223
C	-1.593838	5.048081	-1.882579
H	-0.585734	4.655977	-1.871588
C	-1.993564	5.977179	-0.900542
C	-1.121462	6.430062	0.153694
C	0.100456	5.770725	0.524137

Complex **2** P,A-I

Re	-0.062832	-0.084944	-0.029111
I	0.022124	-0.133329	2.815053
C	-0.093250	-0.100075	-1.928747
O	-0.132843	-0.111280	-3.082287
C	-0.270259	1.862120	0.000499
O	-0.382580	3.003322	0.017642
C	-1.969251	-0.253551	-0.036266
O	-3.115995	-0.358745	-0.051392
N	2.140068	-0.126193	0.041549
C	2.916261	0.960383	-0.050339
H	2.402861	1.911511	-0.079859
C	4.290892	0.892244	-0.112968
H	4.871196	1.802316	-0.181966
C	4.889824	-0.357661	-0.109311
H	5.965245	-0.458158	-0.189483
C	4.101786	-1.488393	-0.012932
H	4.547038	-2.468846	-0.047209
C	2.729104	-1.330844	0.088461
N	1.834906	-2.392537	0.203403
C	0.494254	-2.128078	0.122721
N	-0.126295	-3.306104	0.241270
C	-1.548418	-3.389280	0.532824
H	-1.790543	-2.605478	1.247742
H	-1.760998	-4.354495	0.982043
H	-2.143258	-3.271478	-0.370370
C	0.796755	-4.343286	0.378531
C	2.051580	-3.748183	0.450400
C	3.174313	-4.464018	0.881002
H	4.146704	-4.012843	1.001240
C	2.973732	-5.765315	1.260021
H	3.795163	-6.328855	1.687075
C	1.726750	-6.411370	1.116524
C	1.541947	-7.730018	1.612138
H	2.378704	-8.220501	2.096869
C	0.328100	-8.331374	1.537450
H	0.161503	-9.303403	1.988416
C	-0.725122	-7.747323	0.783040
C	-1.953488	-8.445205	0.613576
H	-2.100453	-9.365396	1.168648
C	-2.916063	-7.974279	-0.216816
H	-3.861906	-8.494248	-0.323251
C	-2.664097	-6.842658	-1.040260
C	-3.575347	-6.469605	-2.046950
H	-4.516107	-7.005511	-2.116340
C	-3.266947	-5.481366	-2.946867
H	-3.970736	-5.210432	-3.725188
C	-2.014110	-4.854772	-2.883041
H	-1.738450	-4.118795	-3.629554
C	-1.127380	-5.172277	-1.884458
H	-0.158041	-4.692236	-1.873757
C	-1.443158	-6.132400	-0.901654
C	-0.534450	-6.504627	0.153184
C	0.623728	-5.738500	0.522480

Complex **2** M,A-Cl

Re	-0.011716	-0.042965	0.037167
Cl	0.927965	-0.383823	2.343124
C	-0.658257	0.161018	-1.737726
O	-1.064299	0.283337	-2.812680
C	-1.815222	-0.226246	0.647460
O	-2.900771	-0.347050	1.013636
C	-0.150131	1.890796	0.317652
O	-0.228156	3.026246	0.461309
N	2.116944	-0.093902	-0.530924
C	2.890603	0.992135	-0.635140
H	2.385591	1.945299	-0.559155
C	4.254448	0.921658	-0.821108
H	4.833726	1.831215	-0.903932
C	4.847477	-0.329544	-0.870781
H	5.920053	-0.431150	-0.981924
C	4.060294	-1.460931	-0.767122
H	4.510792	-2.439518	-0.767138
C	2.691900	-1.302314	-0.624727
N	1.793990	-2.365016	-0.529699
C	0.489838	-2.089058	-0.224650
N	-0.134816	-3.267102	-0.147319
C	-1.585617	-3.366511	-0.152658
H	-1.974245	-2.575098	-0.789117
H	-1.870557	-4.329227	-0.568113
H	-1.993487	-3.270629	0.850957
C	0.757205	-4.316801	-0.367036
C	0.571299	-5.717062	-0.368797
C	-0.492877	-6.441185	0.267969
C	-1.188738	-5.979273	1.442032
C	-0.696512	-4.951832	2.272557
H	0.251739	-4.483631	2.044543
C	-1.383317	-4.547161	3.390017
H	-0.976230	-3.757254	4.010691
C	-2.601671	-5.151196	3.732355
H	-3.149919	-4.811924	4.603461
C	-3.069501	-6.202304	2.985264
H	-3.979871	-6.719308	3.269648
C	-2.360071	-6.663145	1.859520
C	-2.755700	-7.852786	1.188115
H	-3.662949	-8.353348	1.508805
C	-1.961812	-8.397656	0.233405
H	-2.205031	-9.357343	-0.209445
C	-0.789968	-7.727420	-0.216081
C	0.109496	-8.377212	-1.104156
H	-0.131245	-9.380313	-1.438691
C	1.285369	-7.794012	-1.448856
H	2.021283	-8.328425	-2.039174
C	1.550802	-6.442315	-1.100589
C	2.746294	-5.817486	-1.517805
H	3.480304	-6.417758	-2.042895
C	3.003878	-4.492513	-1.281323
H	3.935563	-4.059470	-1.610345
C	1.974011	-3.736804	-0.708758

Complex **2** P,C-Cl

Re	-0.017982	-0.029617	0.034455
Cl	-0.945155	0.365152	2.335871
C	0.597399	-0.322741	-1.739486
O	0.978030	-0.510454	-2.814339
C	1.194032	-1.373997	0.653056
O	1.918021	-2.189689	1.024090
C	1.381811	1.310927	0.315657
O	2.198601	2.102546	0.464396
N	-1.622189	1.366164	-0.542786
C	-1.459162	2.688489	-0.659102
H	-0.441955	3.050111	-0.595936
C	-2.513732	3.556944	-0.841363
H	-2.326729	4.618095	-0.934429
C	-3.797062	3.035504	-0.872882
H	-4.657359	3.685036	-0.978143
C	-3.980401	1.670253	-0.758949
H	-4.973691	1.253013	-0.744222
C	-2.862949	0.863316	-0.623917
N	-2.917716	-0.526346	-0.524202
C	-1.769670	-1.203842	-0.220117
N	-2.105939	-2.494289	-0.140823
C	-1.103033	-3.547478	-0.141697
H	-0.282904	-3.230081	-0.781274
H	-1.543644	-4.452485	-0.550765
H	-0.735990	-3.746015	0.862576
C	-3.473195	-2.665877	-0.361563
C	-4.284685	-3.822926	-0.365885
C	-3.994573	-5.078983	0.268065
C	-3.169535	-5.216171	1.441594
C	-2.831419	-4.130268	2.274810
H	-3.206915	-3.141198	2.048717
C	-2.054788	-4.303595	3.393355
H	-1.816462	-3.449013	4.016089
C	-1.573937	-5.575920	3.734203
H	-0.943065	-5.702424	4.606275
C	-1.944648	-6.662641	2.983669
H	-1.630114	-7.661855	3.265975
C	-2.776344	-6.515083	1.857003
C	-3.294847	-7.655355	1.183712
H	-2.970289	-8.639728	1.503253
C	-4.247069	-7.513197	0.229169
H	-4.721782	-8.381078	-0.215566
C	-4.650651	-6.224093	-0.217708
C	-5.752759	-6.089665	-1.104672
H	-6.257500	-6.988994	-1.439926
C	-6.219863	-4.862754	-1.447339
H	-7.123363	-4.753994	-2.036832
C	-5.496879	-3.690907	-1.097411
C	-5.953315	-2.421599	-1.514369
H	-6.899634	-2.366416	-2.039867
C	-5.245456	-1.272882	-1.277427
H	-5.635643	-0.323066	-1.607811
C	-3.976999	-1.415476	-0.703358

Complex **2** M,C-Cl

Re	-0.023631	0.027283	-0.061746
Cl	-0.329527	0.271046	2.414371
C	0.304212	-0.113819	-1.928002
O	0.493167	-0.193396	-3.065237
C	-1.816687	0.547019	-0.476291
O	-2.892134	0.862504	-0.744658
C	-0.617978	-1.837088	-0.012810
O	-0.952254	-2.934437	0.002908
N	2.090906	-0.344733	0.443647
C	2.632912	-1.562336	0.555408
H	1.951630	-2.396945	0.462107
C	3.979975	-1.762646	0.767904
H	4.366745	-2.768828	0.855882
C	4.807082	-0.653266	0.838047
H	5.876069	-0.765606	0.971187
C	4.260684	0.611326	0.725493
H	4.894561	1.482640	0.738953
C	2.890545	0.725718	0.557187
N	2.223585	1.945142	0.443248
C	0.901026	1.937044	0.095300
N	0.522909	3.216734	0.033753
C	-0.881335	3.595861	0.014670
H	-1.419733	2.925793	0.680727
H	-0.977326	4.612371	0.384147
H	-1.292173	3.535797	-0.990867
C	1.593078	4.066384	0.317225
C	1.682663	5.475969	0.370194
C	0.800692	6.418856	-0.260299
C	0.062285	6.147540	-1.467767
C	0.364070	5.071735	-2.327364
H	1.192337	4.415520	-2.095882
C	-0.351336	4.855753	-3.478785
H	-0.088616	4.025523	-4.124250
C	-1.411173	5.705218	-3.827101
H	-1.985547	5.516330	-4.726515
C	-1.684680	6.799909	-3.047161
H	-2.463198	7.499896	-3.331759
C	-0.935484	7.066617	-1.885031
C	-1.109785	8.285574	-1.173754
H	-1.889352	8.967839	-1.494844
C	-0.255521	8.625526	-0.177511
H	-0.318681	9.596758	0.301152
C	0.746546	7.720107	0.270218
C	1.726473	8.148181	1.206040
H	1.675565	9.166074	1.576532
C	2.753419	7.332895	1.554322
H	3.560161	7.689526	2.184869
C	2.760047	5.969083	1.156517
C	3.796176	5.109344	1.581509
H	4.613894	5.536986	2.149918
C	3.798185	3.768329	1.301804
H	4.613567	3.148581	1.640479
C	2.660543	3.249477	0.673166

Complex **2** P,A-Cl

Re	-0.006881	-0.041034	-0.057982
Cl	-0.162934	-0.360164	2.423529
C	0.211308	0.214694	-1.927958
O	0.339284	0.358361	-3.067401
C	-1.275140	-1.416923	-0.451591
O	-2.033722	-2.246486	-0.705403
C	-1.480138	1.249018	-0.037785
O	-2.337136	2.011617	-0.040354
N	1.617756	1.369762	0.433032
C	1.459842	2.694728	0.525335
H	0.448650	3.062193	0.416685
C	2.512556	3.558970	0.736847
H	2.329582	4.622550	0.807741
C	3.789782	3.029807	0.828829
H	4.649398	3.674895	0.963292
C	3.968163	1.662336	0.736452
H	4.958331	1.238669	0.767504
C	2.851508	0.860894	0.564954
N	2.904341	-0.528864	0.464763
C	1.766161	-1.202342	0.116359
N	2.101053	-2.493763	0.051822
C	1.093023	-3.542138	0.027696
H	0.289547	-3.252285	0.700602
H	1.536442	-4.466387	0.385345
H	0.704851	-3.691870	-0.977447
C	3.456235	-2.671281	0.332466
C	4.259419	-3.833160	0.377239
C	3.988197	-5.091351	-0.260998
C	3.213021	-5.230885	-1.467817
C	2.916661	-4.147739	-2.320165
H	3.290989	-3.160693	-2.083752
C	2.188133	-4.323185	-3.470292
H	1.984423	-3.472072	-4.109857
C	1.714317	-5.594459	-3.824543
H	1.121356	-5.722224	-4.722650
C	2.044857	-6.678733	-3.052148
H	1.735644	-7.677507	-3.341680
C	2.828392	-6.529569	-1.891660
C	3.307987	-7.668890	-1.188678
H	2.989226	-8.652942	-1.514880
C	4.218474	-7.527111	-0.194245
H	4.665229	-8.395429	0.277708
C	4.612840	-6.237995	0.260905
C	5.674800	-6.105911	1.195912
H	6.156124	-7.006756	1.560190
C	6.135514	-4.880257	1.551460
H	7.011693	-4.774409	2.181358
C	5.438218	-3.705277	1.161950
C	5.883565	-2.436750	1.593076
H	6.805292	-2.384869	2.160911
C	5.194184	-1.284718	1.320058
H	5.575324	-0.336169	1.664437
C	3.951062	-1.422419	0.691749

VIII. References

[1] N. O. Foglia, D. Maganas, and F. Neese, J. Chem. Phys. **157** (2022) 084120.

[2] F. Neese, and E. I. Solomon, Inorg. Chem. **38** (1999) 1847.

[3] D. Ganyushin, and F. Neese, J. Chem. Phys. **128** (2008) 114117.

[4] M. Atanasov, D. Aravena, E. Suturina, E. Bill, D. Maganas, and F. Neese, Coordination Chemistry Reviews **289** (2015) 177.

[5] F. Neese, J Chem Phys **122** (2005) 34107.

[6] K. Mori, T. P. Goumans, E. van Lenthe, and F. Wang, Phys. Chem. Chem. Phys. **16** (2014) 14523.

[7] B. de Souza, F. Neese, and R. Izsák, J. Chem. Phys. **148** (2018) 034104.

[8] B. de Souza, G. Farias, F. Neese, and R. Izsák, J. Chem. Phys. **150** (2019) 214102.

[9] R. Ianconescu, and E. Pollak, J. Phys. Chem. A **108** (2004) 7778.

[10] J. Tatchen, and E. Pollak, J. Chem. Phys. **128** (2008) 164303.

[11] Y. Niu, Q. Peng, C. Deng, X. Gao, and Z. Shuai, J. Phys. Chem. A **114** (2010) 7817.

[12] Q. Peng, Y. Niu, C. Deng, and Z. Shuai, Chem. Phys. **370** (2010) 215.

[13] R. Improta, G. Scalmani, M. J. Frisch, and V. Barone, J. Chem. Phys. **127** (2007) 074504.

[14] V. Barone, J. Bloino, M. Biczysko, and F. Santoro, J. Chem. Theory Comput. **5** (2009) 540.

[15] A. Baiardi, J. Bloino, and V. Barone, J. Chem. Theory Comput. **9** (2013) 4097.

[16] Y. Liu, J. Cerezo, G. Mazzeo, N. Lin, X. Zhao, G. Longhi, S. Abbate, and F. Santoro, J. Chem. Theory Comput. **12** (2016) 2799.

[17] R. Englman, and J. Jortner, Mol. Phys. **18** (1970) 145.

[18] G. Baryshnikov, B. Minaev, and H. Agren, Chem Rev **117** (2017) 6500.

[19] K. C. Mishra, and J. Collins, Optical Materials: X **15** (2022) 100190.

[20] C. Bach, H. Willner, F. Aubke, C. Wang, S. J. Rettig, and J. Trotter, Angew. Chem. Int. Ed. Engl. **35** (1996) 1974.

[21] O. Demel, J. Pittner, and F. Neese, J Chem Theory Comput **11** (2015) 3104.

[22] D. G. Liakos, and F. Neese, J Chem Theory Comput **11** (2015) 2137.

[23] A. K. Dutta, M. Nooijen, F. Neese, and R. Izsák, J. Chem. Theory Comput. **14** (2018) 72.

[24] A. K. Dutta, F. Neese, and R. Izsák, J. Chem. Phys. **145** (2016) 034102.

[25] A. Dreuw, and M. Head-Gordon, Chem Rev **105** (2005) 4009.

[26] A. D. Becke, Phys Rev A Gen Phys **38** (1988) 3098.

[27] J. P. Perdew, Phys Rev B **33** (1986) 8822.

[28] J. P. Perdew, K. Burke, and Y. Wang, Phys. Rev. B: Condens. Matter **54** (1996) 16533.

[29] C. Adamo, and V. Barone, J. Chem. Phys. **110** (1999) 6158.

[30] J. P. Perdew, M. Ernzerhof, and K. Burke, J. Chem. Phys. **105** (1996) 9982.

[31] J. P. Perdew, K. Burke, and M. Ernzerhof, Phys. Rev. Lett. **77** (1996) 3865.

[32] A. D. Becke, The Journal of Chemical Physics **98** (1993) 1372.

[33] P. J. Stephens, F. J. Devlin, C. F. Chabalowski, and M. J. Frisch, The Journal of physical chemistry **98** (1994) 11623.

[34] A. Becke, 1993).

[35] C. Lee, W. Yang, and R. G. Parr, Phys Rev B **37** (1988) 785.

[36] Y. Zhao, and D. G. Truhlar, Theor Chem Acc **120** (2008) 215.

[37] T. Yanai, D. P. Tew, and N. C. Handy, Chemical Physics Letters **393** (2004) 51.

[38] J.-D. Chai, and M. Head-Gordon, The Journal of Chemical Physics **128** (2008)

[39] S. Grimme, J. Chem. Phys. **124** (2006) 034108.

[40] A. Dittmer, R. Izsák, F. Neese, and D. Maganas, Inorg. Chem. **58** (2019) 9303.

[41] R. Shafei, D. Maganas, P. J. Strobel, P. J. Schmidt, W. Schnick, and F. Neese, J. Am. Chem. Soc. **144** (2022) 8038.